論文 / 著書情報
Article / Book Information

題目(和文)	
Title(English)	Improvement of Primary Human Hepatocyte Cell Attachment through EPAC2 Activation and Unraveling WFS1 Selective Degradation
著者(和文)	HELENA Grace Aprilia
Author(English)	Grace Aprilia Helena
出典(和文)	学位:博士(工学), 学位授与機関:東京科学大学, 報告番号:甲第331号, 授与年月日:2025年3月26日, 学位の種別:課程博士, 審査員:粂 昭苑,白木 伸明,田口 英樹,田川 陽一,三重 正和
Citation(English)	Degree:Doctor (Engineering), Conferring organization: Institute of Science Tokyo, Report number:甲第331号, Conferred date:2025/3/26, Degree Type:Course doctor, Examiner:,,,,
学位種別(和文)	博士論文
Type(English)	Doctoral Thesis

Doctoral Degree Dissertation

Improvement of Primary Human Hepatocyte Cell Attachment through EPAC2 Activation and Unraveling WFS1 Selective Degradation

Grace Aprilia Helena

School of Life Science and Technology
Institute of Science Tokyo

Table of Contents

Table of Figures

List of Table

List of Supplementary Data

Glossary

007	EPAC1 activator (8-pCPT-2'-O-Me-cAMP) (Cayman Chemical, 7143)
007-AM	EPAC1 activator (8-pCPT-2'-O-Me-cAMP-AM) (Merck Millipore, SML-3072)
8-Br-cAMP	PKA activator (Tocris Bioscience, 1140)
cAMP	3',5'-cyclic adenosine monophosphate
D-MEM	Dulbecco's Modified Eagle's Medium (Gibco, 11965092)
DAPI	4′,6-diamidino-2-phenylindole
ELISA	Enzyme-Linked Immunosorbent Assay
EPAC2	Rap guanine nucleotide exchange factor (GEF) 4
ER	Endoplasmic Reticulum
ESI-09	General EPAC inhibitor (Sigma Aldrich, 500506)
Fkbp2	Mouse Fk-506 isoform 2
Forskolin	adenylate cyclase (BioGems, 6652995)
HEP	Cellartis® Power™ Primary HEP Medium (Takara Bio, Y20020)
IBMX	Isobutylmethylxanthine, 1-Methyl-3-Isobutylxanthine (2885842, BioGems)
iPSC	Induced Pluripotent Stem Cell
iPSC-Hep	Induced pluripotent stem cell-derived hepatocyte
KEGG	Kyoto Encyclopedia of Genes and Genomes
LTMM	Cellartis® Enhanced hiPS-HEP Long-Term Maintenance Medium (Takara Bio, Y30052)
M4	Kume-Shiraki Laboratory late stage iPS-Hep Medium
MAM	Mitochondria-Associated Membrane
MM	Cellartis® Hepatocyte Maintenance Medium (Takara Bio, Y30051)
mRNA	Messenger Ribonucleic Acid
Opti	Optiplate (Sekisui Xenotech, K8200)
pAd	Adenovirus destination vector pAd/CMV/V5/Dest (Invitrogen, V49320)
PBS	Phosphate Buffered Saline
PBS-T	PBS with 0.1% Tween
PCR	Polymerase Chain Reaction
pENTR1A	Golden gate entry vector (Invitrogen, A10462)
PHH	Primary Human Hepatocyte
PLA	Proximity Ligation Assay
RT-qPCR	Reverse Transcription qPCR (quantitative PCR)
S-220	EPAC2-specific inhibitor (Sp-Bnt-8-cAMPS) (Biolog.de, B 046-05)
Sec61a1	Mouse Sec61a1
WFS1	Wolfram Syndrome 1 (Wolframin)
WS	Wolfram Syndrome

Chapter I: Introduction

Improvement of Primary Human Hepatocyte Cell Attachment through EPAC2 Activation

Introduction

Primary Human Hepatocyte (PHH) is the gold standard model for pharmacological studies. However, it often loses its attachment properties due to the isolation processes from donors. This study focuses on improving its attachment by optimizing the seeding procedure and medium composition. Additionally, the specific activation of EPAC2, a cyclic AMP effector, significantly enhanced the attachment of the so-called 'suspension type' (low attachment) PHH. The procedure and medium composition established in this study present a promising approach to improving PHH versatility in related fields.

Experiment method

Commercially available suspension PHH was subjected to various culture conditions based on BSA concentrations, small molecule compositions, and inhibitor/activator addition of M4 (Kume-Shiraki's Lab iPS-Hep late-stage differentiation medium). PHH was cultured for a short period (4 to 24 hours) or a long period (up to 7 days). PHH cultured for 4-24 hours was subjected to immunocytochemistry with Phalloidin, Albumin, and DAPI for cell attachment quantification. PHH cultured for a long-term period was subjected to CYP3A4 activity assay, immunocytochemistry, and RT-qPCR.

Results and Discussion

Activation of cAMP through the addition of both IBMX and Forskolin coupled with BSA elimination from M4 medium increased early PHH attachment. Furthermore, adjustment of seeding density is also crucial to increase its attachment. Delving further into the cAMP effector, the EPAC2-specific activator, S-220, was found to potently increase PHH attachment at low concentrations. Moreover, Culturing PHH in M4 BSA- medium with cAMP activators seemed to improve PHH functional marker, CYP3A4 activity, and bile canaliculi formation.

However, culturing PHH in M4 BSA- compared to BSA+ in the long term might pose a detrimental effect on PHH viability and albumin secretion.

Unraveling WFS1 Selective Degradation

Introduction

WFS1 is an endoplasmic reticulum (ER) protein whose mutations are associated with Wolfram Syndrome (WS). A previous study discovered that c-terminal truncated mutant WFS1 W837X and Y652X showed faster degradation in MIN6 (mouse insulinoma) cells than HEK293T (human embryonic) cells. Comparative analysis of proteins identified in MIN6 and HEK293T through TurboID assay was performed to search for interacting candidates possibly involved in WFS1 degradation.

Experiment method

Adenovirus was used to transiently transfect confluent MIN6. The harvested crude protein was then processed with a subcellular fractionation kit to isolate membrane-organelle fraction. The membrane-organelle fraction was subjected to biotinylated protein enrichment with avidin beads and trypsinization. The eluted fraction was then subjected to LC-MS/MS analysis. The resulting data was filtered, tidied, explored, and visualized with R.

Results and Discussion

Primary, secondary, and tertiary candidates that were detected in the WFS1 (WT)-TurboID assay were identified. From these candidates, many ER chaperone proteins were identified in the dataset. This leads to a hypothesis: the loss of the C-terminal in WFS1 W837X and Y652X might lead to a loss of interaction with the chaperone, leading to faster protein turnover. The primary focus in this study was the primary candidates: Sec61a1 and Fkbp2, which possess chaperone functions. As for Sec61a1, other functions, such as ER membrane protein insertion mediator, were also considered. This study also confirmed the direct interaction between WFS1-Sec61a1 and WFS1-Fkbp2 through PLA (Proximity Ligation Assay).

Chapter II: Improvement of Primary Human Hepatocyte Cell Attachment through EPAC2 Activation

Section I: Background

Primary Human Hepatocyte

As a center of metabolic processing, liver holds an essential role in metabolism, biosynthesis, nutrient storage, detoxification, and bioactivation of drugs. Boasting to demonstrate similar *in-vivo* response towards drug insults, the main component, the *Primary Human Hepatocyte*, or PHH, was renowned as the gold standard for model cells in drug toxicity research (Vinken & Hengstler, 2018). Godoy and colleagues have curated a plethora of studies that utilized PHH as the main research subject, emphasizing it as an indispensable model for pharmacological studies (Godoy et al., 2013).

The isolation of PHH involves a long and tedious series of steps that require a high level of practical expertise to ensure its quality. Prior to the invention of the infamous 2-step perfusion isolation protocol method in the late 1970s, hepatocytes were initially isolated through mechanical force, which yielded low-quality hepatocytes (Longmuir & Ap Rees, 1956). The establishment of the 2-step perfusion method provided a less invasive procedure which leads to a higher yield of quality of hepatocytes (Green et al., 2017; Horner et al., 2019; Kegel et al., 2016; S. M. L. Lee et al., 2013). The protocol starts with the cannulation to the specimen's blood vessel, followed by Ca^{2+}-free EGTA perfusion to disrupt the desmosome, allowing cell-cell detachment of the cells (S. M. L. Lee et al., 2013; Seglen, 1976). Enzymatic digestion by collagenase is then performed to dissociate the cells from the ECM (Extracellular Matrix), mainly composed of collagen (Bedossa & Paradis, 2003; S. M. L. Lee et al., 2013). The Isolated cells go through a purification process by centrifuging the cells in Percoll (low-density solution) (Horner et al., 2019).

Following the isolation procedure, cryopreservation is performed to ensure the availability of cryopreserved PHH for future use. The first hepatocyte cryopreservation protocol was published in the late 1980s, utilizing slow-freezing cryoprotectants such as DMSO, FBS, and other high-density solutions (Loretz et al., 1989). The PHH cryopreservation method has been evolving until now, adding additional steps such as tweaks in the base protocol. Aiming for better post-thaw cell viability and activity (De Vries et al., 2018; T. D. R. Lloyd et al., 2004; Saliem et al., 2012). Despite the evolving cryopreservation protocol, PHH is still negatively affected by the process to some extent. Terry and colleagues have performed extensive studies of the PHH functional damage and reduction of PHH attachment resulting from the cryopreservation process (Terry et al., 2005, 2010).

Due to the lengthy and harsh processing steps performed, cryopreserved PHH received significant performance reduction compared to freshly isolated PHH (Sosef et al., 2005; Terry et al., 2005). Studies have documented the reduction of cell attachment in cryopreserved PHH (Ölander et al., 2019; Sosef et al., 2005; Terry et al., 2005). Although the donor-to-donor differences also played a role in post-thaw PHH attachment, the reduction of PHH attachment was generally correlated to the reduction dedifferentiation of PHH based on the observed reduction of albumin secretion, cell metabolism, viability, and activity observed after the thawing the cells (Terry et al., 2005). Not only in 2D culture, Baze and colleagues also documented that PHH spheroid formation is significantly dependent on PHH attachment or palatability (Baze et al., 2018). Therefore, attachability is essential to maintain PHH functionality and versatility in an *in vitro* culture system.

Based on its attachment grade, commercially available PHH is generally divided into “Suspension” (low attachment PHH) and “Plateable” (high attachment PHH) (Baze et al., 2018; Bell et al., 2016; Moeller et al., 2012). The plateable PHH was identified demonstrated 80-90% cell attachment making it suit able for long-term studies and various pharmacological

studies (Lauschke et al., 2019; Moeller et al., 2012; Shoemaker et al., 2020). Although the suspension PHH is generally more available, its use is limited to short-term studies, which hinders the pharmacological studies that require it to be cultured for an extended period (Lauschke et al., 2019; Shoemaker et al., 2020). This study aims to increase PHH attachment by using suspension PHH as the model cell in order to increase its range of *in-vitro* versatility. In contrast, hopefully increases long-term culturable hepatocyte availability for medical and pharmacological studies.

Cell Attachment

In-vitro mammalian cell culture was designed to mimic the intricate *in-vivo* environment to sustain the cells outside the body. Culture medium was added to mimic the function of blood, which delivers nutrients and mediates metabolism clearance. The cells are maintained in an incubator that maintains the temperature at 37 °C, which mimics body temperature, while providing a steady supply of CO_2, which mimics gas exchange by the lung. Most mammalian cells exhibited a preference for an attachment-promoting culture system; hence, the early cell culture system *in vitro* generally utilized substrates that promote cell attachment (Hacking & Khademhosseini, 2013).

Cell attachment is comprised of cell-substrate interactions that govern cell functions, activity, and differentiation (Ruoslahti, 1996). Morphologically, attached cells display a flattened appearance with irregular cell shape and cellular process extension. Studies in the past revealed that cells can attach to TCP (*Tissue Cell Polystyrene*) pretreated with serum. Investigation attempt revealed that instead of directly binding into the TCP surface, the process was comprised of interactions between the transmembrane protein of integrins and specific anchoring proteins from the serum that adsorbed on the surface of TCP (Fredriksson et al., 1998; Gallant & García, 2007). Integrins consist of alpha and beta subunits that act as an adhesion receptor that bind to the anchoring proteins on the substrate (Gallant & García, 2007;

Hynes, 2002). Integrins play a significant role in controlling signaling pathway that governs cytoskeletal organization, cell proliferation, differentiation, apoptosis, and migration (Ruoslahti & Reed, 1994).

The importance of cell attachment mediated by integrin towards osteogenic differentiation of hMSC (Mesenchymal Stem Cell) was previously reported (Ogura et al., 2004). A more detailed study by McBeath and colleagues demonstrated the role of cell attachment and morphology on hMSC differentiation (McBeath et al., 1996).

PHH Cell Attachment

In the liver, ECM (Extracellular Matrix) is considered a minor component of the organ. Although ECM makes up less than 3% of the relative tissue section area (Geerts, 2001), it possesses important roles in orchestrating hepatocyte differentiation state and regenerative capability (Friedman, 2005; Schuppan et al., 2001). Liver ECM showed site-specific zonation in its component (Schuppan et al., 2001). The liver's ECM is comprised of 20 types of collagens, predominantly Collagen I, Collagen III, and Collagen IV as the structural components (Klaas et al., 2016).

Hepatocyte survival and differentiation are heavily affected by cell-matrix interactions (Gkretsi, Bowen, et al., 2007). Past studies have reported that the loss of cell-matrix interactions induced dedifferentiation of hepatocytes (Bucher et al., 1990; T. H. Kim et al., 1998). Furthermore, *in-vitro* hepatocyte was found to prefer complex matrices such as Matrigel and collagen (Lindblad et al., 1991). Although the mechanism has not been fully elucidated, evidence suggests that cell attachment is essential in maintaining in-vitro PHH culture (Bucher et al., 1990).

PHH possesses various integrin adhesion molecules that mediate cell attachment to ECM (Klaas et al., 2016; Pinkse et al., 2004, 2005). Integrin-linked was also reported to be involved in PHH survival, differentiation, and even CYP3A4 activity (Gkretsi et al., 2008; Gkretsi, Bowen, et al., 2007; Gkretsi, Mars, et al., 2007; Jonsson-Schmunk et al., 2016; T. H. Kim et al., 1998; Pinkse et al., 2004). Hepatocyte generally binds to the arginine-glycine-aspartic acid (RGD) domain of the matrix component through, most notably, the $\alpha_v\beta_1$ and $\alpha_1\beta_1$ integrins (Pinkse et al., 2004; Richter et al., 2011; Ruoslahti, 1996).

As a primary cell, PHH is sourced from dead donors and goes through multiple steps of cell harvest, isolation, and purification (Horner et al., 2019). These processes resulted in the

loss of cell-cell contact, signaling, and reduction of cell-matrix interaction (cell attachment) (Sosef et al., 2005; Stéphenne et al., 2010). Methods to optimize cryopreserved PHH attachment have long been studied by primarily emphasizing matrix type or medium composition. Freshly isolated PHH attached to various substrates such as serum-treated, polystyrene, collagen I, and Matrigel (Gjessing & Seglen, 1980b; Kikkawa et al., 2011; Rubin et al., 1981). Unfortunately, cryopreserved PHH showed a partial reduction in its attachment, preventing the cells from forming a confluent monolayer on most matrices, leading to cell death and a shortened cell culture period (Ölander et al., 2019; Terry et al., 2007). A more comprehensive study also revealed that low attachment hinders the pharmacological studies that mainly require PHH to be cultured for an extended period (Lauschke et al., 2019).

Studies in the past have made various attempts to improve PHH attachment. Kan and colleagues initially proposed fibronectin as a solution to improve PHH attachment (Kan et al., 1982). Years after, it was revealed that although fibronectin addition improved PHH attachment, the cells showed signs of over-spreading and over-time increase of stress fiber production and reduction of cell maturity (Mooney et al., 1992). Olander and colleagues also reported that the addition of apoptosis inhibitor Z-VAD-FMK improved PHH survival and attachment, although the mechanism that governs the PHH attachment process remains unknown (Ölander et al., 2019). Decades ago, many studies also revealed that BSA reduced cell attachment interactions by hindering direct cell-matrix interactions (Gjessing & Seglen, 1980a; Junker & Heine, 1987; Kan et al., 1982). Furthermore, it was reported that seeding density played a substantial role in maintaining hepatocyte maturity and affected PHH attachment by the cell-cell connection and hepatocyte's self-secreting growth factor characteristic (Gjessing & Seglen, 1980a; L. Qiao & Farrell, 1999; Yamasaki et al., 2020).

A correlation between hepatocyte cell-matrix attachment and its differentiation state was observed in the study of rat hepatocytes (T. H. Kim et al., 1998). Furthermore, it was discovered

that the interaction between integrin and collagen is essential in regulating epithelial cell differentiation (Yeh et al., 2012). The phenotypic adherent characteristic may be the reason why plateable PHH is usable in long-term culture without significantly losing its identity while maintaining its viability. Therefore, the improvement of PHH attachment may help widen the versatility of PHH for long-term research while improving its function.

cAMP

Cyclic Adenosine Monophosphate (cAMP) acts as a second messenger that relay the extracellular signal within the cytoplasm (Yan et al., 2016). cAMP is synthesized from Adenosine Triphosphate (ATP) through Adenylyl Cyclase (AC) and regulated through hydrolysis by Phosphodiesterase (PDE) (Maurice et al., 2003). There are compounds that improve cAMP concentration. One of them is IBMX (3-isobutyl-1-methylxanthine). It improves cAMP activity through PDE inhibition (Huai et al., 2004). Another compound, Forskolin, works synergistically with IBMX by activating Adenylyl Cyclase (AC), the enzyme responsible for cAMP synthesis (Hurley, 1999; Seamon et al., 1981).

As one of the second messengers, cAMP is involved in various cellular functions such as metabolism, transcription, and growth in cells. There are two main downstream effectors, protein kinase A (PKA) and exchange factor directly activated by cAMP (EPAC) (Cheng et al., 2008). Protein PKA is directly activated by cAMP, releasing active C subunits that phosphorylate a multitude of metabolite enzymes and regulate various cellular processes, including cell adhesion (Howe, 2004; Whittard & Akiyama, 2001). cAMP also binds to EPAC and directly activates Rap protein that regulates cellular functions such as cell adhesion, cell-cell junction, and many more (Bos et al., 2003; Cheng et al., 2008).

EPAC

EPAC protein possesses two main isoforms, EPAC1 and EPAC2, which are respectively encoded by Rapgef3 and Rapgef4 genes (Hoivik et al., 2013; Lezoualc'H et al., 2016; Niimura et al., 2009). Both isoforms are regulated by cAMP. Rapgef3 synthesizes one 4-kb mRNA that constitutes the EPAC1 protein, whereas EPAC2 (Rapgef4) goes through differential splicing that generates three different isoforms EPAC2A, EPAC2B, and EPAC2C (Bos, 2006) (Hoivik et al., 2013; Niimura et al., 2009). These isoforms exhibit restricted expression patterns, which causes them to be found on specific cell types (Lezoualc'H et al., 2016).

One of the most renowned cellular functions of EPAC is the ability to enhance cell adhesion. Studies have revealed the EPAC overexpression effect on HEK293 cells induced cell flattening and improved cell adhesion (J. Qiao et al., 2002). Other studies also proved that cAMP-Epac-Rap1 has a role in regulating cell spreading and adhesion (Enserink et al., 2004). The less common isoform of EPAC, with the name EPAC2C, is found to be only expressed in the liver (Sugawara et al., 2016; Ueno et al., 2001b). DNA Methylation on alternative promoters regulates this tissue-specific expression of EPAC (Hoivik et al., 2013). Currently, the detailed role of EPAC2C in the liver has not been fully understood.

Section II: Experimental Methods

PHH Culture

Commercially available cryopreserved suspension-type Primary Human Hepatocytes (PHH) (Sekisui Xenotech Lot no. H789 and H877, AMY>4.0×10^6 cells/vial) were thawed with ThawSTAR™ (Biocision), then decanted into 14 mL of 37°C OptiThaw medium (Sekisui Xenotech). The cell suspension was then sampled for 10 µL and then mixed with 10 µL for automated cell quantification in the cell counting chamber (Invitrogen™ Countess II Automated Cell Countess; ThermoFisher). The cell suspension was centrifuged at 100×g at 25°C for 5 minutes. The cell pellets were resuspended to the desired cell density with the treatment media, plated into 96-well plates at 75 µL /well (Collagen Type I-Coated, Flat-Bottom Microplates plate, Gibco™), and incubated at 37°C for 4 h, followed by complete volume medium change. The cells were incubated for the required period with medium change every 24 h. The medium list for **Result 3.1** can be seen in **Table 1**. The chemical list for **Result 3.4**, **Result 3.6**, and **Result 3.7** is listed in **Table 2**. The composition of the M4 medium can be found in **Supplementary Table 2**.

Table 1 *Medium List*

Medium Name	Company, Catalog Number
Optiplate	Sekisui Xenotech, K8200
HCM (Hepatocyte Culture Medium SingleQuotsTM Kit)	Lonza, CC-4182
MM (Cellartis® Hepatocyte Maintenance Medium)	Takara Bio, -
LTMM (Cellartis Enhanced hiPS-HEP Long-Term Maintenance Medium)	Takara bio, Y30052
HEP (Cellartis Enhanced hiPS-HEP Long-Term Maintenance Medium)	Takara Bio, Y20020
M4 Medium	Kume-Shiraki Lab's iPS-Hep maintenance medium

Table 2 *List of cAMP-Related Chemical Used*

Chemical Name	Company, Catalog Number	Role
007	Tocris, 1645	EPAC1 Activator
007-AM	Tocris, 4853	EPAC1 Activator
ESI-09	Sigma Aldrich, 500506	EPAC inhibitor
S-220	Biolog.de, B 046	EPAC2 Activator
8-Br-cAMP	Tocris, 1140	PKA Activator

RT-qPCR (Reverse Transcriptase qPCR) analysis

RNA was extracted from PHH using the Cica geneus® RNA Prep Kit for Tissue (Kanto Chemical #08057-96). 2.5 µg RNA was reverse-transcribed using PrimeScript™ RT Master Mix (Takara Bio). For RT-qPCR analysis, the mRNA expression was quantified using SyberGreen on a StepOne Plus (Applied Biosystems, Foster City). The PCR conditions were as follows: initial denaturation at 95℃ for 30 seconds (s), then denaturation at 95℃ for 5 s, annealing, and extension at 60℃ for 30 s, for up to 40 cycles. β-ACTIN and glyceraldehyde-3-phosphate dehydrogenase (GAPDH) were used as internal controls. Target mRNA levels were expressed as fold-changes against human adult hepatocytes (=1). Primer details are listed in **Supplementary Table 1**.

Measurement for CYP3A metabolites by LC-MS/MS

CYP3A activity in PHH after 5 Days of culture was evaluated. PHH plated for 4 h, or 48 h were used as references. iPS-hep or PHH cultures were washed with warm William's E media supplemented with PS, L-Gln, and Primary Hepatocyte Maintenance Supplements (ThermoFisher, CM4000). Assays were started by adding media containing 5 µM midazolam (Wako). The volume of media added was 500 µL to the PHH, 300 µL to the upper, and 600 µL to the lower chamber. 0.5, 1, and 2 h, 60 µL of supernatants were collected from the upper and lower chamber and kept at -80℃ until performing LC-MS/MS analysis of the metabolite, 1'-OH midazolam. For iPS-hep, midazolam was added to both the upper and lower chambers.

Supernatants from both the upper and lower chambers were collected and combined. The collected supernatants were extracted by adding acetonitrile containing an internal standard, 1‘-OH midazolam 13C3, and were quantified by LC-MS/MS with the liquid chromatography, Nexera I LC-2040C 3D (Shimadzu) and the mass spectrometer, LCMS-8050 (Shimadzu), using Inertsil ODS-3, 2.1×33 mm, 3 μm column (GL Sciences) (detailed LC-MS/MS analysis condition of the metabolite, 1’OH midazolam is in Supplementary Table S2). Protein amount per well was quantified using the Pierce BCA protein assay kit (ThermoFisher, 23225). Metabolite concentrations were normalized with protein amounts.

Immunocytochemistry & Phalloidin Staining

Cells were fixed with 4% paraformaldehyde (Nacalai Tesque) in PBS (Phosphate Buffered Saline), permeabilized with 0.1% Triton X-100 (Nacalai Tesque) and blocked with 20% Blocking One (Nacalai Tesque) in PBST (0.1% Tween-20 in PBS). Antibodies were diluted in 20% Blocking One in PBST (0.1% Tween-20 in PBS). Cells were treated with goat anti-Albumin (ALB; A80-129A, 1:100, Bethyl Laboratories) and incubated at 4°C overnight. PBS was performed three times after the incubation. Cells were counterstained with 6-diamidino-2-phenylindole (DAPI; Roche Diagnostics) as counterstain, along with Donkey Anti-Goat IgG (H+L) whole antibody CF 568 Dye (Biotium, 20106), and Phalloidin-iFluor™ 488 Conjugate anti-AAT (Bioquest, 23115).

Albumin and alpha-fetoprotein ELISA

Albumin secretion into the medium was quantified with a Human Albumin ELISA Kit (Bethylm, E88-129). The process was performed according to the manufacturer’s guide. Alpha-fetoprotein ELISA was performed with the Human AFP Sandwich ELISA Kit (Proteintech, KE00132) according to the manufacturer’s guide.

Live/dead assay

Live/Dead assay was performed with LIVE/DEAD™ Cell Imaging Kit (488/570) (Invitrogen, R37601) according to the manufacturer's guide. Treated cells were visualized with MolecularDevice. Quantification was performed with MetaXpress.

Image acquisition and quantification

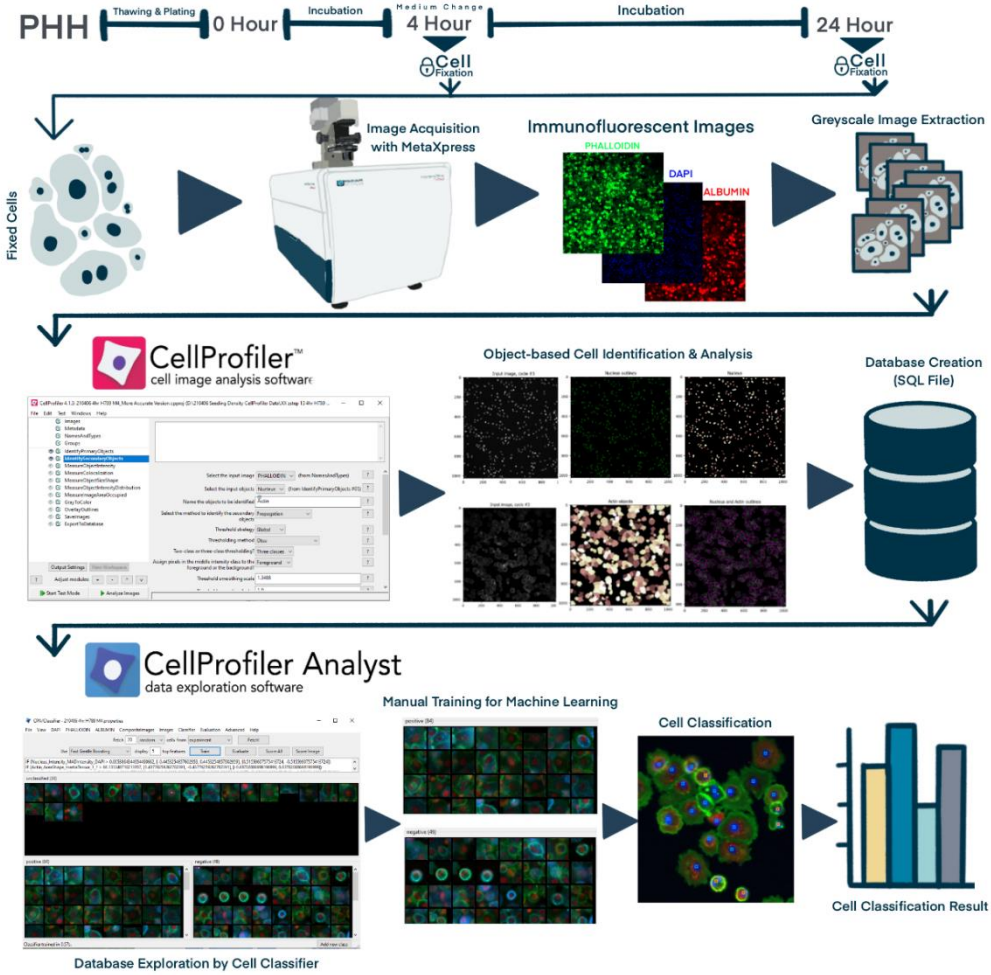

Figure 1 *General workflow of the image quantification procedure*

Image acquisition was generally performed on 4 hours (h) and 24 h DAPI, ALB (Albumin), and Phalloidin stained cells (**Figure 1**). Image acquisition was performed on the stained cells with ImageXpress (Molecular Devices). Image data were then exported to assign the required metadata to the image files. The exported images were then moved into personal PC for analysis and quantification using CellProfiler to identify DAPI staining as the primary object (Nucleus) and phalloidin staining (actin on the periphery) as a secondary object (McQuin et al., 2018). Both objects were connected and identified as one cell. Various parameters such as size, staining intensity, and object distribution were measured and exported as one big database for machine-learning-based cell identification in CellProfiler Analyst (Jones et al., 2008).

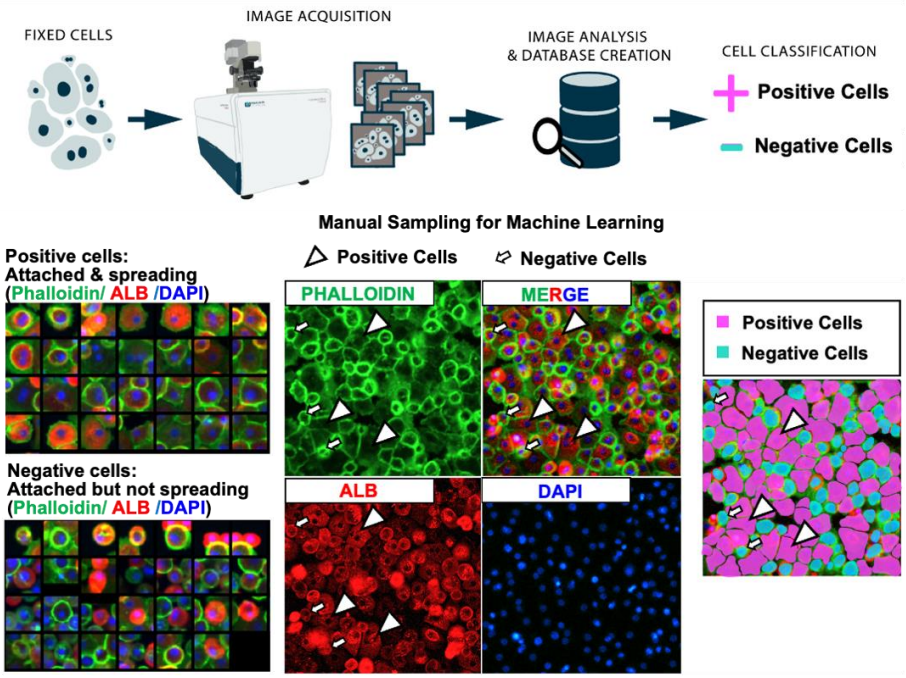

Figure 2 Cell classification with CellProfiler Analyst

The previously created database created in CellProfiler was processed in CellProfiler Analyst by utilizing the cell classifier module as the main data exploration tool. The identified cells within the database were randomly fetched for manual classification as learning material for the software. Manual classification is fundamentally performed based on the morphology of the cells (**Figure 2**). The cells that showed "Attached and Spreading" morphology and connection with the neighboring cells were classified as positive cells. In contrast, the cells that showed circular morphology without any flattening were classified as Negative cells. Based on the manual classification result, the software would create an algorithm based on the Fast Gentle Boosting module to classify the rest of the cells in hundreds of images. The quantification results were finally exported in Microsoft Excel file format and visualized in GraphPad Prism.

Section III: Results

3.1 PHH Showed better attachment in M4 Medium

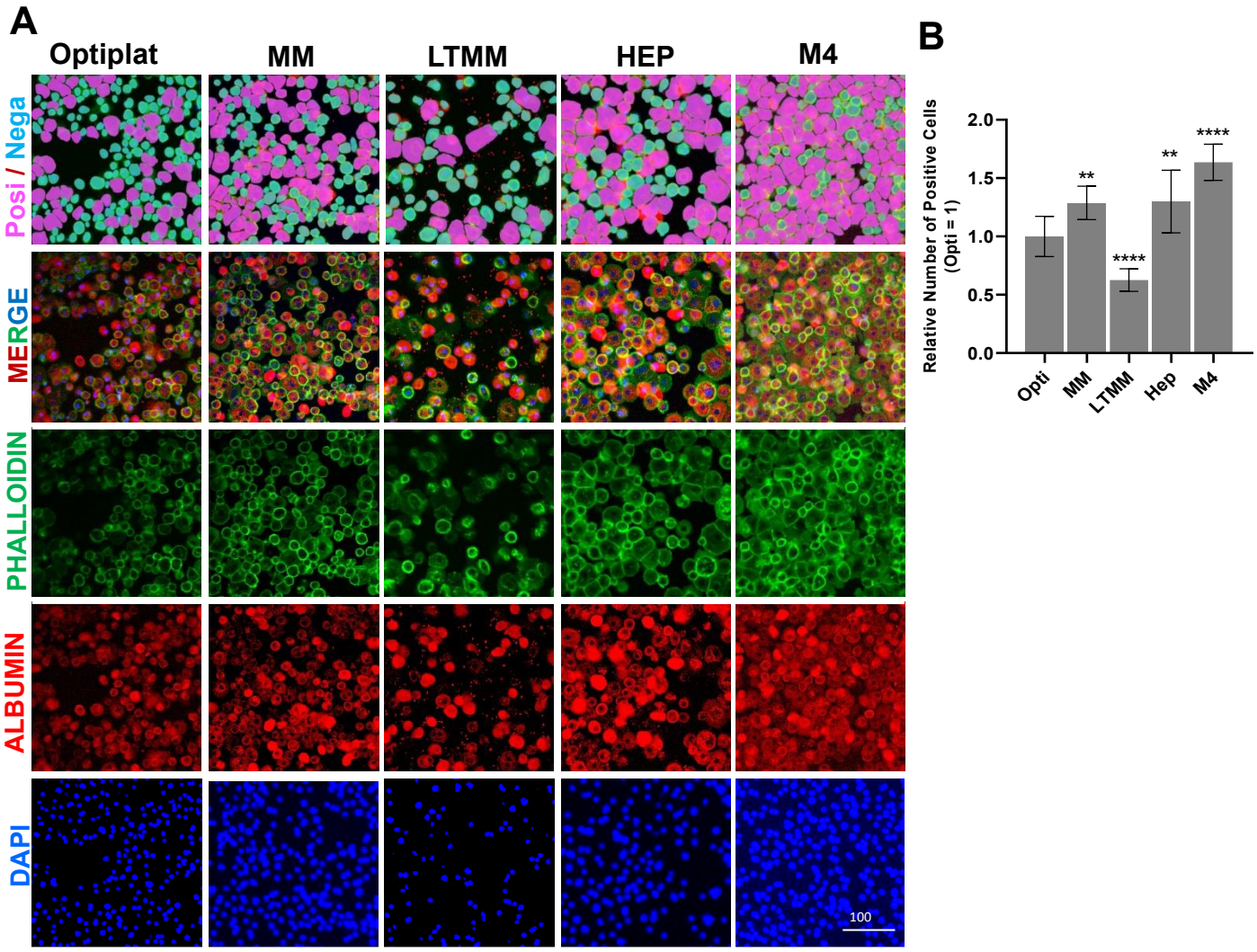

Figure 3 PHH H789 cultured in 5 different media

A) PHH cultured 4 hours (h) in M4 medium or several other commercial media, Optiplate, MM, LTMM, and HEP, classified as positive (magenta) and negative (cyan) based on the staining with phalloidin (green) albumin (red) and DAPI (blue). B) Image quantification of the stained images. Data are expressed as mean ± SD N=10. Differences are shown as *P ≤ 0.05, ** P ≤ 0.01, *** P ≤ 0.001, and **** P ≤ 0.0001 analyzed with one-way ANOVA, Dunnett's multiple comparisons test.

As a preliminary experiment to establish and confirm PHH handling protocol, after the thawing procedure, PHH was plated in five different commercial media (**Table 1**). The quantification process was performed according to the method described in part 2.5. Quantification results revealed that PHH cultured in Kume-Shiraki's Lab M4 media showed relatively higher cell attachment compared to the other commercial media (**Figure 3A**). The

quantification result showed 1.5 times more positive (attached and spreading) cells to Optiplate, the designated plating media by the provider of PHH (Sekisui Xenotech). Furthermore, the cells plated in the M4 medium showed improved cell attachment, sufficient spreading, proper cell-to-cell connections, and even monolayer formation compared to other commercial media at 4 h (**Figure 3**). These results suggest that our M4 is superior in improving early hepatocyte attachment.

3.2 Low BSA Concentration Improved PHH Attachment

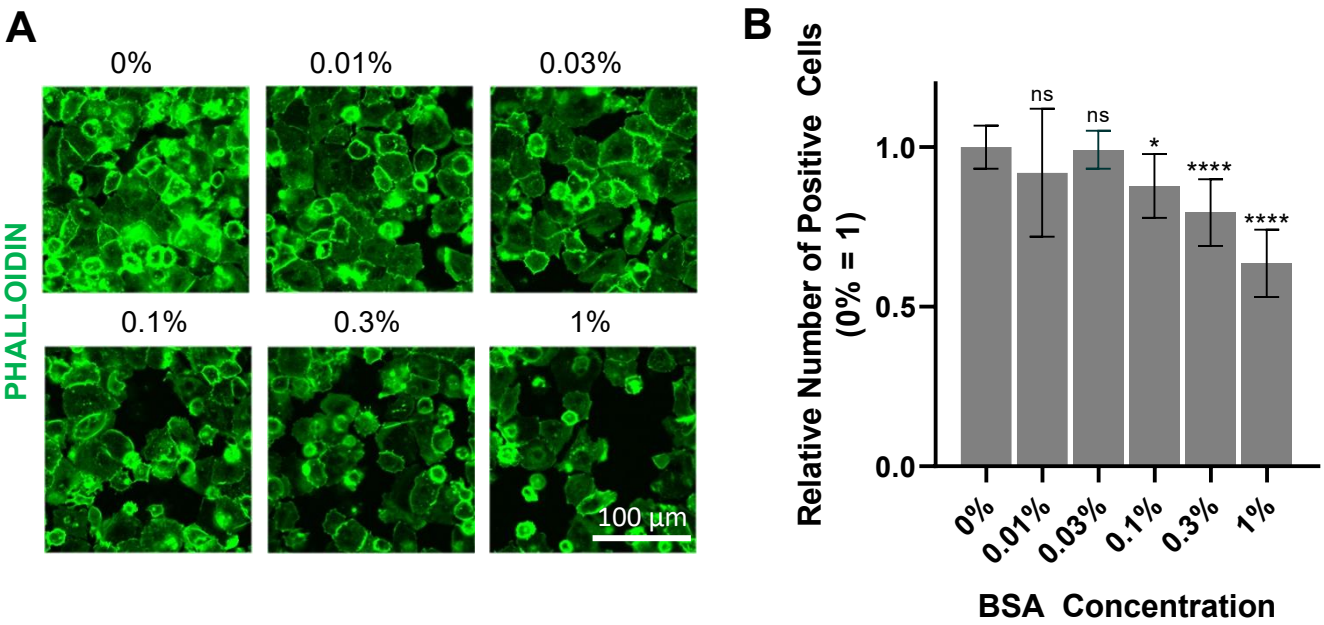

Figure 4 Lower BSA Concentration Improved PHH Attachment

A) Phalloidin staining (green) of 4 h PHH H789 cultured in M4 medium with different BSA concentrations. B) Quantification result of phalloidin staining images. Data are expressed as mean ± SD N=10. Differences are shown as ns $P>0.05$, *$P \leq 0.05$, ** $P \leq 0.01$, *** $P \leq 0.001$, and **** $P \leq 0.0001$ analyzed with one-way ANOVA, Dunnett's multiple comparisons test.

Based on the previous result, the extent of BSA effect on PHH attachment by plating the cells in various concentrations of BSA from 0 to 1% (**Figure 4**). Cells in BSA 1% medium showed the lowest relative number of positive cells. While cells in 0% showed the highest number of positive cells, statistical analysis revealed that the cells in 0.01% and 0.03 % did not show a significant difference to 0%, which implies that lower concentration of BSA in the M4 medium improved PHH cell attachment.

3.3 Seeding Density Affected PHH Attachment

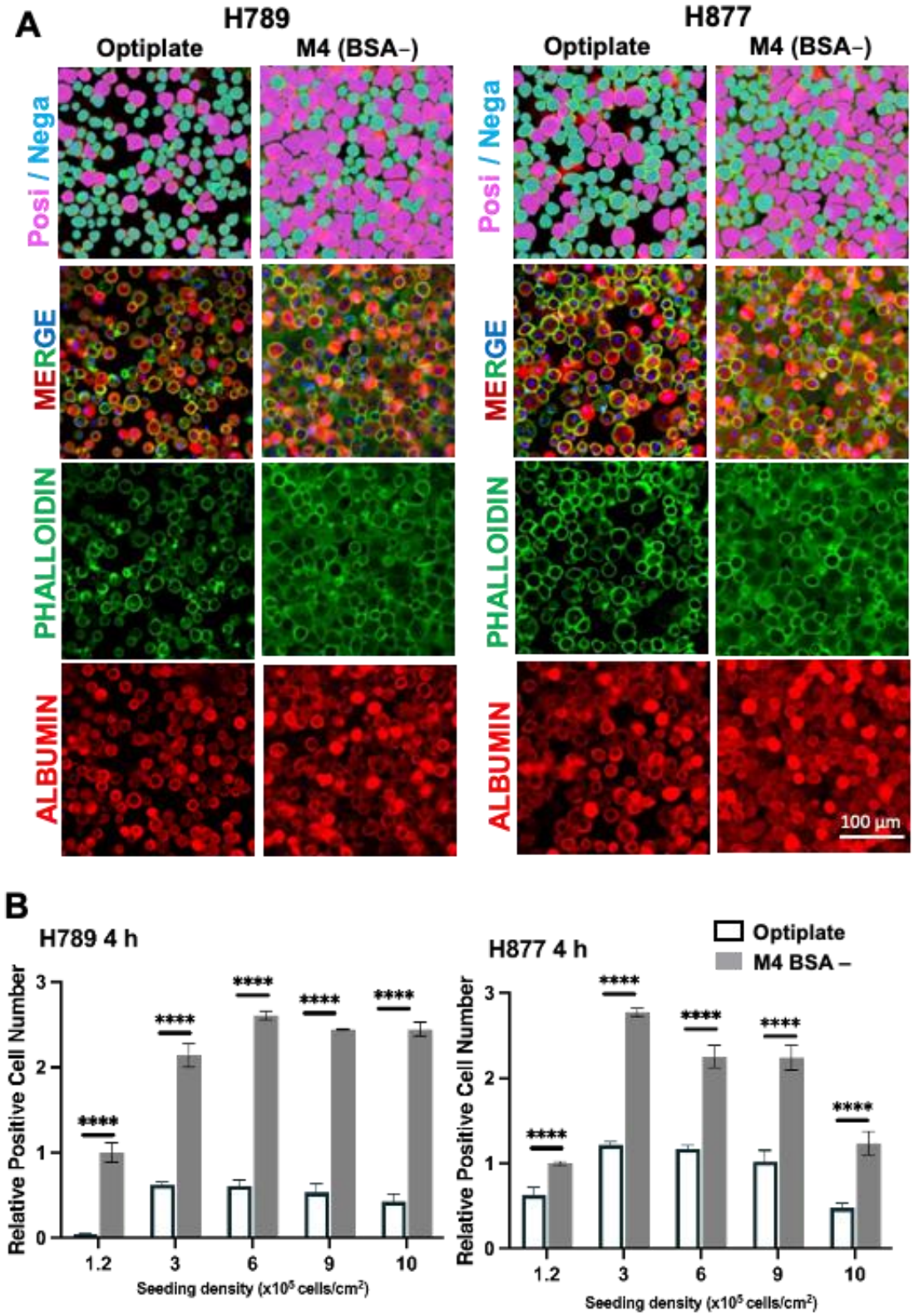

Figure 5 Seeding density effect on Early PHH attachment

A) PHH H789 and H877 in M4 and Optiplate, at 4 h post-plating of 6×10^5 cells/cm^2. The cells were classified as positive (magenta) and negative (cyan) based on the staining with phalloidin (green) albumin (red) and DAPI (blue). B) Quantification result of phalloidin staining images. Data are expressed as mean ± SD N=3. Differences are shown as ns $P > 0.05$, *$P \leq 0.05$, ** $P \leq 0.01$, *** $P \leq 0.001$, and **** $P \leq 0.0001$ analyzed with two-way ANOVA, Sidak's multiple comparisons test.

To confirm the effect of seeding density, we cultured two lots of suspension PHH (H789 and H877) in different seeding densities ranging from 0.4 $x10^5$ to $3.5x10^5$ cells/well in Optiplate (negative control) and our M4 BSA free (BSA–) medium. The cells were cultured for 4 h and subjected to immunostaining. Quantification results revealed that different lots of PHH possessed different attachment capabilities and optimal seeding densities. As observed in **Figure 5**, H877 generally demonstrated better cell adherence and spreading compared to H789. In general, cells seeded at $6x10^5$ cells/cm^2 showed the highest relative number of positive cells compared to the other seeding densities except for H877 4h (**Figure 5B**). H877 exhibited the highest positive cells at $3x10^5$ cells/cm^2. We also discovered that the cells cultured in our M4 BSA– medium showed a higher relative positive cell number than the Optiplate medium. Moreover, the cells plated in higher densities ($9x10^5$ cells/cm^2 and $10x10^5$ cells/cm^2) demonstrated reduced attached cell numbers in 4 hr and all medium treatment results. These findings confirmed that seeding density holds a substantial role in PHH attachment while proving that different lots of PHH possessed different optimal seeding densities.

3.4 IBMX and Forskolin Elimination Reduced PHH Attachment

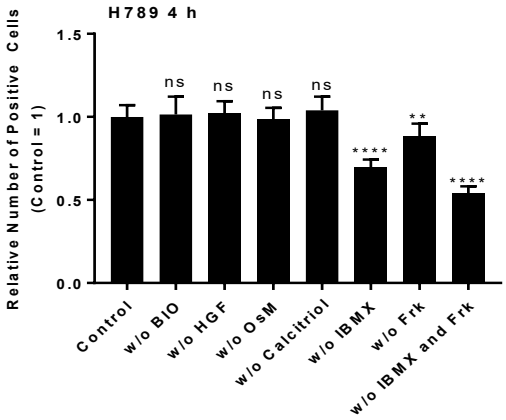

Abbreviation	Meaning
HGF	Hepatocyte Growth Factor
OsM	Oncostatin M
BIO	6-Bromoindirubin-3'-oxime
Calcitriol	Vitamin D3
Frk	Forskolin
IBMX	3-Isobutyl-1-methylxanthine

Figure 6 Quantification Result of PHH cultured in M4 with small molecule elimination

4 h quantification result of PHH in M4 with component elimination and the small molecule abbreviation table. Differences are shown as ns, P>0.05, *P ≤ 0.05, ** P ≤ 0.01, *** P ≤ 0.001, and **** P ≤ 0.0001 analyzed with one-way ANOVA, Dunnett's multiple comparisons test.

Preliminary results revealed M4 as the superior medium in improving PHH attachment. Further experiments were conducted to identify the specific composition of it that caused the positive effect (**Figure 6**). PHH was plated in the M4 medium by eliminating one of its supplements. In comparison to the control (complete M4 medium), the elimination of BIO, HGF (Hepatocyte Growth Factor), OsM (Oncostatin M), and Calcitriol did not show a significant difference in positive cell number. However, the elimination of either or both IBMX (3-isobutyl-1-methylxanthine) and Frk (Forskolin) significantly reduced the relative positive cell number. Elimination of IBMX or Frk elimination alone resulted in roughly 0.75 and 0.9 times reduction to control, respectively. While IBMX or Frk elimination significantly reduced PHH attachment, the elimination of both components from the M4 medium caused higher positive cell reduction of PHH attachment. Both IBMX and Frk were found to synergistically improve cAMP concentration within the cell.

3.5 General Inhibition of EPAC by ESI-09 (EPAC-Specific Inhibitor) Affected PHH Attachment

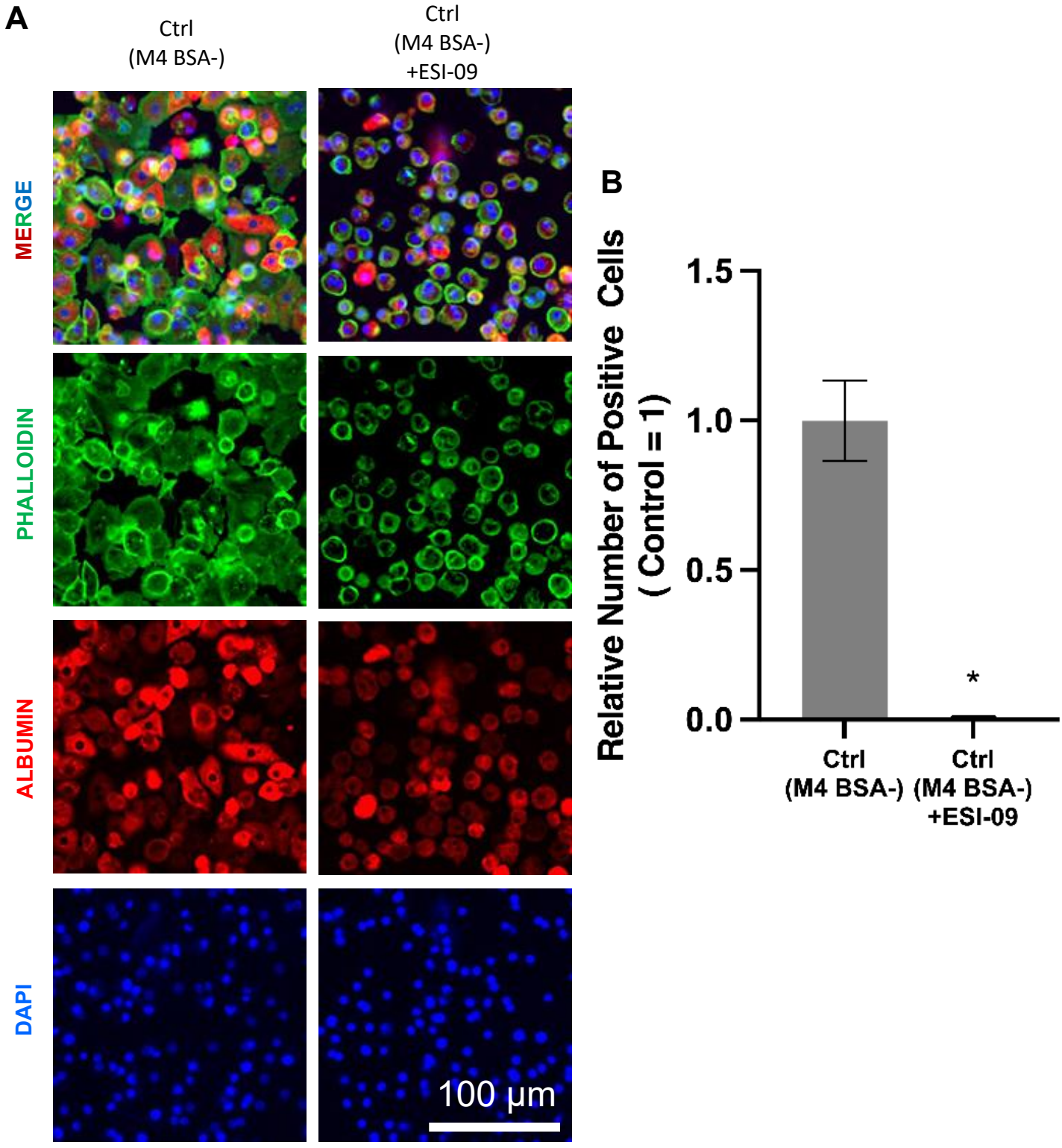

Figure 7 ESI-09 Addition reduced PHH attachment (4 h)

A) Phalloidin staining (green) of 24 h PHH H789 and in M4 BSA- (Control), and M4 BSA- +ESI-09 (6.25 μM). B) Quantification result of phalloidin staining images. ESI-09 Addition reduced PHH attachment (4 h)

As the elimination of cAMP activators IBMX and Frk was found to significantly reduce PHH attachment, an attempt to further elucidate cAMP involvement was performed by adding EPAC-specific inhibitor ESI-09. ESI-09 works by inhibiting all isoforms of EPAC (Zhu et al., 2015). The result in **Figure 7** revealed that the addition of ESI-09 reduced the number of positive PHH in comparison to the control (M4 BSA-), thereby confirming the involvement of EPAC in PHH attachment.

3.6 EPAC1 Activation did not affect PHH Attachment

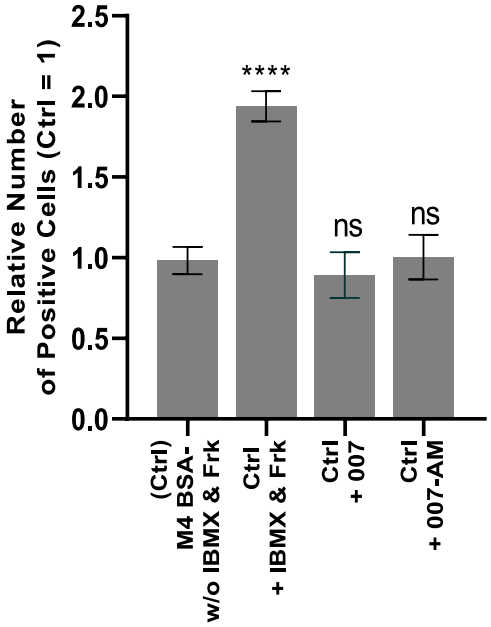

Figure 8 007, 007-AM addition effect on PHH 4 h

A) Phalloidin staining (green) of 24 h PHH H789 and in M4 BSA- (Control), M4 BSA- without IBMX and Forskolin, M4 BSA- w/ 007 or 007-AM B) Quantification result of phalloidin staining Differences are shown as ns, P>0.05, *P ≤ 0.05, ** P ≤ 0.01, *** P ≤ 0.001, and **** P ≤ 0.0001 analyzed with one-way ANOVA, Dunnett's multiple comparisons test.

Based on EPAC inhibition result with ESI-09, another experiment was performed to confirm EPAC1 involvement in PHH attachment by adding EPAC1 activators: 007 (8-pCPT-2′-O-Me-cAMP) and 007-AM (8-pCPT-2′-O-Me-cAMP-AM) (Luchowska-Stańska et al., 2019). PHH was plated in M4 medium w/o IBMX and Frk. Staining results revealed a non-significant difference between control and 007 or 007-AM treatment to M4 BSA- w/o IBMX

and Frk (**Figure 8**). This result was surprising due to the fact that the previous result of EPAC inhibition by ESI-09 showed a significant reduction of attachment PHH. Further literature study revealed that the liver demonstrated a preference of EPAC2C expression to EPAC1 and that EPAC2C is abundantly expressed compared to EPAC1 (Hoivik et al., 2013; Ueno et al., 2001a). This explains the data in **Result 3.5**.

3.7 cAMP Effector Activation Improved PHH Attachment

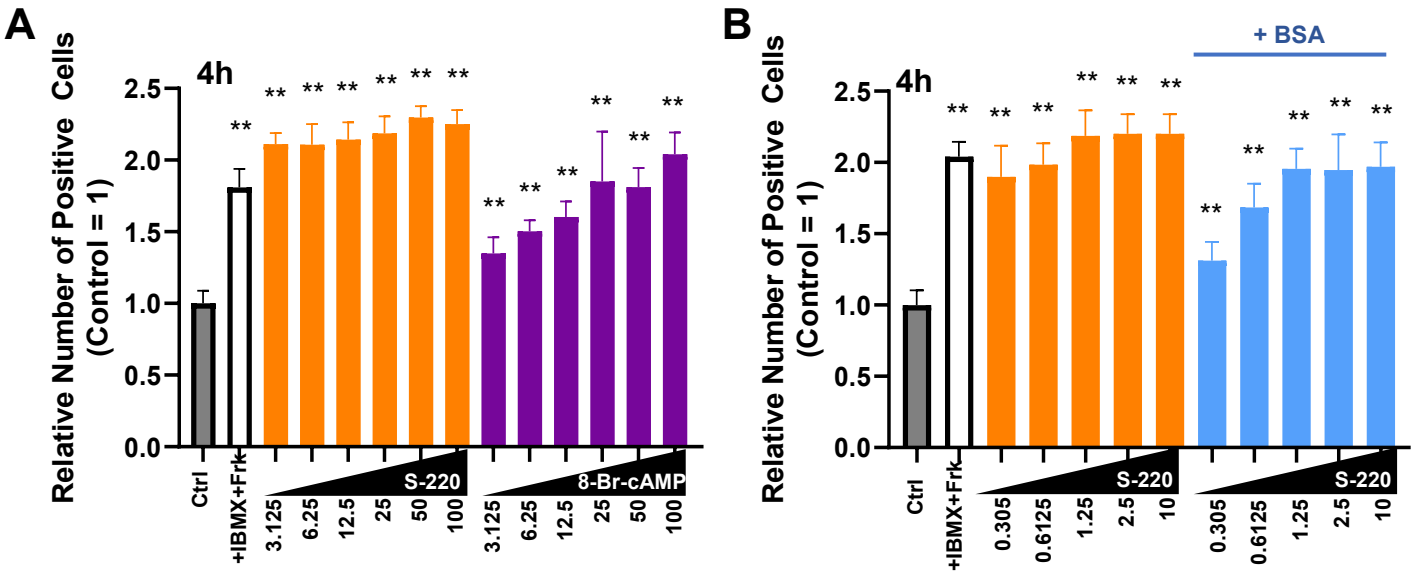

Figure 9 cAMP Activator Addition Effect on PHH Attachment

Quantification results of 4h PHH cultured in M4 BSA– w/ IBMX and Frk (white bar, Positive control), w/o IBMX and Frk (grey bars, Negative control B). S-220 (orange bars) or 8-Br-cAMP (purple bars) C). S-220 in M4 BSA- (orange bars), M4 BSA+ (blue bars). Data are expressed as mean ± SD, N=10 (A) and N=14 (B). Differences are shown as ** $P \leq 0.01$, *** $P \leq 0.001$, and **** $P \leq 0.0001$ analyzed with one-way ANOVA Dunnett's multiple comparisons test.

As implied in **Result 1**, the addition of EPAC1 activator did not affect PHH attachment. As found in the literature study, another experiment was conducted to confirm cAMP effector involvement in PHH attachment (**Figure 9**). This time, PHH was plated with EPAC2 or PKA activator (S-220, 8-Br-cAMP) with a concentration ranging from 3.125 to 100 µM. As predicted, the S-220 addition greatly improved PHH attachment (**Figure 9A**, red bars) and even showed a higher positive cell number than the positive control (white bar) even at the

lowest concentration (3.125 μM). Although the 8-Br-cAMP addition (blue bar) result showed an improvement of positive cell number to negative control (gray bar), the effect was not as potent as the S-220 treatment. These results suggested that activation of EPAC2 may hold a bigger role in the PHH attachment mechanism to PKA.

A further experiment was performed with an even lower concentration of S-220 ranging from (0.305 to 10 μM) with additional w/o BSA (**Figure 9B**, orange bars) and w/ BSA (**Figure 9B**, light-blue bars) treatments. The result revealed that even at the lowest concentration (0.305 μM), S-220 showed a higher positive cell number than the negative control (grey bar). In general, w/o BSA medium showed higher positive cell number in every concentration of S-220 compared to w/ BSA medium. These results further confirmed the involvement of EPAC2 activation PHH attachment.

3.8 Long-term culture of PHH in M4

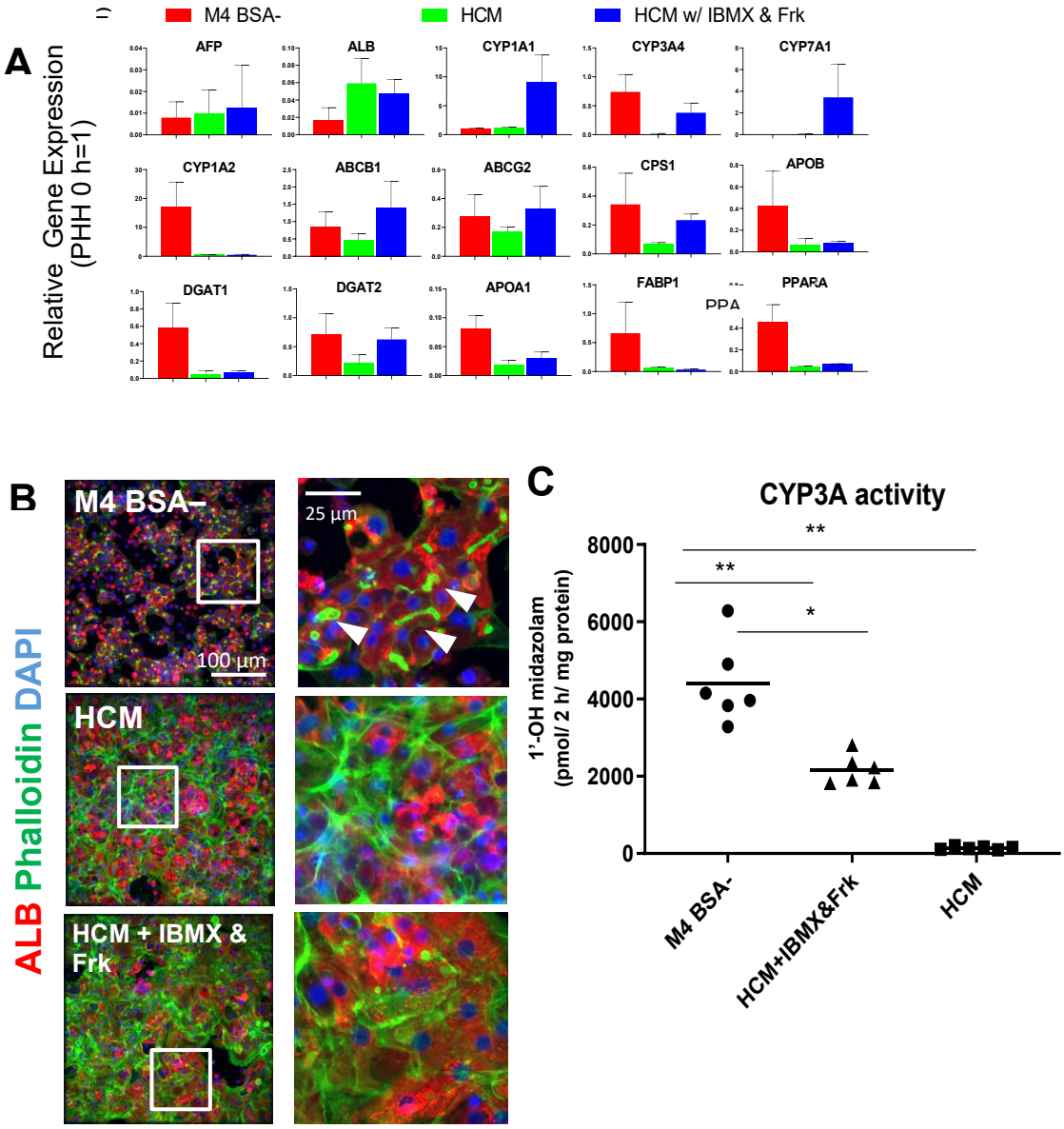

Figure 10 cAMP activators addition effect on Long-Term Culture

A) qPCR result of PHH day 7 cultured in M4 BSA– (red bars), HCM (green bars), and HCM w/ IBMX and Frk (blue bars). Data are expressed as mean ± SD N=3. B) Staining images of PHH day 7 cultured in M4 BSA–, HCM, and HCM w/ IBMX and FRK with anti-ALB antibody (red), phalloidin (green) and DAPI (blue). C) CYP3A4 activity of PHH measured by midazolam metabolite on day 7 after plating in M4 BSA-, HBM, and HBM w/ IBMX and Frk. Data are expressed as mean ± SD N=3. Differences are shown as ** $P \leq 0.01$ analyzed with one-way ANOVA Dunnett's multiple comparisons test.

Thus far, the observation was only performed on 4 h and 24 h time points. Further examination was performed to observe the effect of M4 BSA- medium on PHH. PHH was plated and maintained in three different media: M4 BSA-, HCM (Lonza), and HCM with IBMX and Frk addition for 7 days **(Figure 10**). The RT-PCR results revealed the reduction of mature hepatocytes in HCM treatment, such as *CYP3A4, CYP1A2, CPS1, FABP1*, etc., was observed (**Figure 10**). Interestingly IBMX and Frk addition to HCM resulted in a slight improvement in several but not all markers (**Figure 10A**, blue bars). Observation of PHH morphology after 7 days showed that the cells M4 BSA–revealed the morphology in which singular cells can still be distinguished and positive cells with phalloidin staining at the periphery (**Figure 10B**). However, cells cultured in HCM exhibited abundant actin stress fibers revealed by phalloidin staining. The addition of IBMX and Forskolin slightly improved the morphology by reducing the stress fiber formation and even shows formation of bile canaliculi structure (**Figure 10B**, left). CYP3A activity assay revealed that PHH cultured in M4 BSA– showed the best CYP3A activity, while those cultured in HCM showed the lowest CYP3A activity (**Figure 10C**). Interestingly, PHH cultured in HCM with the addition of IBMX and Forskolin showed improved CYP3A4 activity in comparison to the HCM medium alone.

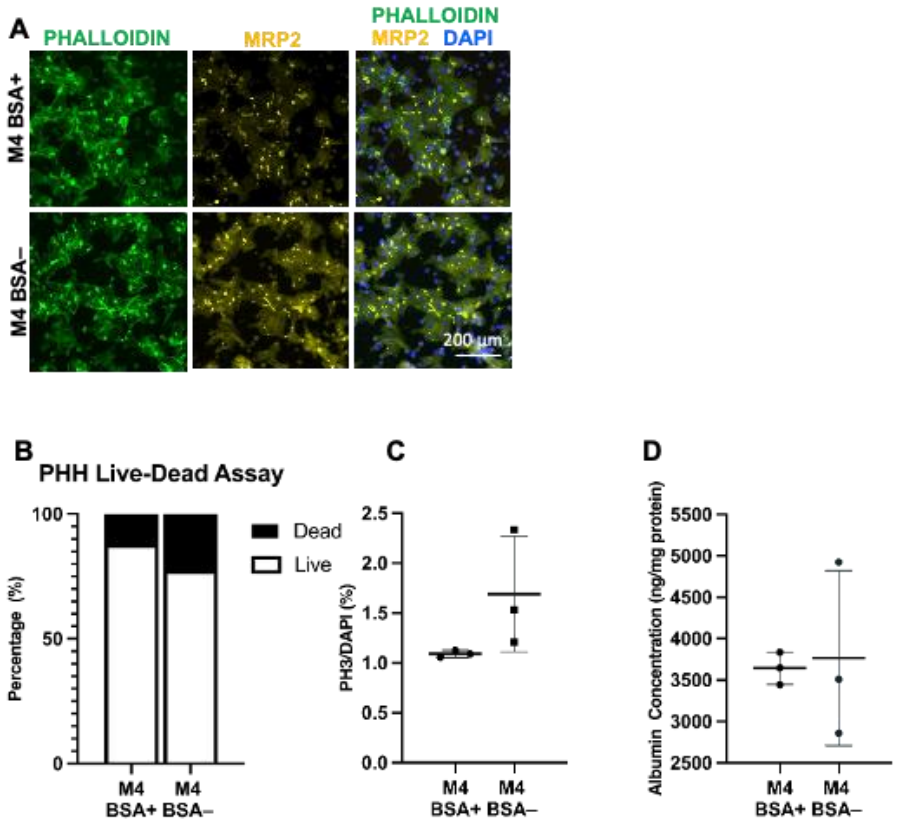

Figure 11 Long-term cultured PHH in M4 BSA+/–

A) Staining images of day 7 PHH cultured in M4 BSA+ and M4 BSA–, with Phalloidin (green), anti-MRP2 (yellow), and DAPI (blue). B) Live-dead assay of D7 PHH. C). PH3+ staining/DAPI for cell proliferation (n=3). D) Albumin secretion of D7 PHH (n=3) assayed by ELISA.

BSA is essential in maintaining medium osmolarity and growth factor delivery in a cell medium. Elimination of BSA is a concern that might affect the PHH function. Anther long-term experiment was performed to assess PHH functionality in M4 BSA- long-term culture (7 Days). The result in **Figure 11** shows that PHH cultured in either M4 BSA+ or BSA- condition showed bile canaliculi formation marked with the colocalization of MRP2 and phalloidin. However, Live-Dead assay on D7 PHH in M4 BSA- exhibited a higher percentage of dead cells. PH3 staining was also performed to quantify proliferative PHH. The result revealed that PHH in BSA- showed relatively higher variety between replicates. Furthermore, although not statistically significant, BSA removal from the M4 medium also affected the albumin secretion relatively compared to M4 BSA+.

The results further confirm that IBMX and Frk addition not only positively improved PHH early attachment but also prevented over-spreading and stress fiber formation in long-term culture while also improving CYP3A4 activity and hepatic gene expression. Furthermore, BSA removal from the medium might be beneficial for early PHH attachment but detrimental in long-term culture.

Section IV: Discussion

Optimization of PHH Culture Medium and Protocol

This research reported the novel use of iPS-derived hepatocyte medium (M4) for PHH culture (**Result 3.1**). Not only did it improve cell attachment, this medium also demonstrated the capability to maintain the prolonged culture of PHH (**Result 3.8**). Further investigation attempt in **Result 3.2** revealed that a lower BSA concentration version of this medium enhanced PHH attachment. Past studies have reported the inhibitory effect of BSA on cell attachment (Han et al., 2008; Kan et al., 1982; Y. L. Kim et al., 2006). Rubin and colleagues proposed that BSA hinders interactions between cell attachment receptors such as integrin with the binding site of the cell matrix (Rubin et al., 1981); thereby preventing the establishment of a focal adhesion complex which discouraged cell spreading (Cavalcanti-Adam et al., 2007).

Protocol optimization was performed by testing optimal seeding density for suspension PHH (**Result 3.3**). The results revealed lot-to-lot differences between optimal seeding density with H789 at 600,000 cells/cm^2 and H877 at 300,000 cells/cm^2 (96-well plate) for cell attachment. Furthermor e, instead of enhancing PHH attachment, plating the cells with a density higher than the optimal number reduced cell attachment or anoikis. In adherent cell culture, cell-cell and cell-matrix contacts are required to maintain differentiated cell behavior (Hacking & Khademhosseini, 2013). Past studies have explained the importance of the right seeding density in hepatocyte plating protocols and also reported the same phenomenon (Swift & Brouwer, 2010). The loss of cell-cell connections is attributed to the loss of differentiated properties or even associated with the cancer cell EMS (Epithelial to Mesenchymal) transition phenomenon (Choi & Diehl, 2009). Hepatocyte itself critically requires cell-cell contact to function and survive. It creates bile canaliculi with neighboring cells as the secretory channel for the bile (Belicova et al., 2021). Seeding density is important in maintaining hepatocyte differentiation state as the right seeding density encourages cell-cell contact, and therefore

allowing bile secretory functions like *in-vivo* hepatocytes (Belicova et al., 2021; Swift & Brouwer, 2010). Lower seeding density was found to encourage hepatocyte dedifferentiation, while optimal seeding density allows the maintenance of its differentiated state and functions (Machide et al., 2006; Mesnil et al., 1987).

Another investigation attempt was performed in **Result 3.4** to identify components in the M4 medium responsible for enhanced PHH attachment. The results revealed that the elimination of either one or both IBMX and Forskolin from the medium resulted in a significant reduction of PHH attachment. IBMX and forskolin work synergistically by improving cAMP intracellular concentration. IBMX inhibits phosphodiesterase (PDE), the enzyme responsible for cAMP degradation (Huai et al., 2004). Forskolin works by activating Adenylyl Cyclase (AC), which synthetizes cAMP (Seamon et al., 1981).

cAMP Involvement in PHH Attachment

In this research, the presence of IBMX and Forskolin in the medium plays a role in enhancing PHH to collagen matrix attachment (**Result 3.4**). As previously stated in the previous discussion, IBMX and Forskolin synergistically improve intracellular cAMP concentration, thereby named cAMP activators. cAMP is the second messenger that relays extracellular signals, orchestrating various signaling pathways in cell function (Yan et al., 2016). The cAMP signaling pathway started by activation of its main effectors, PKA and EPAC. PKA works by phosphorylating downstream proteins that predominantly regulate cell metabolism (London et al., 2020; Sassone-Corsi, 2012; Yan et al., 2016). On the other hand, EPAC works by activating the Rap proteins, which, in turn, activate other genes related to structure-related properties such as cell motility, cell junctions, and cell attachment (Borland et al., 2009; Bos et al., 2003; Gloerich et al., 2010; Rangarajan et al., 2003).

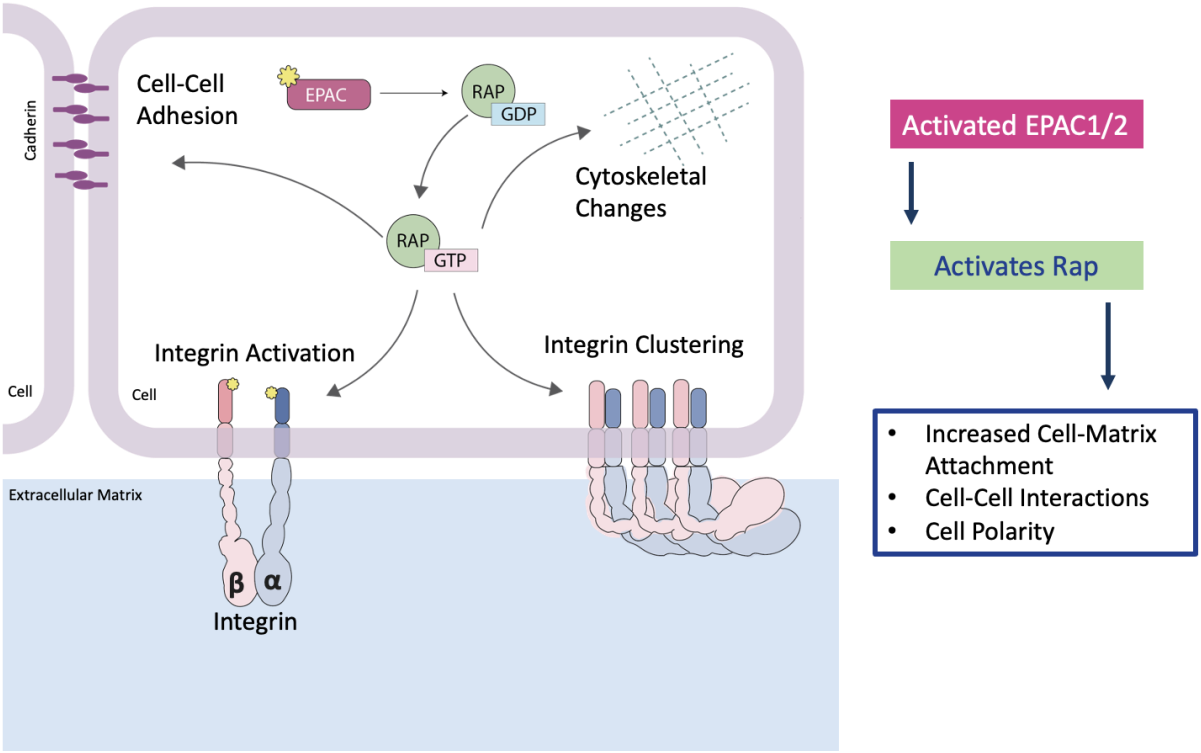

Figure 12 A schematic representation of the involvement of Epac in the integrin-mediated cell adhesion adapted from (Bos et al., 2003; Kinbara et al., 2003; Zhang et al., 2017)

Attempts to further confirm cAMP involvement in PHH attachment were performed by adding PKA or EPAC activators or inhibitors to the PHH medium (**Table 2**). In **Result 3.5**, the addition of general EPAC Inhibitor (ESI-09) into M4 BSA- reduced PHH attachment, confirming the cAMP-EPAC pathway involvement in PHH attachment. Based on these results, it was expected that EPAC1 activators' addition into M4 BSA- medium without (w/o) IBMX and Forskolin was expected to improve PHH attachment. However, in **Result 3.6**, EPAC1 activators (007 or 007-AM) addition did not pose any significant effect on cell attachment. Lezoualc'H and colleagues have summarized past studies regarding the EPAC isoforms and their organ-specific expression (Lezoualc'H et al., 2016). It was revealed that EPAC possessed a liver-specific isoform called EPAC2C, whose functions are still largely unknown (Sugawara et al., 2016; Ueno et al., 2001b).

Based on the previous literature, another experiment was performed to confirm not only cAMP-EPAC but also cAMP-PKA involvement in PHH attachment. In **Result 3.7A**, EPAC2

activator (S-220) or PKA activator (8-Br-cAMP) was added to M4 BSA- medium w/o IBMX and Forskolin. The results revealed that EPAC2 activation by S-220 in the lowest concentration (3.125 μM) resulted in a higher amount of positive (attached) cells compared to the positive control or PKA activator (8-Br-cAMP).

Because PHH in the lowest S-220 concentration demonstrated superior enhancement of PHH attachment, a further experiment was performed to investigate the effect of even lower concentrations of S-220 and BSA addition on PHH attachment (**Result 3.7A**). Again, it was confirmed that even the lowest S-220 concentration (0.305 μM) in M4 without BSA showed a positive cell number close to the positive control. These results confirmed the dominancy of EPAC2 in regulating PHH cell attachment as opposed to the mainstream literature that lean towards EPAC1 activation in other cell attachment (Bos et al., 2003; Gloerich et al., 2010; Rangarajan et al., 2003).

Although this research has briefly confirmed the cAMP-EPAC2 role in PHH attachment, the further mechanism is still unknown. Past studies have investigated the relationship between integrin and EPAC activation (Bos et al., 2003; Rangarajan et al., 2003). Menter and colleagues have elaborated on the inside-out and outside-in integrin regulation mechanisms (Menter & Dubois, 2012). In the inside-out mechanism, Integrin was reportedly regulated by Rap, which is part of the cAMP-EPAC-Rap pathway (**Figure 12**). Because of the minuscule amount of literature that investigated EPAC2's role in cell attachment, the result is relatively novel. Hence, further elucidation is required to confirm the overall signaling mechanism of cAMP-EPAC2 in cell attachment.

In relation to **Result 3.7B**, BSA was confirmed as GDI (Guanine Nucleotide Dissociation Inhibitor), which inhibits G-Protein Subunit $G\alpha_s$ from activating AC (Adenylyl Cyclase, the protein responsible for cAMP production. As a result, BSA addition reduced the intracellular concentration of cAMP (Du & Patel, 2003). Integrin $\alpha_v\beta_1$ and $\alpha_1\beta_1$ were known

as the main adhesion receptors of PHH (Pinkse et al., 2004; Richter et al., 2011). It was reported that BSA hinders the binding process between integrin and RGD sites on anchor protein found in ECM, thus reducing cell attachment and discouraging flattened cell morphology (Blaauboer & Paine, 1979; Gjessing & Seglen, 1980a; Ruoslahti, 1996).

Based on the composition of M4 used in **Supplementary Table 2**, other chemicals in M4 may also contribute to PHH attachment. In the outside-in integrin regulation mechanism, there are studies that also focused on the crosstalk between integrin and HGF (Hepatocyte Growth Factor) Receptor (C-Met) in cell attachment mechanism (Gkretsi et al., 2008). A more comprehensive study by Beviglia and colleagues further elucidated HGF involvement in integrin-mediated cell adhesion through Focal Adhesion Kinase (FAK) activation (Beviglia & Kramer, 1999). In this research, cAMP may bypass the signal transduction required from HGF or integrin, which directly activates the downstream target, thereby increasing the cell attachment in a more efficient manner. However, further investigation needs to be performed to confirm this notion.

Long-Term Culture of PHH in M4 BSA- Medium

In **Result 3.8**, long-term culture of PHH in M4 BSA- medium maintained PHH genetic profile and CYP3 activity and inhibited stress fiber formation compared to the cells cultured in HCM commercial medium. Furthermore, the addition of IBMX and Forskolin to the HCM medium attenuated the detrimental long-term culture effects on PHH. In relation to cAMP activation by IBMX and Forskolin, previous studies have reported that cAMP intracellular increase resulted in arrays of positive effects such as aiding in cell differentiation, cell functions, attenuating cell apoptosis and many more (Kabeya et al., 2018; Y. Wang et al., 2006; Yan et al., 2016). Further explanation regarding the stress fiber formation observed in PHH in HCM may be due to the addition of EGF, which was previously reported to enhance stress fiber formation (Ojaniemi & Vuori, 1997)

Chapter III: Unraveling WFS1 Selective Degradation

Section I: Literature Studies and Background

Literature Studies

Wolfram Syndrome and WFS1

Wolfram Syndrome (WS) is a severe recessive autosomal disease whose symptoms include late-onset diabetes mellitus and neurodegeneration. WS was first discovered by Wolfram and Wagener in 1983 (Urano, 2016). This disease affects a complex array of systems known as DIDMOAD (Diabetes Insipidus, Diabetes Mellitus, Optic Atrophy, and Deafness) (Matsunaga et al., 2014). This syndrome is mainly caused by mutations of *WFS1* (Wolfram syndrome gene-1), which encodes the WFS1 protein. Approximately 1 in 770,000 of the general population is subject to this disease. This categorizes WS as a rare prevalence. The general symptoms of WS primarily appear in childhood and juvenile, starting with late-onset diabetes mellitus, which progressively escalates to hearing loss and neurological disorders (E. M. Lee et al., 2023).

The etiology of WS is tightly linked to ER (Endoplasmic Reticulum) stress and intracellular homeostasis (Fonseca et al., 2010). Impairment of WFS1 leads to calcium homeostasis disruption, escalates ER stress, and, ultimately, apoptosis (Pallotta et al., 2019). WS is often undiagnosed, and a curative therapy has yet to be discovered. This

WFS1: Structure, Function, Localization, and Known Functions

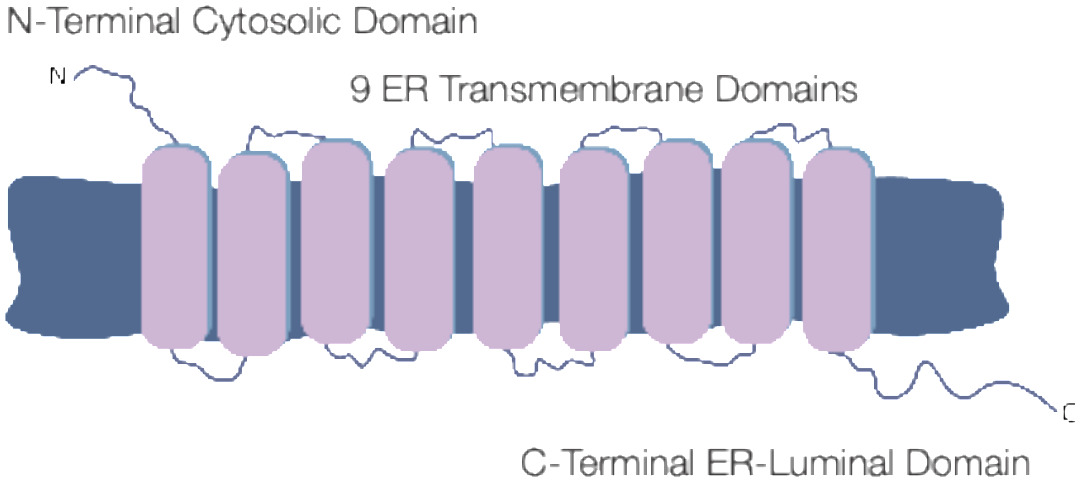

Figure 13 WFS1 Structure

The *WFS1* gene, known as *wolframin*, is a gene that is solely responsible for Wolfram Syndrome disease. This protein consists of 890 amino acids and is a transmembrane protein predominantly localized into the ER (Endoplasmic Reticulum) membrane. The protein consists of three domains: the N-cytosolic domain, the transmembrane domain, and the C-terminal domain that faces the ER lumen (**Figure 13**). Attempts to elucidate each of the WFS1 domains have been made and revealed that the N-terminal cytosolic domain of WFS1 is responsible for proinsulin trafficking to the Golgi (L. Wang et al., 2021). Furthermore, the transmembrane domain is required for ER-membrane localization and stability (Lim et al., 2023), while the C-terminal domain is recognized by cargo proteins such as proinsulin, playing a role in its transport mechanism (L. Wang et al., 2021).

WFS1 was first reported to be mainly involved in calcium homeostasis (Fonseca et al., 2010; Ishihara et al., 2004; Ueda et al., 2005), ER stress response (Ueda et al., 2005), and proinsulin folding (L. Wang et al., 2021). Furthermore, it is hypothesized to be involved in a multitude of intracellular processes, and yet, its endogenous function is still left to be discovered. In these past 20 years, studies of WFS1 mainly focused on elucidating its mutant variants, localization, architecture, calcium signaling, and its role in ER-stress regulation.

Fonseca and colleagues have identified WFS1 as a key player in ER stress and ER's UPR (Unfolded Protein Response) regulation (Fonseca et al., 2010). On the onset of ER stress, ATF6 localizes into the Golgi body to be cleaved. Cleaved ATF6 localizes into the nucleus to aid the transcriptions of genes required in ER-stress response. Overexpression of these genes will pose a great burden for cells, which might lead to apoptosis. WFS1 mitigates ER stress response by interacting with ATF6 (Activating Transcription Factor-6), attenuating UPR while handling ER-stress response which prevents apoptosis (Fonseca et al., 2010). WFS1 acts as an ATF6 stabilizer, preventing it from undergoing proteolytic cleavage in tandem with HRD1, thereby attenuating ER-Stress response back to homeostasis (Fonseca et al., 2010).

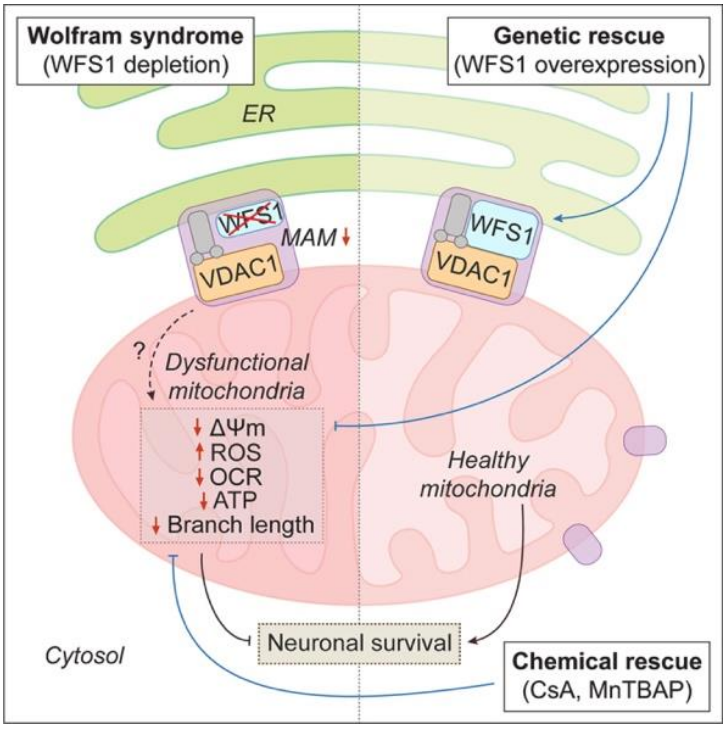

Figure 14 WFS1 Role in MAM Interactions (Zatyka et al., 2023).

In recent years, the focus of studies has shifted towards the role of WFS1 in cell metabolism involving MAM (Mitochondria-Associated Membrane) and protein trafficking, specifically proinsulin processing. WFS1 has been reported to localize into the ER-mitochondria contact site, MAM (Mitochondria-Associated Membrane) (Zatyka et al., 2023). It is found to interact with VDAC1 (Voltage-Dependent Anion Channel-1). VDAC1 itself acts as a regulator of

metabolism and calcium homeostasis in mitochondria and is implied to facilitate the transfer of calcium from ER to mitochondria. WFS1 regulates this transfer by ensuring the regulation of calcium channels such as IP3R (Inositol 1,4,5-trisphosphate receptors) that directly transfer calcium from ER to mitochondria. The disruption of WFS1-VDAC1 interaction might lead to mitochondrial malfunction and the release of apoptotic factors such as Cytochrome C and metabolism dysfunction (**Figure 14**) (Zatyka et al., 2023).

Protein Degradation Pathways: Proteasome, Autophagy, and Beyond

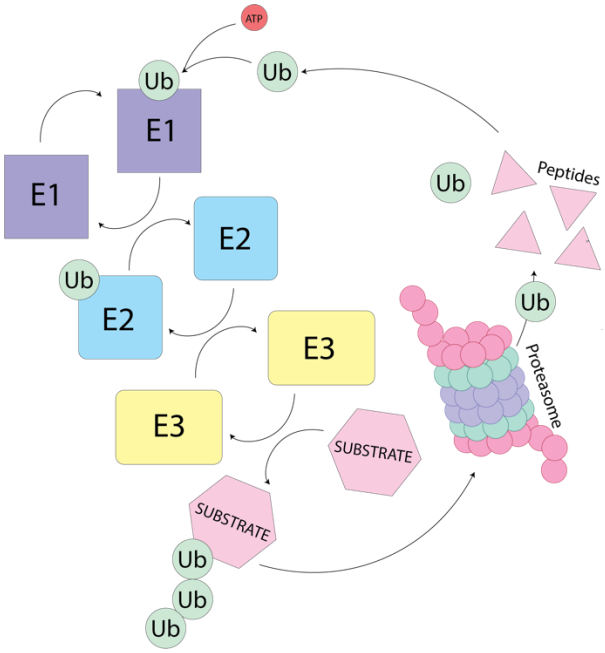

Figure 15 Illustration of Ubiquitin-Proteasome Degradation

The maintenance of cellular homeostasis is supported by solid protein degradation systems. In mammalian cells, the protein degradation pathway is primarily divided into ubiquitin-proteasomal degradation and autophagy. Independent from the primary pathways, EV (Extracellular Vesicle)-based protein degradation has also been reported (Van Niel et al., 2018).

The ubiquitin-proteasomal degradation occurs in the cytoplasm and primarily targets short-lived and misfolded proteins. Target proteins undergo enzymatic processes, including E1 activating enzymes, E2 conjugating enzymes, and E3 ubiquitin ligase (**Figure 15**) (Zhao et al., 2022). The ubiquitinated proteins are then identified and degraded by the 26s proteasome. This

process requires hydrolysis of ATP due to the energy necessary to unfold the protein (Smith et al., 2005).

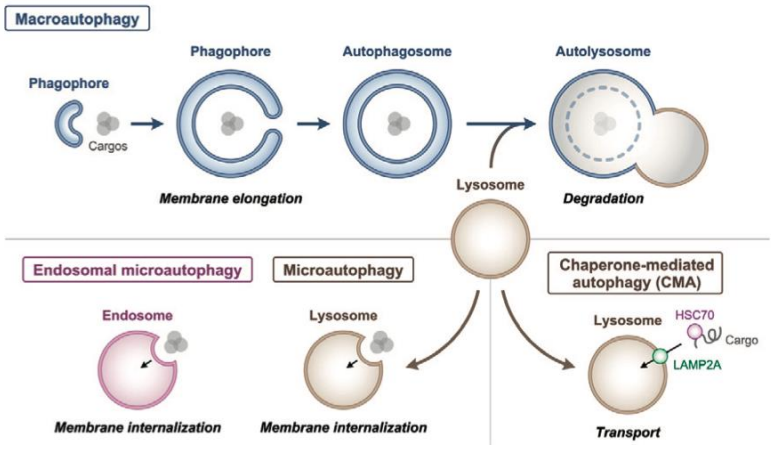

Figure *16* Autophagy mechanism (Yamamoto & Matsui, 2024)

Autophagy, on the other hand, is a mechanism reserved to target long-lived target proteins, protein aggregates, and damaged organelles. The mechanism involves the formation of an autophagosome, which will then engulf the damaged organelle or aggregated protein and finally be subjected to lysosome fusion for degradation (Abounit et al., 2012). Autophagy is generally divided into three types: macroautophagy, microautophagy, and Chaperone-Mediated Autophagy (CMA) (**Figure 16**) (Yamamoto & Matsui, 2024). Macroautophagy is mainly involved in the degradation of cytoplasmic materials into autophagosomes, and elongation of the autophagosome membrane. The closed autophagosome is then fused with the lysosome to sequester the cytoplasmic cargo. Microautophagy involves the direct internalization of the target protein into the lysosome. CMA starts with the tagging of a target protein that possesses a KFREQ-like motif by Hsc70 (Heat shock cognate 70) chaperone. This tagged protein will be recruited by LAMP2A protein for lysosomal degradation (Yamamoto & Matsui, 2024). Recent studies have discovered further variations of autophagy, such as ER-phagy, mitophagy, aggrephagy, and other autophagy mechanisms (Fleming et al., 2022).

Recent studies have reported the crosstalk between Proteasomal degradation and autophagy (Yu & Hua, 2023). Shrestha and colleagues have also investigated the synergistic role of ERAD (ER-Associated Degradation), which involves the ubiquitin-proteasome system and ER-phagy in the β-cell (Shrestha, Liu, et al., 2020). These studies show that protein degradation is a complex intertwined process that involves myriads of other factors and components within mammalian cells.

Known Mechanisms of WFS1 Regulation and Degradation

The currently known mechanism for WFS1 degradation is the ER-associated degradation (ERAD) pathway involving E3 ubiquitin ligase HRD1 as the key regulator. WFS1 was proven to interact with HRD1, facilitating its ubiquitination and degradation by proteasome (Fonseca et al., 2010). Other studies have also identified another E3 ubiquitin ligase, SMURF1 as a regulator of WFS1 degradation (Guo et al., 2011).

Proximity Labeling in the Studies of Protein-Protein Interaction

Past studies about protein-protein interactions mainly rely on co-immunoprecipitation and yeast two-hybrid screens. However, these assays often fail to capture transient and weak interactions, which might be crucial in elucidating protein-protein interaction networks. In 2012, a revolutionary study developed BioID, the early predecessor of proximity labeling. ~~protein~~ BioID was developed from E. *coli* BirA through directed mutation (Roux et al., 2012). BioID showed a promising means of proximity labeling; however, the exposure time needed for biotin treatment was deemed as too long (roughly 18 hours) (Roux et al., 2012). The enhanced version of BioID, BioID2, was developed from *Aquifex aeoliqus* and showed a promising increase in the labeling duration required (D. I. Kim et al., 2016).

Following the discovery of BioID variants, other proximity labeling, such as APEX and APEX2 (Ascorbate Peroxidase), was developed. These enzymes were derived from pea (*Pisum sativum*) and utilized another substrate, biotin-phenol (Hung et al., 2016). As years went by, other directed-mutation variants of BirA were further developed with enhanced biotinylation speed, lower toxicity, and higher specificity, which is widely known as TurboID (Branon et al., 2018). TurboID allows biotinylating time in only 10-15 minutes. Multiple other variants, such as AirID, which promises more specific labeling, and PhoxID, which promises non-protein proximity labeling, have been steadily developed (Kido et al., 2020; Takato et al., 2024).

Despite the tremendous development over the years, proximity labeling still has several limitations to overcome. First, as proximity labeling can label the interacting protein within 10-

20 nm radius, non-specific labeling might occur, thus hindering data interpretation. To overcome this limitation, robust controls followed by proper data analysis and interpretation. These factors are crucial to capture the correct protein-protein interaction landscape. Second, most of the proximity labeling methods developed to date mainly rely on protein fusion, which may affect native protein interaction. The recent development of PhoxID seemed to overcome this matter. However, as PhoxID is still limited to proteins with receptor functions, further development might be required for it to be indiscriminately used for various proteins (Takato et al., 2024).

Background

WFS1 C-terminal Mutant Selective Degradation in Two Different Cell Lines

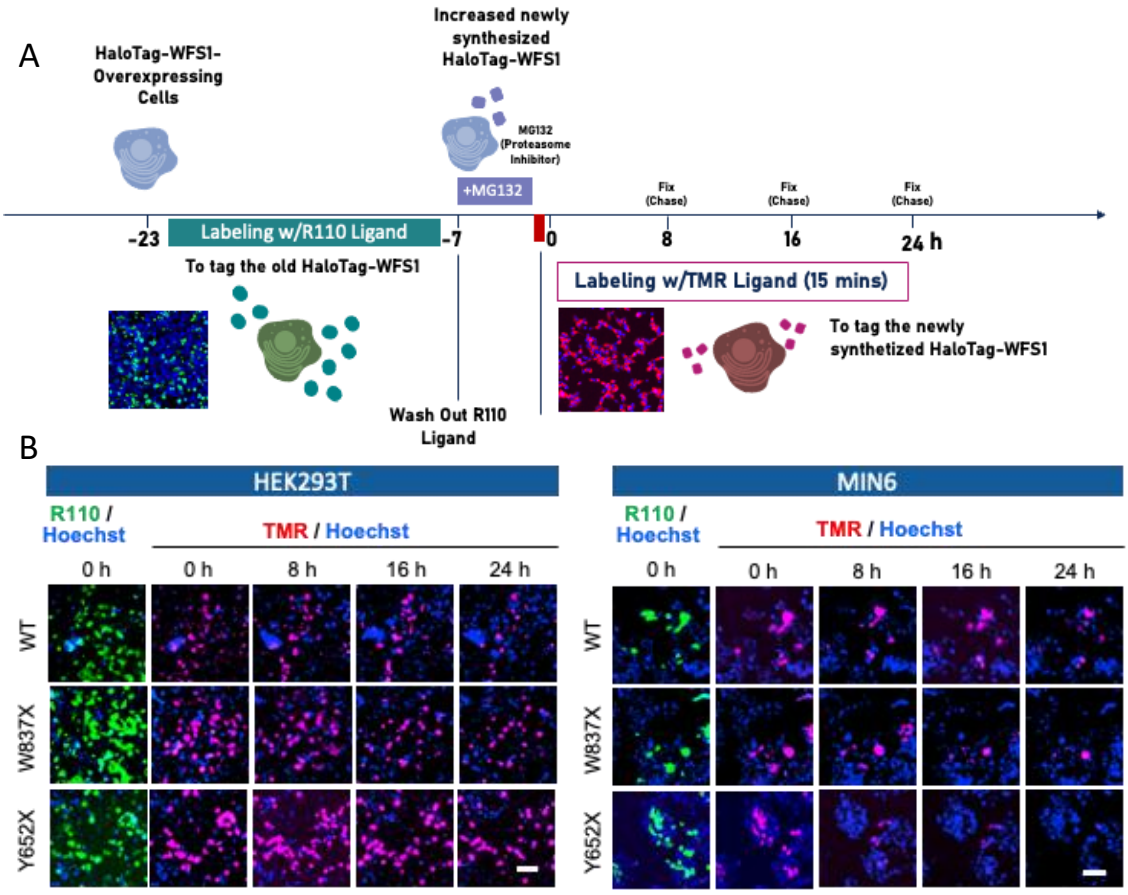

Figure 17 WFS1 Selective Degradation in HEK293T VS MIN6 (Tokuma et al., 2023)

A. Schematic illustration of HaloTag-based pulse-chase assay B. the pulse-chase result of previous study about hWFS1 Selective Degradation in two different cell lines: HEK293T vs MIN6. Scale bar = 50 μm

Matsunaga and colleagues have previously categorized c-terminally truncated WFS1 mutants W837X and Y652X as Group 1 in terms of WS manifestation (Matsunaga et al., 2014). The patients with these mutations exhibited earlier onset of diabetes mellitus compared to other groups at an average age of 4.4±1.9 years and optic atrophy at an average age of 9.6±6.9 years (Matsunaga et al., 2014). These Group 1 mutations are labeled as severe as compared to Group 2 and Group 3 WFS1 mutations.

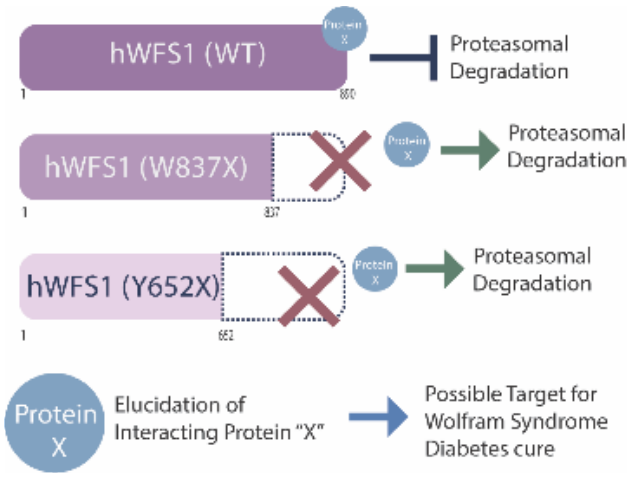

Figure 18 Elucidation of WFS1`s Selective Degradation in MIN6

We previously highlighted the effect of human WFS1 C-terminal truncated mutations W837X and Y652X to on WFS1 protein stability in two different cell lines: MIN6 and HEK293T (**Figure 17**) (Tokuma et al., 2023). We performed HaloTag-based pulse-chase assay in WFS1 WT (Wild Type), W837X mutant, and Y652X in two different cell lines: MIN6 (Mouse Insulinoma) and HEK293T (Kidney Embryonic) cell lines. WFS1 mutants exhibited a faster degradation rate in MIN6 than HEK293T. The study implicates possible beta-cell-specific regulation and degradation mechanisms for the C-terminally truncated WFS1. Elucidation of this mechanism might lead to the discovery of a possible diabetes cure specific to WS (**Figure 18**).

Objective and Scope

Objective

The primary objective of this dissertation is to investigate the mechanism of WFS1 mutant degradation in the MIN6 cell line through the identification of interacting protein candidates with the proximity labeling method TurboID.

Scopes

This dissertation explores WFS1 degradation based on the following scopes

1. **Evaluation of interacting protein candidates with TurboID**

   Data exploration of identified interacting protein candidates from LC-MS/MS results.

2. **WFS1 degradation pathway investigation**

   Identifying the molecular pathways involved, such as proteasomal or autophagy degradation, responsible for WFS1 turnover.

3. **Functional implications**

   Exploring the impact of candidate gene knockdown on WFS1 mutant stability in MIN6.

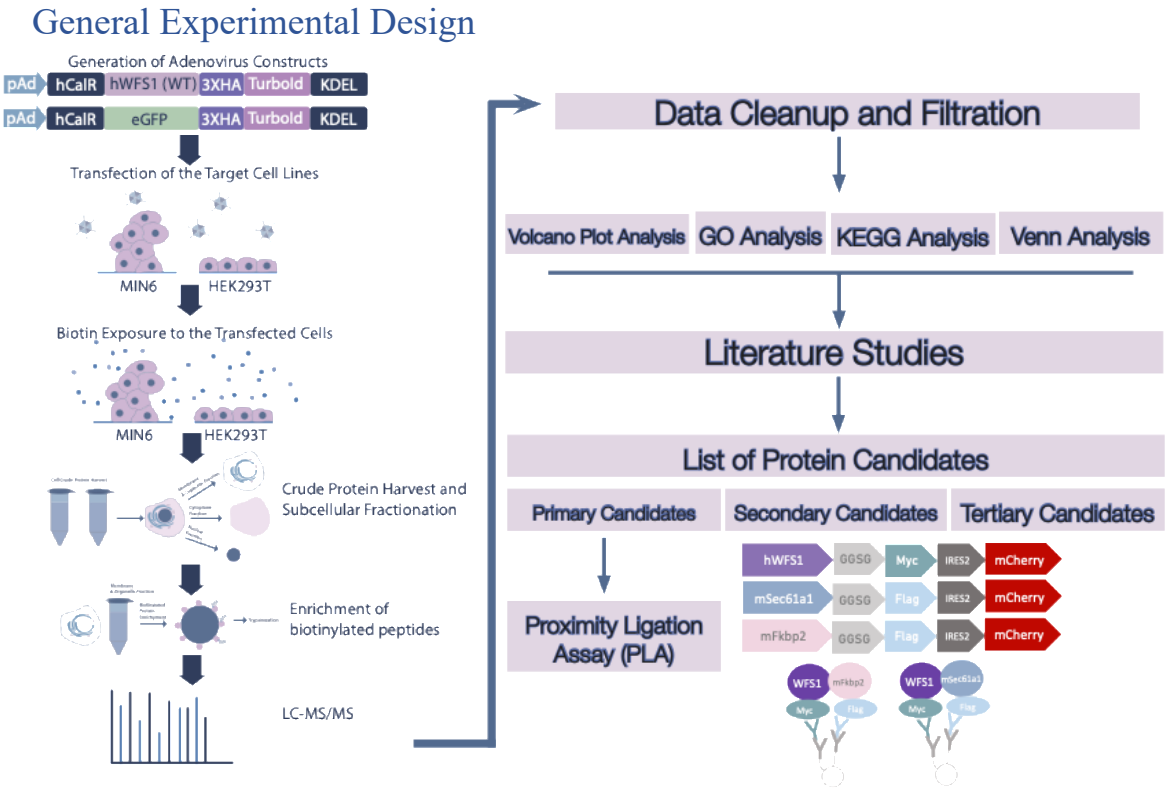

Figure 19 Experimental Design

A. Adenovirus Constructs Used in This Study: The C-terminal of the protein was tagged with a 3xHA tag along with the TurboID sequence. The expression cassette was positioned between the ER-colocalization sequence (hCalR) and KDEL. B. Schematic Illustration of the TurboID Mechanism: The TurboID protein promiscuously biotinylates proteins in close proximity, tagging them for further downstream workflows.C. Schematic Illustration of Experimental Methods: Adenovirus constructs were generated using the Gateway Cloning System. The resulting adenovirus crude stocks were transfected into both MIN6 and HEK293T cells and incubated for 2 days. The transfected cells were then exposed to 50 μM biotin for 30 minutes to enable biotinylation by TurboID. Subsequently, the cells underwent crude protein extraction and subcellular fractionation. The organelle fraction was subjected to trypsin digestion, and biotinylated proteins were enriched, eluted, and analyzed with LC-MS/MS. D. Acquired LC-MS/MS peptide motifs were analyzed and filtered to generate protein candidates for further analysis. Proximity Ligation Assay (PLA) was performed to confirm the interactions between WFS1 and primary candidates.

The general experimental design refers to the **Figure 19**. Experiment was begun by constructing the required adenovirus overexpression vectors with the Gateway Cloning system (Thermofisher, A10462, V49320). The expression cassette consisted of N-terminal hCalR and C-terminal KDEL sequence for ER localization (Miki et al., 2016). Following the hCalR sequence, tested gene such as WFS1 (WT) or eGFP (enhanced Green Fluorescent Protein) was

added, followed by 3X HA (Hemaglutinin tag) and TurboID (Cho et al., 2020). The resulting adenovirus vector was lipofected into HEK293A for Adenovirus production. From here, the crude virus extract was used to transiently transfect confluent MIN6. After transfection, MIN6 cells were incubated for 2 days and subjected to 50 μM for 30 minutes. The harvested crude protein was then processed with a subcellular fractionation kit (GLScience, 7510-11400) to isolate membrane-organelle fraction. The membrane-organelle fraction was subjected to biotinylated protein enrichment with avidin beads and trypsinization. The eluted fraction was then subjected to LC-MS/MS analysis.

Cell Lines

Cell Lines

MIN6 Cells

MIN6 cells were acquired from J. Miyazaki form Osaka University (Miyazaki et al., 1990). MIN6 cells used in this dissertation are all under the passage number of 25. The cells were routinely maintained in 10 cm dish (Corning, 430167) coated with 0.1% gelatin and maintained in EB (Embryoid Body) medium (**Supplementary Table** *7*). MIN6 cells were maintained in a cell incubator at 37°C, 90-95% humidity, and 5% CO_2. As MIN6 cells divide relatively slowly compared to HEK293-derived cells, medium change can be performed once every 3-4 days. $1x10^6$ cells will approximately reach confluence in 2 weeks. Careful planning is required for the experiment. Attention must be paid to their morphology. MIN6 cells formed pseudo islets, therefore, should form small colonies that grow on top of each other. If the cells seem to show flattened and wide morphology, it is better to use fresh stock.

At 80% confluence, the cells must be passaged. At the time of passage, confluent MIN6 cells in 10 cm dishes were washed in 10 mL D-PBS (-) (Nacalai, 14249-95). After wash, the cells were subjected to 1 mL 0.25% Trypsin (Gibco, 25200056) treatment for 5 minutes and then neutralized with 4 mL of EB medium. The cell suspension was subjected to Trypan Blue exclusion by sampling 10 μL of to be mixed with 10 μL Trypan Blue (Gibco, 15250061). The

mix was then added into the counting chamber for automated counting (Invitrogen, AMQAX2000). The cells were homogenized with a disposable pasteur pipette and centrifuged at 1000 rpm, 25°C, for 5 minutes. The supernatant was discarded and the pellet was resuspended with fresh, pre-warmed EB medium to be seeded in a gelatin-coated 10 cm dish or other culture format. Depending on the purpose of the experiment, MIN6 can be subjected to a cell strainer to produce a single cell for the purpose of a colocalization study (PluriStrainer, SKU 43-50070-51).

HEK29T & HEK293A Cells

HEK293T cells were acquired from Riken BioResource Center (BRC) (Graham et al., 1977). All HEK293T cells used in this dissertation were under the passage number of 30. HEK293A cells were purchased from Thermofisher (Thermofisher, R70507). HEK293A cells used in this dissertation are all under the passage number of 20.

The cells were routinely maintained in 10 cm dish (Corning, 430167) in a high glucose EB (Embryoid Body) medium (**Supplementary Table** *7*). They were maintained in a cell incubator at 37°C, 90-95% humidity, and 5% CO_2. Depending on the initial seeding density, medium change can be performed once every 2-4 days. $1x10^6$ cells will approximately reach confluence in 3-4 days. Careful observation must be performed every day to avoid over-confluence.

At 80% confluence, the cells must be passaged. At the time of passage, confluent cells in 10 cm dishes were washed in 10 mL D-PBS(-) (Nacalai, 14249-95). After washing, the cells were subjected to 1 mL 0.25% Trypsin (Gibco, 25200056) treatment for 5 minutes and then neutralized with 4 mL of EB medium. The cell suspension was subjected to Trypan Blue exclusion by sampling 10 μL of to be mixed with 10 μL Trypan Blue (Gibco, 15250061). The mix was then added into the counting chamber for automated counting (Invitrogen, AMQAX2000). The cells were homogenized with a disposable Pasteur pipette and centrifuged at 1000 rpm, 25°C, for 5 minutes. The supernatant was discarded and the pellet was

resuspended with fresh, pre-warmed EB medium to be seeded in a gelatin-coated 10 cm dish or other culture format.

Constructs

Adenovirus Overexpression Construct for TurboID

Gateway Cloning System was used to construct adenovirus overexpression vectors. The gateway vectors used in this dissertation were pENTR1A (entry vector) (Invitrogen, A10462) and pAD/CMV/V5/Dest (destination vector) (Thermofisher, V49320) as the Adenovirus destination vector. Insertion of the required cassette was performed through homologous recombination with NEB (New England Biolabs) HiFi DNA Assembly (NEB, E2621S).

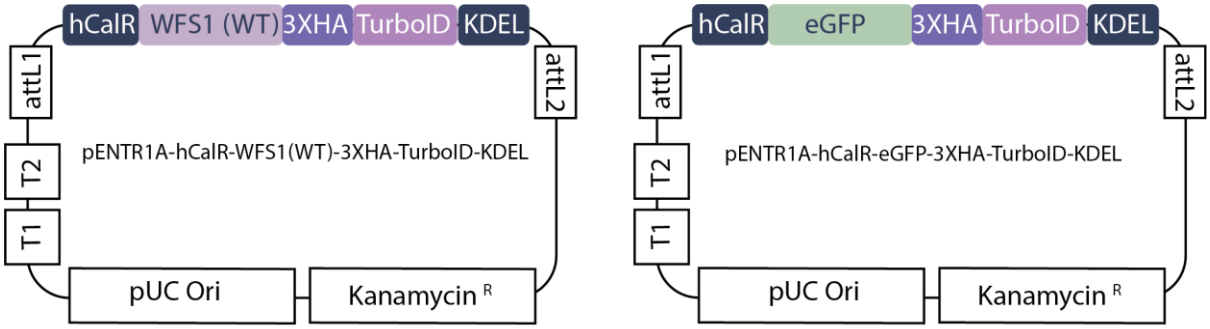

Figure 20 pENTR1A Plasmid Construct Maps

In-silico construct simulation was previously performed in SnapGene software. In this software, inversed PCR and 20-25 homologue arms primers (forward and reverse) for inserts were designed. Designed oligo sequences were synthetized by Eurofin Genomics. For vector backbone, inversed PCR with previously designed primers were performed on pENTR1A-hCalR-mCherry-KDEL with High Fidelity PCR Enzyme KOD Fx Neo (Toyobo, KFX-201). This was done to eliminate the mCherry Sequence, linearize and amplify the vector. The reaction was run on gel electrophoresis and the expected band size was sliced and purified using the Monarch Gel Extraction Kit (NEB, T1120S). The purified DNA was then subjected to DpnI digestion to eliminate possible background (Nippon Genetics, FG-DpnI) for 3 hours.

The enzymatic reaction was then purified with the Zymogen DNA Clean-Up Kit (Zymogen, D4013).

Inserts from the origin plasmid were amplified with previously designed 20-25 homologue arm addition primers with PCR by using (Toyobo, KFX-201). Amplified inserts were gel-purified with Monarch Gel Extraction Kit (NEB, T1120S). Homologous recombination was performed with NEB (New England Biolabs) HiFi DNA Assembly (NEB, E2621S) according to the manufacturer protocol while adjusting to the DNA purification yields. The resulting reaction was then transformed into a home-made competent DH5α E. *coli* (Takara, 9057) and plated on 50 μg/mL Kanamycin LB (Luria-Bertani) Agar plate. The transformed cells were incubated at 37°C overnight (16-18 hours). On the following day, colony PCR was performed in tandem with a replica plate. The replica plate was incubated at 37°C overnight (16-18 hours) and kept at 4°C until further use. Positive colonies were cultured in 3 mL Liquid LB medium overnight and subjected to plasmid purification with FastGene miniprep plasmid purification kit (Nippon gene, FG-90502). Positive colonies were sequenced (Instiute of Science Tokyo's Sequencing Facility). Sequence analysis was performed in SnapGene software. The resulting plasmids: pENTR1A-hCalrR-WFS1(WT)-3XHA-TurboID-KDEL and pENTR1A-hCalR-eGFP-3XHA-TurboID-KDEL were stored at -20°C until further use (**Figure 20**).

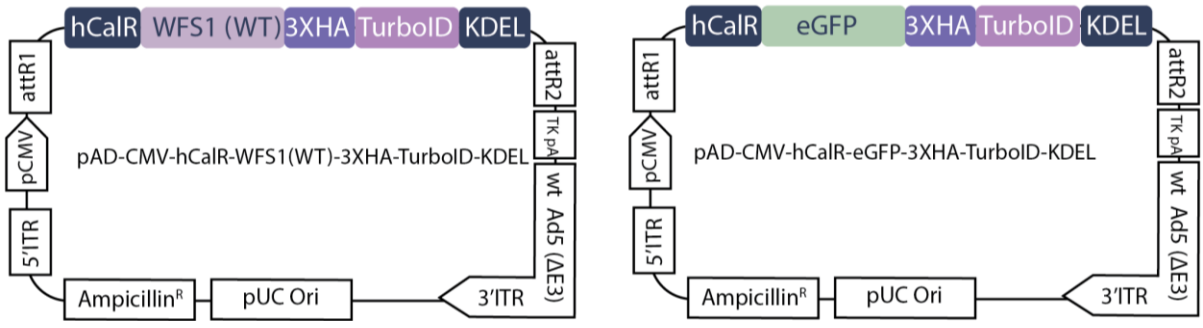

Figure 21 *Adenovirus Construct Plasmid Maps*

Confirmed pENTR1A vector with inserts was then subjected to L/R reaction with L/R Clonase II (Invitrogen, 11791020) to insert the cassette into pAD/CMV/V5/Dest . The reaction resulted in adenovirus vectors: pAd-CMV-hCalR-WFS1 (WT)-3XHA-TurboID-KDEL and pAD-CMV-hCalR-eGFP-3XHA-TurboID-KDEL (**Figure 21**). L/R reaction was performed according to the manufacturer`s protocol while adjusting to the yield of pENTR1A. The resulting reaction was transformed into DH5α E. *coli* (Takara, 9057) and plated on 100 µg/mL Penicillin LB (Luria-Bertani) Agar plate. The transformed cells were incubated at 37°C overnight (16-18 hours). The resulting colonies were processed with the same steps to the pENTR1A process.The confirmed colonies were then cultured in an Erlenmeyer flask containing 50 mL liquid LB medium with 50 µg/mL Ampicillin overnight. On the following day, the culture was subjected to midiprep transfection grade plasmid purification with a Qiagen Midiprep Kit (Qiagen, 12145). The resulting plasmid was stored at -20°C until further use.

Vector Construction for PLA Assay

Assembly of the cassette was performed through homologous recombination with NEB (New England Biolabs) HiFi DNA Assembly (NEB, E2621S).

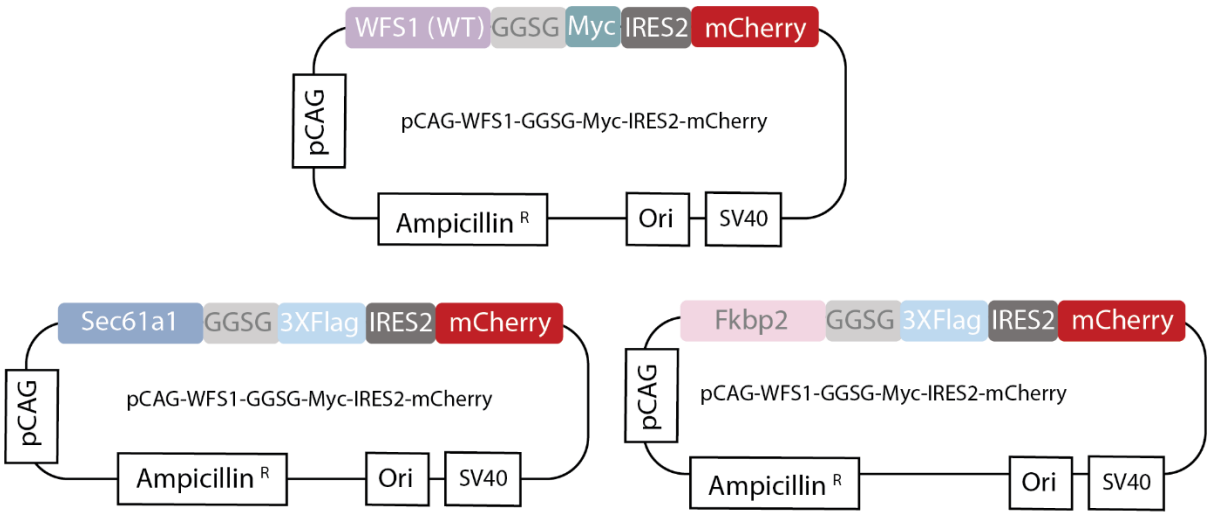

Figure 22 PLA Plasmid Construct Maps

In-silico construct simulation was previously performed using SnapGene software. In this software, inversed PCR and 20-25 homolog arms primers (forward and reverse) for inserts were designed. Designed oligo sequences were synthetized by Eurofin Genomics. For vector backbone, inversed PCR with previously designed primers was performed on pCAG-IRES2-mCherry (Laboratory inventory) with High Fidelity PCR Enzyme KOD One Blue (Toyobo, KMM-201). This was done to linearize and amplify the vector. The reaction was run on gel electrophoresis, and the expected band size was sliced and purified using the Monarch Gel Extraction Kit (NEB, T1120S). The purified DNA was then subjected to DpnI digestion to eliminate possible background (Nippon Genetics, FG-DpnI) for 3 hours. The enzymatic reaction was then purified with the Zymogen DNA Clean-Up Kit (Zymogen, D4013).

Inserts from the origin plasmid were amplified with previously designed 20-25 homologue arm addition primers with PCR by using KOD One Blue (Toyobo, KMM-201). Amplified inserts were gel-purified with Monarch Gel Extraction Kit (NEB, T1120S). Homologue recombination was performed with NEB (New England Biolabs) HiFi DNA Assembly (NEB, E2621S) according to the manufacturer protocol while adjusting to the DNA purification yields. The resulting reaction was then transformed into either home-made competent DH5α E. *coli* (Takara, 9057) or SURE2 (Agilent, 200152) and plated on 100 μg/mL Ampicillin LB (Luria-Bertani) Agar plate. The transformed cells were incubated at 37°C overnight (16-18 hours). On the following day, colony PCR was performed, and a replica plate was made using methods similar to the pENTR1A and pAD-CMV-V5-Dest methods. The confirmed pCAG colonies were then subjected to midiprep transfection grade plasmid purification with Qiagen Plasmid Midi Kit (Qiagen, 12145). Then resulting plasmis: pCAG-WFS(WT)-GGSG-Myc-IRES2-mCherry, pCAG-Sec61a1-GGSG-3X Flag-IRES2-mCherry, and pCAG-Fkbp2-GGSG-3X Flag-IRES2-mCherry (**Figure 22**) were stored at -20°C until further use.

Lipofection

Lipofection was performed on the intended cell line with Lipofectamine 3000 (Thermofisher, L3000001) according to the manufacturer`s protocol at optimal cell confluence and health.

Adenovirus Generation

HEK293A has to be at 70-90% confluency before transfection. The confluent HEK293A cells in 10 cm dish were passaged by first washing the cells with 10 mL D-PBS(-) (Nacalai, 14249-95). After washing, the cells were subjected to 1 mL 0.25% Trypsin (Gibco, 25200056) treatment for 5 minutes and then neutralized with 4 mL of EB medium. The cell suspension was subjected to Trypan Blue exclusion by sampling 10 µL of to be mixed with 10 µL TrypanBlue (Gibco, 15250061). The mix was then added into the counting chamber for automated counting (Invitrogen, AMQAX2000). The cells were homogenized with a disposable Pasteur pipette and centrifuged at 1000 rpm, 25°C, for 5 minutes. The supernatant was discarded, and the pellet was resuspended with fresh, pre-warmed EB medium to be seeded in a 6-well plate with a density of $5x10^5$ cells/well. The cells were incubated overnight.

On the following day, lipofection was performed according to the manufacturer`s protocol. The transfected cells were incubated for a week while observing for plaque formation daily. When the cells started to 90% detached from the plate, they were scraped and moved into a 15 mL tube. The cell suspension was then subjected to 3X (-80°C-37°C) freeze-thaw cycles to free virus particles from the cells. After freeze-thawing the cells, the cell suspension was centrifuged at 13,000 rpm, 25°C, for 20 minutes. The supernatant containing the virus particles was aliquoted into screw cap cryotubes (Sarstedt, 72379). The crude viral stock was then stored at -80°C until further use. While working stock can be kept at 4°C.

Assays

TurboID-LC-MS/MS assay

For this experiment, MIN6 cells (~1×10^7 cells per 10 cm dish) were seeded and cultured in standard conditions. Adenoviruses expressing TurboID fused to the intended protein were

added to the culture medium at 1-10% of the total volume to facilitate infection. After 48 hours, biotin (Sigma-Aldrich, B4501) was added to the medium to a final concentration of 50 μM. The cells were incubated for 30 minutes at 37°C, allowing biotinylation of proteins in proximity. Incubation time can be optimized to minimize background and increase specificity. After incubation, the cells were washed three times with 10 mL of PBS (Nacalai Tesque, 14249-95) and subjected to subcellular fractionation with SF-PTS Kit (GLSciences, 7510-11400).

Protein concentrations in membrane-organelle fraction samples were determined using the Pierce™ BCA Protein Assay Kit (Thermo Fisher Scientific, 23250). Samples containing 500 μg of total protein were adjusted to a final volume of 500 μL using MilliQ water. To block free cysteine residues, iodoacetamide (FUJIFILM Wako Pure Chemical, 144-48-9) was added to a final concentration of 50 mM, and the reaction was incubated for 30 minutes in the dark. The alkylation reaction was terminated by light exposure.

To enrich biotinylated proteins, magnetic beads (Dynabeads™ Biotin Binder; Thermo Fisher Scientific, 11047) were used. The beads were washed three times with TBS (Tris-Buffered Saline) (Nacalai Tesque, 30557-95) using a magnetic stand. 50 μL of the washed beads were added to each sample, and the mixture was rotated at room temperature for 1 hour. After incubation, the beads were sequentially washed three times with TBS containing 0.2% SDS (Nacalai Tesque, 30359-35), three times with TBS containing 1 M urea (Nacalai Tesque, 35993-15), and three times with TBS. Finally, the beads were resuspended in 100 μL of TBS containing 1 M urea.

Proteolytic digestion was performed by adding 2 μL of LysC-Trypsin mix (Promega, V5071) to the resuspended beads, followed by incubation at 37°C with gentle rotation overnight. After digestion, the beads were separated, and the supernatant containing peptides was collected. Samples were desalted using C-Tips (Nikkyo Technos, 2110-00002) and dried

using a SpeedVac concentrator (Thermo Fisher Scientific, SPD131DDA). The dried peptides were reconstituted in 20 µL of binding solution, consisting of 0.1% trifluoroacetic acid (TFA; Sigma-Aldrich, 302031) and 2% acetonitrile (FUJIFILM Wako Pure Chemical, 013-12041), and centrifuged at 20,000 × g at 4°C for 5 minutes. The supernatant was transferred to LC-MS vials (Tokyo Glass, 0170-29-51-03).

Samples were analyzed by liquid chromatography-tandem mass spectrometry (LC-MS/MS) using a Q-Exactive system coupled with an Easy-nLC 1000 (Thermo Fisher Scientific) in collaboration with the Taguchi Laboratory. The LC-MS/MS results were used to identify proteins biotinylated by TurboID and analyzed with Thermofisher Scientific`s Proteome Discoverer software.

PLA Assay

PLA Assay was performed using Merck's Duolink® In Situ Assay Kit. The method basically follows the manufacturer`s protocol with the addition of a counterstaining step post-final reaction.

Transfected MIN6 cells were fixed in 2% PFA for 15 minutes and continued with 4% PFA for 20 minutes. These cells were then washed 3x with PBS-T (phosphate-buffered saline with 0.1% Tween). The cells were then subjected to permeabilization with 0.1% Triton-X (Nacalai, 35501-02) for 5 minutes on ice, followed by 3x PBS-T washes. The cells were then blocked by using Duolink® Blocking Solution (Merck, DUO82049) in a pre-warmed humidity chamber at 37°C for 60 minutes. Subsequently, primary antibodies specific to the target proteins were diluted in Duolink® Antibody Diluent and added to the samples. The samples were incubated with primary antibodies overnight at 4°C, depending on antibody requirements inside a humidity chamber.

After primary antibody incubation, samples were subjected to 2x Wash Buffer A washes 5 minutes each. The samples were then probed with Duolink® PLA probes: Anti-Rabbit PLUS (Merck, DUO92002) and Anti-Mouse MINUS (Merck, DUO92004) diluted in

the antibody diluent. These antibody diluents were added to the samples and the samples were incubated at 37°C for 1 hour in a humidity chamber. After incubation, 2x Wash Buffer A washes were performed for 5 minutes each.

The ligation step was performed by first diluting the 5x Ligation Buffer with high-purity water and adding ligase enzyme immediately prior to use, was added to the samples. The samples were incubated at 37°C for 30 minutes to form circular DNA formation if the PLA probes were near each other (≤40 nm). After the ligation, samples were washed 2x in Wash Buffer A for 5 minutes each. The following step was the amplification of the circular DNA. This was done by first preparing a diluted 5x Amplification Buffer with high-purity water and adding polymerase enzyme immediately prior to use. The amplification reaction was carried out at 37°C for 100 minutes in a humidity chamber.

After amplification, the samples were processed for counter-staining. The samples were washed in Wash Buffer B twice for 10 minutes duration each. 1X Wash buffer A was applied after. The samples were then subjected to secondary antibody staining (for localization) or DAPI diluted in Duolink antibody diluent®. The samples were then incubated at 37°C for 40 minutes in a humidity chamber. After incubation, the samples were washed in 1x Wash Buffer A for 2 x 2 minutes and 0.01x Wash Buffer B for 1 minute. The leftover buffer was discarded, and the samples were mounted with a Vectashield mounting medium for fluorescence (Vector Laboratories, H-1000-10). Samples were then observed with an LSM780 confocal microscope.

Data Analysis

Data filtration and tidy-up was performed with Microsoft Excel then analyzed with R.

Packages used in R can be viewed in **Supplementary Table 8**.

Section III: Results

3.1 GO (Gene Ontology) analysis of MIN6 TurboID LC-MS/MS Result showed enrichment in ER-resident protein.

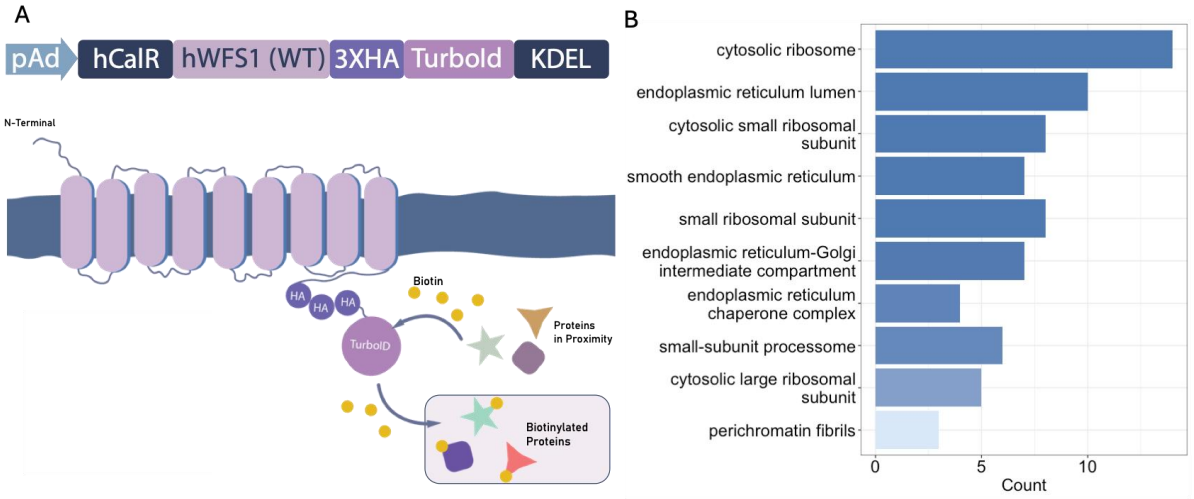

Figure 23 Construct Design and GO Analysis of Peptide Motifs Detected in MIN6 Membrane-Organelle Fraction.

A. Vector construct of adenovirus was purposefully designed to target interacting protein on the C-terminal ER luminal region B. GO Analysis of MIN6 membrane-organelle fraction

To elucidate the c-terminal interacting protein involved in WFS1 degradation, a WFS1 adenovirus vector was designed. The vector construct (**Figure 21**) was designed to capture interacting protein at the C-terminal ER luminal region. hCalR-KDEL ER localization sequence was added to minimize non-specific protein capture and ensure ER protein resident enrichment. Kit-isolated membrane-organelle fraction was analyzed for LC-MS/MS and the resulting data was analyzed using Gene Ontology. The resulting GO Analysis of MIN6 membrane-organelle fraction revealed mainly cytosolic and endoplasmic-reticulum resident protein enrichment.

GO analysis result (**Figure 23**) suggested that despite the isolation of membrane-organelle fraction, pure ER-only could not be attained as the highest enrichment was cytosolic ribosome. Despite the impurity, endoplasmic-reticulum resident enrichment can be detected and further analyzed.

3.2 *In-silico* analysis resulted in primary, secondary, and tertiary protein candidates.

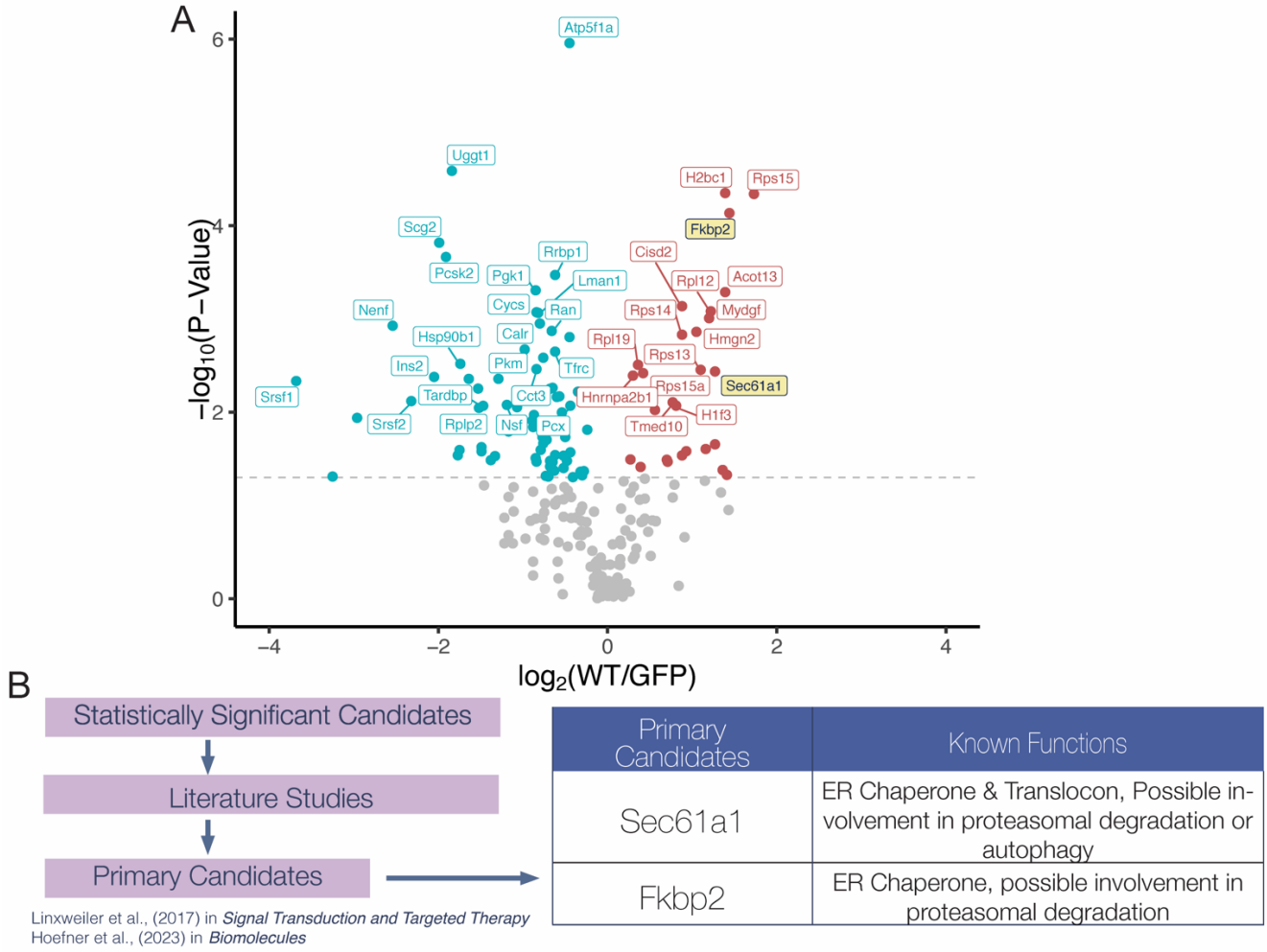

Figure 24 Volcano Plot Analysis and Primary Interacting Protein Candidates

A. Volcano Plot of log2(abundance) against -log10(P-value) for biotinylated proteins detected in MIN6 WT versus eGFP. Y-axis cutoff: P-value ≤ 0.05. B. A list of statistically and literature-significant protein candidates .

The resulting data from LC-MS/MS was further analyzed based on statistical significance and subjected to volcano plot analysis. The candidates with $p<0.05$ were identified and further analyzed through literature studies. The selected candidates were Sec61a1 and Fkbp2 (**Figure 24**).

Sec61a1 is a translocon protein subunit that is responsible for plasma membrane protein localization (Linxweiler et al., 2017). Aside from the translocon function, Sec61a1 possesed chaperone function which aids protein to properly fold. The presence of Sec61a1 is crucial for protein retrotranslocation and might be a key player in WFS1 proteasomal degradation

(Linxweiler et al., 2017). Sec61a1 also interacts with Sec62 and Sec63, performing a complex with proteins that were involved in ER autophagy (Linxweiler et al., 2017; Shrestha, Reinert, et al., 2020). Therefore, Sec61a1 was chosen as the primary candidate.

Fkbp2 was found to be enriched in beta-cells (Hoefner et al., 2023). It was also reported to aid proinsulin folding. Aside from the chaperone function, this candidate protein is also included in a protein family that interacts with the IP3R protein that is involved in autophagy regulation (Hoefner et al., 2023). Therefore, Fkbp2 might be an important chaperone in WFS1 folding and degradation.

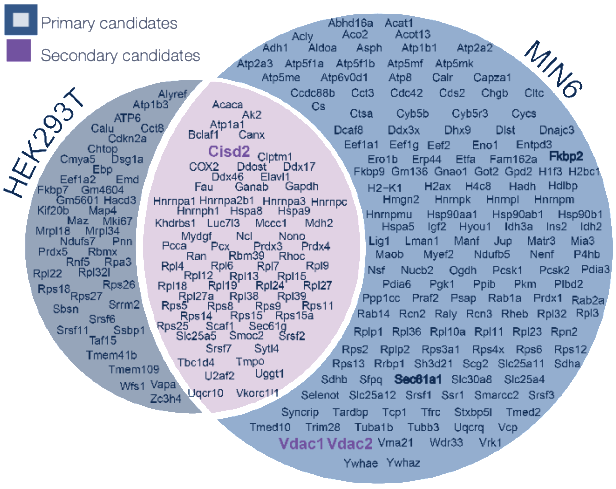

Set	# of Proteins
HEK293T only	44
MIN6-only	155
HEK293T and MIN6	71

Literature Studies
Secondary Candidates

Secondary Candidates	Known Functions
Cisd2	Possible involvement in autophagy
Vdac1	MAM Interaction, metabolite exchange, autophagy regulator (Beclin-1 interactor)
Vdac2	Metabolite echange, autophagy regulator

Figure 25 Venn Diagram Analysis and Secondary Protein Candidates

Venn Diagram of peptide motifs identified with LC-MS/MS after biotinylated protein enrichment. Sec61a1 and Fkbp2 were detected exclusively in the MIN6-only dataset. Further literature analysis of the identified proteins revealed secondary candidates potentially associated with protein autophagy. (Proteins detected in HEK293 were translated into MIN6 protein symbols for comparison purposes).

To further identify protein candidates detected in MIN6, the dataset was compared to HEK293T dataset through venn diagram (**Figure 25**). As observed in **Figure 25**, Fkbp2 and Sec61a1 were only detected in MIN6 and not HEK293T. The result further confirmed the possibility of primary candidates involvement in WFS1 degradation in MIN6.

From the diagram, further literature study revealed there were candidates that have been confirmed to interact with WFS1 such as Vdac1 and Vdac2 (Zatyka et al., 2023). As seen in **Figure 25,** Vdac1 and Vdac2 were only detected in MIN6. Other interesting secondary

candidate was Cisd2 which mutation was reported as the cause of WS2 (Loncke et al., 2021; Rosanio et al., 2022). Other notable function of Cisd2 is as a Bcl2 interactor, together, they form a complex that regulate autophagy (Chang et al., 2012)

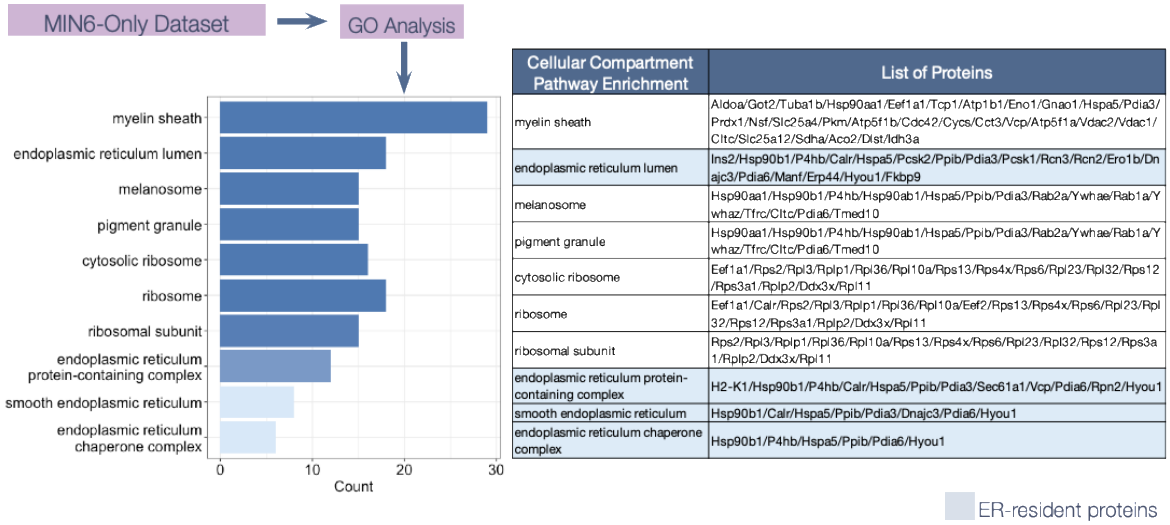

Cellular Compartment Pathway Enrichment	List of Proteins
myelin sheath	Aldoa/Got2/Tuba1b/Hsp90aa1/Eef1a1/Tcp1/Atp1b1/Eno1/Gnao1/Hspa5/Pdia3/Prdx1/Nsf/Slc25a4/Pkm/Atp5f1b/Cdc42/Cycs/Cct3/Vcp/Atp5f1a/Vdac2/Vdac1/Cltc/Slc25a12/Sdha/Aco2/Dlst/Idh3a
endoplasmic reticulum lumen	Ins2/Hsp90b1/P4hb/Calr/Hspa5/Pcsk2/Ppib/Pdia3/Pcsk1/Rcn3/Rcn2/Ero1b/Dnajc3/Pdia6/Manf/Erp44/Hyou1/Fkbp9
melanosome	Hsp90aa1/Hsp90b1/P4hb/Hsp90ab1/Hspa5/Ppib/Pdia3/Rab2a/Ywhae/Rab1a/Ywhaz/Tfrc/Cltc/Pdia6/Tmed10
pigment granule	Hsp90aa1/Hsp90b1/P4hb/Hsp90ab1/Hspa5/Ppib/Pdia3/Rab2a/Ywhae/Rab1a/Ywhaz/Tfrc/Cltc/Pdia6/Tmed10
cytosolic ribosome	Eef1a1/Rps2/Rpl3/Rplp1/Rpl36/Rpl10a/Rps13/Rps4x/Rps6/Rpl23/Rpl32/Rps12/Rps3a1/Rplp2/Ddx3x/Rpl11
ribosome	Eef1a1/Calr/Rps2/Rpl3/Rplp1/Rpl36/Rpl10a/Eef2/Rps13/Rps4x/Rps6/Rpl23/Rpl32/Rps12/Rps3a1/Rplp2/Ddx3x/Rpl11
ribosomal subunit	Rps2/Rpl3/Rplp1/Rpl36/Rpl10a/Rps13/Rps4x/Rps6/Rpl23/Rpl32/Rps12/Rps3a1/Rplp2/Ddx3x/Rpl11
endoplasmic reticulum protein-containing complex	H2-K1/Hsp90b1/P4hb/Calr/Hspa5/Ppib/Pdia3/Sec61a1/Vcp/Pdia6/Rpn2/Hyou1
smooth endoplasmic reticulum	Hsp90b1/Calr/Hspa5/Ppib/Pdia3/Dnajc3/Pdia6/Hyou1
endoplasmic reticulum chaperone complex	Hsp90b1/P4hb/Hspa5/Ppib/Pdia6/Hyou1

Figure 26 MIN6-Only Dataset GO Analysis

GO Enrichment Analysis for Cellular Compartment (CC) and the list of genes based on the Venn diagram in Figure 28 revealed enrichment of ER-resident proteins associated with protein folding (chaperone).

The list of proteins detected only in the MIN6-only dataset (**Figure 25**) was further subjected to GO analysis to filter out tertiary candidates (**Figure 26**). GO enrichment for cellular compartment pathway enrichment in ER-resident proteins (highlighted in blue) further reveals possible tertiary candidates such as Calr, Hyou1 et cetera. However, due to the copious number of proteins, further filtration of these datasets was required to narrow down the proteins for the tertiary candidates.

To address the matter, KEGG (Kyoto Encyclopedia of Genes and Genomes) pathway analysis was performed (**Figure 27).** This was done to identify the pathway enriched in the MIN6-only dataset and to visualize the cellular process based on the available KEGG database. The resulting analysis revealed the enrichment of the protein processing pathway in the endoplasmic reticulum. Assuming that candidate proteins involved in WFS1 WT degradation might be a crucial member of the ER protein processing pathway, the proteins included in this

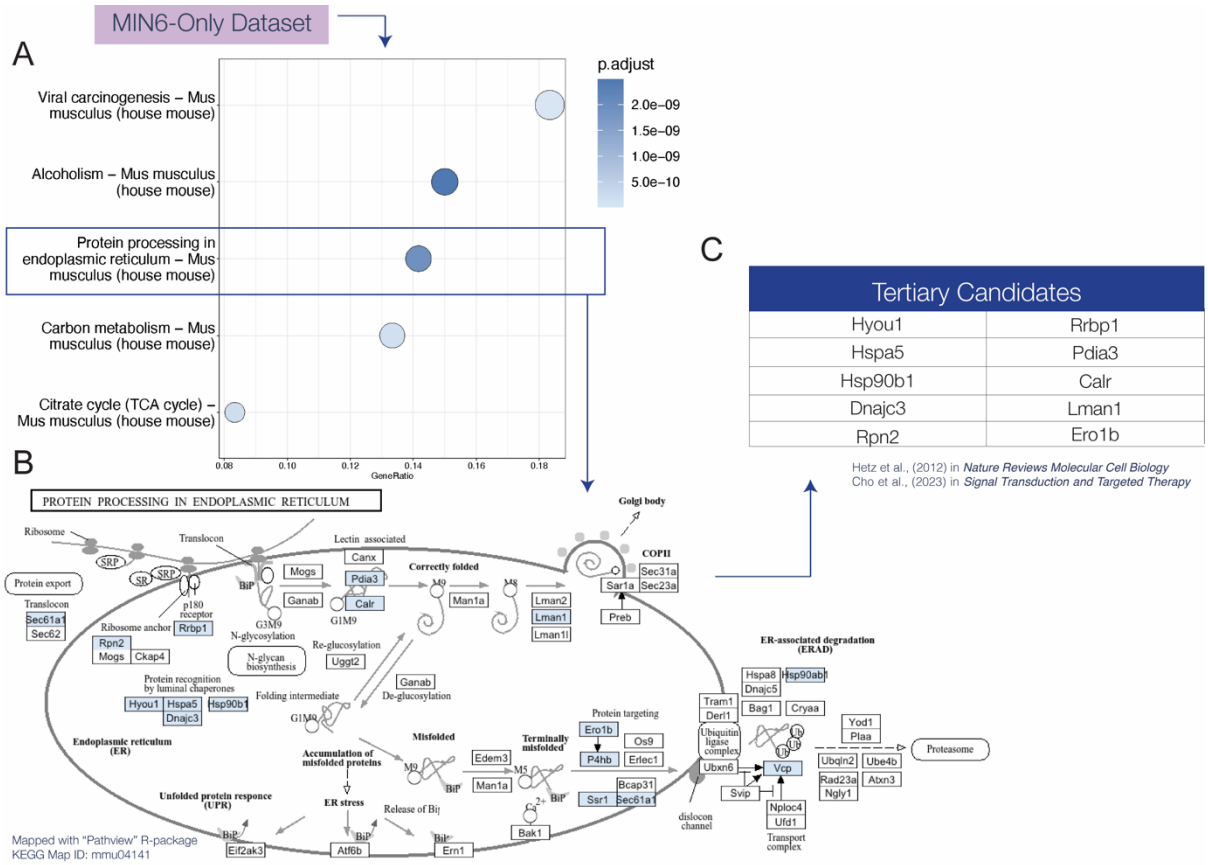

Figure 27 KEGG Analysis of MIN6-Only Dataset

A. KEGG Pathway Enrichment Analysis of peptide motifs identified in the MIN6-only dataset. B. Schematic Illustration of the Protein Processing KEGG Pathway (mmu04141). Further elimination through literature studies resulted in the tertiary candidate proteins.

pathway were mounted into the KEGG map database by highlighting the map in blue to map out and nail down the possible tertiary candidates (**Figure 27**). ER protein processing consists of several steps: protein translation, transport, recognition by ER chaperones for assisted folding, glycosylation, retro-translocation, and degradation. As viewed in **Figure 27B,** KEGG pathway map, the detected proteins revealed that after translation, WFS1 (WT) might be subjected to glycosylation as seen from the detected proteins Pdia3, Calr, and Lman1. From

there, WFS1 WT might be processed through chaperone-assisted folding by Hyou1, Hspa5, Hsp90b1, and Dnajc3.

To maintain WFS1 WT homeostasis within the cells, the degradation process might involve recognition by Ero1b for ER-associated degradation by proteasome with the aid of Vcp protein. The analysis revealed which process in ER-protein processing proteins is identified within the whole WFS1 WT processing pathway. As shown in **Figure 27B,** KEGG map, the protein complexes that were all highlighted in blue are ER-luminal chaperones that consisted of Hyou1, Hspa5, Hsp90b1 and Dnajc3. Aside from the chaperone function, these proteins were also involved in UPR and ER stress response (Sharma et al., 2008). This increased the likelihood of these proteins' involvement in WFS1 degradation. Therefore, these proteins were chosen as top priorities in tertiary candidates (**Figure 27C**). Other proteins highlighted in the KEGG pathway map were identified as the second priority of tertiary target proteins.

3.3 PLA Assay Result Showed Interactions between WFS1 (WT) and Primary Protein Candidate

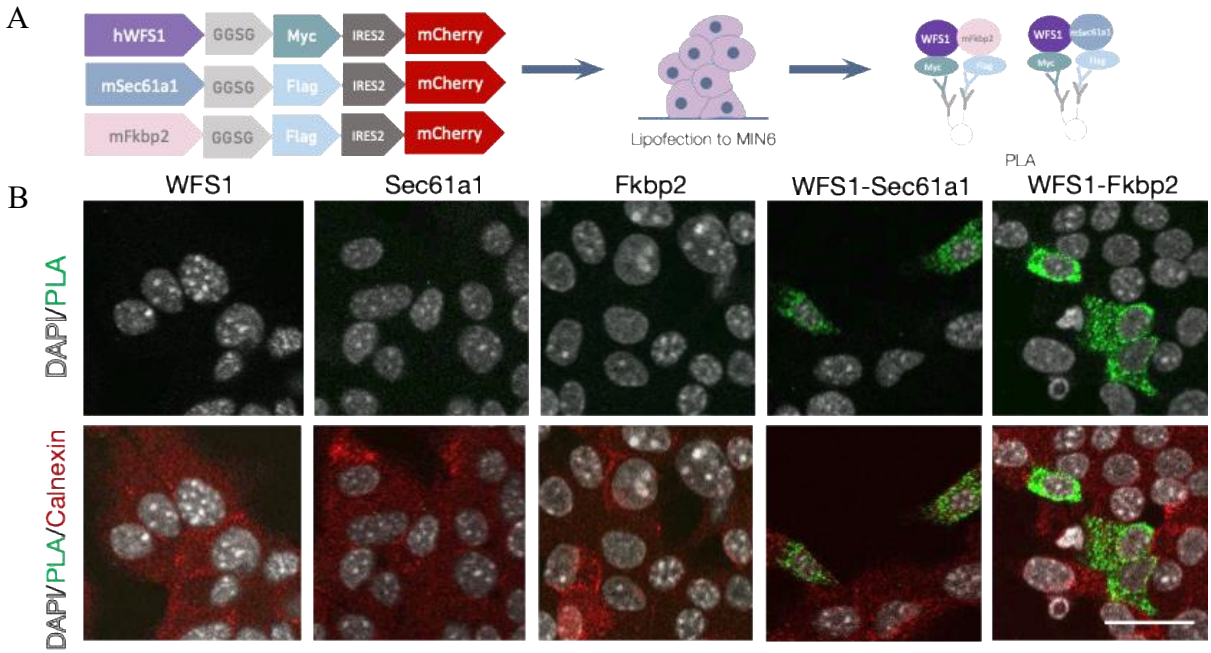

Figure 28 *Immunocyctochemistry Images of PLA Result*

A. Schematic Illustration of the PLA workflow. B. Immunochemistry Image of the PLA assay in MIN6 cells, 3 days post-lipofection. The PLA results showed positive signals in cells transfected with either WFS1-Sec61a1 or WFS1-Fkbp2, with little to no signal was found in negative and single-antibody controls. Calnexin was used as an ER marker. Scale bar = 25 µm.

PLA assay was performed to confirm the interactions between WFS1 (WT) and primary candidate proteins Sec61a1 and Fkbp2 in the MIN6 (**Figure 28**). Each of the constructs was singularly transfected into MIN6 as negative control followed by WFS1-Sec61a1 or WFS1-Fkbp2 cotransfection. The result showed that minimal to no PLA signal was detected in a single transfection MIN6. Meanwhile, WFS1-Sec61a1 and WFS1-Fkbp2 showed clear, strong and positive PLA signals, confirming the interactions between WFS1 and primary candidates.

Section IV: Discussion

Mechanistic Insights into WFS1 degradation: A hypothesis

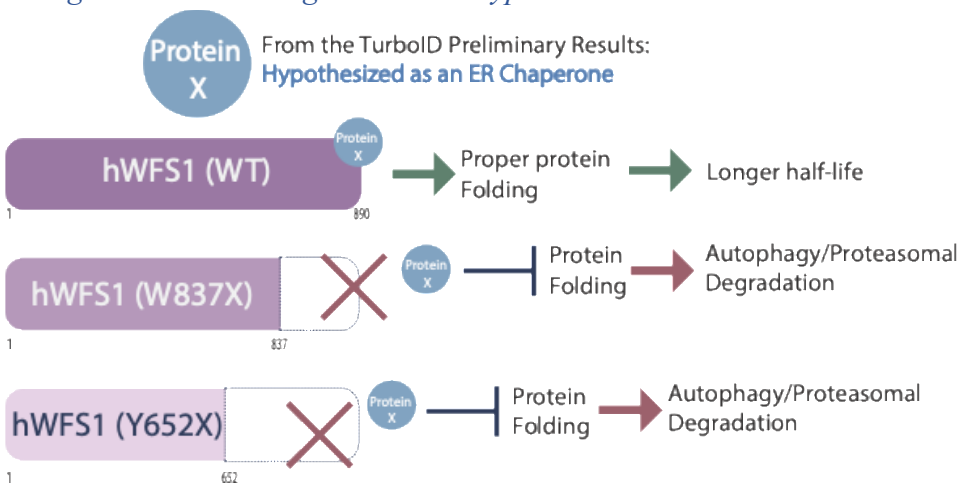

Figure 29 *Hypothesized Mechanism of WFS1`s MIN6-Specific Degradation*

Based on these results, primary, secondary, and tertiary protein candidates have been identified. Analysis of identified protein revealed enrichment of ER-processing proteins and chaperones (**Figure 27**). The previously identified primary candidates, Sec61a and Fkbp2 (**Figure 24**), were also found to possess chaperone functions (Hoefner et al., 2023; Linxweiler et al., 2017). Rewinding back to the goal of this dissertation: Identifying the proteins responsible for WFS1 mutant degradation, the proteins involved might be the chaperone responsible for assisting WFS1 protein folding. Therefore, as a hypothesis, in the MIN6 cell line, the loss of the c-terminal region of WFS1 mutants in W837X and Y652X might be crucial for WFS1 overall folding. This might cause protein misfolding, which might be detected and processed for relatively higher protein turnover through proteasomal degradation in the previous study (Tokuma et al., 2023).

Further elucidation should first focus on further elucidating the detailed mechanism of these candidate proteins in regulating WFS1 WT versus mutant. The first priority should be focused on quantitively significant candidates, Sec61a1 and Fkbp2, followed by the secondary, and tertiary candidates.

Primary candidates: Sec61a1 and Fkbp2

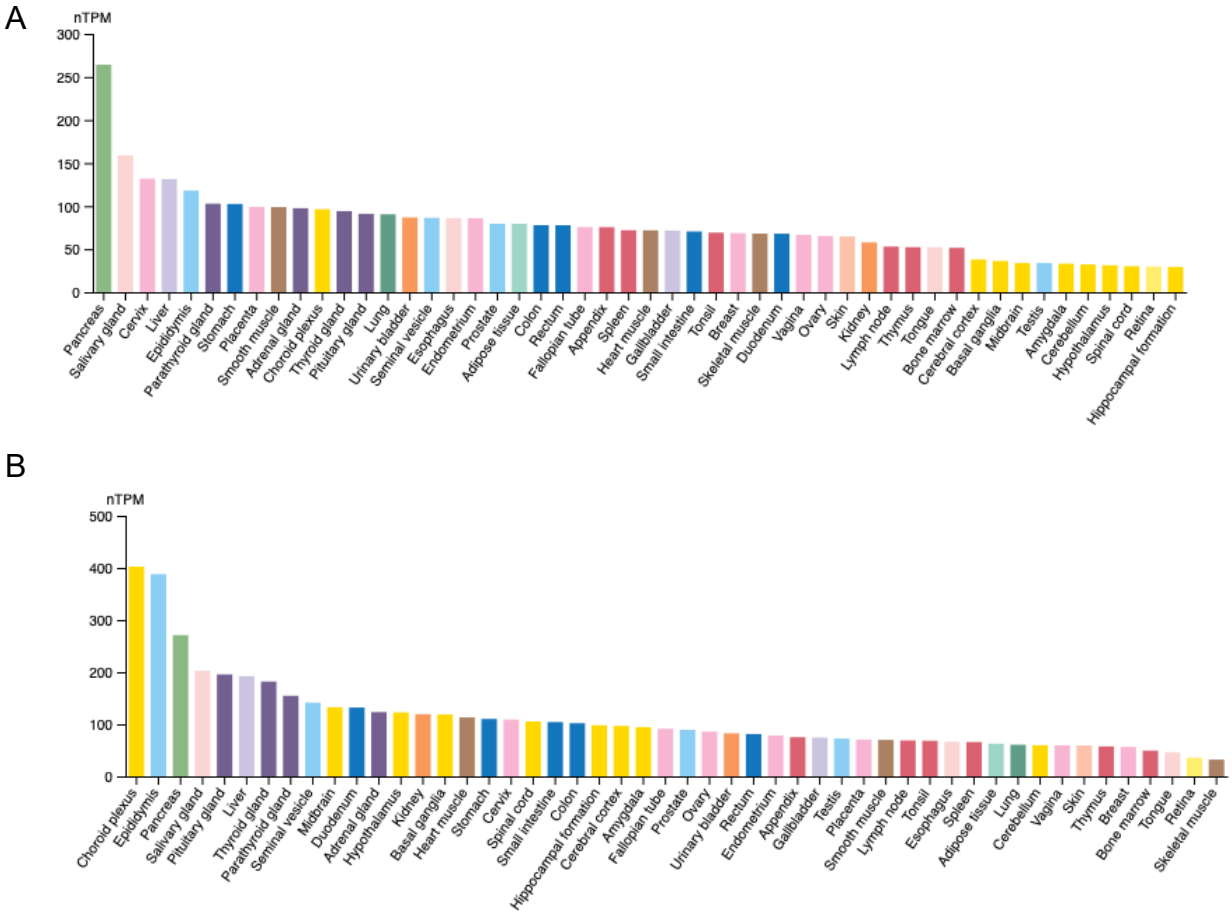

Figure 30 *Consensus dataset form Human RNA Expression Overview for human SEC61A1 and FKBP2*

A. SEC61A1 (from: https://www.proteinatlas.org/ENSG00000058262-SEC61A1/tissue) and B. FKBP2 (from; https://www.proteinatlas.org/ENSG00000173486-FKBP2/tissue)

The main focus was put on the primary protein candidates identified through statistical analysis and abundance through volcano plot analysis: Sec61a1 and Fkbp2 (**Figure 24**). In humans, these two proteins were found to be enriched in the pancreas (**Figure 30**). Previous studies have reported that Sec61a1 mutation causes diabetes in mice and ER stress in the MIN6 cell line (D. J. Lloyd et al., 2009). Hoefner and colleagues have also elucidated the apoptotic effect of Fkbp2 in pancreatic β-cells, emphasizing its crucial chaperone activity in modulating protein folding (Hoefner et al., 2023). This evidence further suggests the importance of the primary protein candidates in β-cell homeostasis and protein degradation.

To date, the mechanism of WFS1 and primary protein candidates' interaction in MIN6 has not been reported. In this dissertation, aside from *in-silico* analysis, the PLA assay was performed to confirm the direct interaction of each of these proteins with WFS1 (WT) (**Figure 29**). The result revealed that WFS1 indeed directly interacts with each of the primary candidates. Aside from the chaperone function, other renowned Sec61a1 functions in membrane protein insertion might play a crucial role in WFS1 (WT) protein turnover. Sec61a1 functions as a protein that mediates the protein localization to the ER membrane (Wu & Hegde, 2023). The C-terminal region of WFS1 might be important for recognition by Sec61a1 and ER-membrane localization. The loss of the c-terminal region in W837X and Y652X might cause these proteins to be contained within the ER-lumen, aggregate, and subjected to protein degradation.

Limitations and Future Directions

In this dissertation, preliminary research was performed to elucidate the mechanism of WFS1 mutant degradation in MIN6. This study identified primary, secondary, and tertiary candidates based on *in-silico* analysis from fusion TurboID protein biotinylation. Despite the confirmed WFS1-primary candidate interaction from the PLA assay, further study needs to be performed to sufficiently confirm the direct effect of the candidate protein overexpression, knockdown and rescue on WFS1 mutant degradation. Other methods, such as the addition of candidate-specific inhibitors, should also be considered.

Chapter IV: Conclusions

Improvement of Primary Human Hepatocyte Cell Attachment through EPAC2 Activation

Summary of Key Findings

In this dissertation, activation of cAMP through the addition of both IBMX and Forskolin coupled with BSA elimination from M4 medium increased early PHH attachment. Furthermore, adjustment of seeding density is also crucial in increasing the attachment. Delving further into the cAMP effector, the EPAC2-specific activator, S-220, was found to potently increase PHH attachment at low concentrations. Moreover, Culturing PHH in M4 BSA- medium with a cAMP activator seemed to improve PHH functional marker, CYP3A4 activity, and bile canaliculi formation. However, culturing PHH in M4 BSA- compared to BSA+ in the long-term posed a detrimental effect towards PHH viability and albumin secretion.

Broader Implication and Future Prospects

The identification of EPAC2-specific activator, S-2220, as a potent small molecule for PHH attachment, may significantly contribute towards pharmacological studies that require PHH as the primary model. This small molecule might be beneficial for increasing early PHH attachment and maintenance. However, further study still needs to be performed to assess its effect on other PHH functions. Elucidation of the EPAC2 cell attachment pathway may also be beneficial in studying cell attachment not only in PHH but also in other type of cells.

Unraveling WFS1 Selective Degradation

Summary of Key Findings

In this dissertation, primary, secondary, and tertiary candidates that were detected in WFS1 (WT)-TurboID were identified. Primary candidates were identified through statistical analysis and literature study. Secondary candidates were identified through Venn diagram analysis and literature study. Tertiary candidates were identified through the KEGG pathway enrichment and mapping. From these candidates, ER chaperone was identified among a copious number of proteins identified. This leads to a possible WFS1 mutant degradation mechanism hypothesis: the loss of C-terminal in WFS1 W837X and Y652X might lead to a loss of interaction with chaperone, leading to faster protein turnover.

The primary focus in this study was the primary candidates: Sec61a1 and Fkbp2, which possess chaperone functions. As for Sec61a1, other functions, such as ER membrane protein insertion mediator, were also considered. This study also confirmed the direct interaction between WFS1-Sec61a1 and WFS1-Fkbp2 through PLA assay.

Broader Implications and Future Prospects

Even though the confirmation of WFS1-primary candidates' interactions has been confirmed, future studies should focus on elucidating the detailed mechanism and as a possible target of a cure for WS late-onset diabetes.

Acknowledgement

I would like to convey my deepest gratitude to:

Prof. Shoen Kume as the principal investigator during the course of my study.

Associate Prof. Nobuaki Shiraki for the supervision during PHH project

Dr. Daisuke Sakano for the supervision during WFS1 project

Prof. Hideki Taguchi for facilitating LC-MS/MS experiment

Prof. Tatsuya Niwa for facilitating LC-MS/MS experiment

Teruhiko Watanabe for the contribution in PHH project (LC/MS-MS)

Dr. Tokuma Hiraku for providing the plasmid material and as a prior predecessor of WFS1 project

Dr. Airi Inoue for the contribution and superfision in WFS1 TurboID, LC-MS/MS Experiment

Yusuke Kato for the contribution in LC-MS/MS experiment

All Kume-Shiraki Lab Members for supporting the me throughout my study

Institute of Science Tokyo`s Life Science & Technology Sequencing Facility for handling sequencing requests

References

Abounit, K., Scarabelli, T. M., & McCauley, R. B. (2012). Autophagy in mammalian cells. *World Journal of Biological Chemistry*, *3*(1). https://doi.org/10.4331/wjbc.v3.i1.1

Baze, A., Parmentier, C., Hendriks, D. F. G., Hurrell, T., Heyd, B., Bachellier, P., Schuster, C., Ingelman-Sundberg, M., & Richert, L. (2018). Three-Dimensional Spheroid Primary Human Hepatocytes in Monoculture and Coculture with Nonparenchymal Cells. *Https://Home.Liebertpub.Com/Tec*, *24*(9), 534–545. https://doi.org/10.1089/TEN.TEC.2018.0134

Bedossa, P., & Paradis, V. (2003). Liver extracellular matrix in health and disease. *The Journal of Pathology*, *200*(4), 504–515. https://doi.org/10.1002/PATH.1397

Belicova, L., Repnik, U., Delpierre, J., Gralinska, E., Seifert, S., Valenzuela, J. I., Morales-Navarrete, H. A., Franke, C., Räägel, H., Shcherbinina, E., Prikazchikova, T., Koteliansky, V., Vingron, M., Kalaidzidis, Y. L., Zatsepin, T., & Zerial, M. (2021). Anisotropic expansion of hepatocyte lumina enforced by apical bulkheads. *Journal of Cell Biology*, *220*(10). https://doi.org/10.1083/JCB.202103003/VIDEO-1

Bell, C. C., Hendriks, D. F. G., Moro, S. M. L., Ellis, E., Walsh, J., Renblom, A., Fredriksson Puigvert, L., Dankers, A. C. A., Jacobs, F., Snoeys, J., Sison-Young, R. L., Jenkins, R. E., Nordling, Å., Mkrtchian, S., Park, B. K., Kitteringham, N. R., Goldring, C. E. P., Lauschke, V. M., & Ingelman-Sundberg, M. (2016). Characterization of primary human hepatocyte spheroids as a model system for drug-induced liver injury, liver function and disease. *Scientific Reports*, *6*(October 2015), 25187. https://doi.org/10.1038/srep25187

Beviglia, L., & Kramer, R. H. (1999). HGF INDUCES FAK ACTIVATION AND INTEGRIN-MEDIATED ADHESION IN MTLn3 BREAST CARCINOMA CELLS. *J. Cancer*, *83*, 640–649. https://doi.org/10.1002/(SICI)1097-0215(19991126)83:5

Blaauboer, B. J., & Paine, A. J. (1979). Attachment of rat hepatocytes to plastic substrata in the absence of serum requires protein synthesis. *Biochemical and Biophysical Research Communications*, *90*(1), 368–374. https://doi.org/10.1016/0006-291X(79)91634-6

Borland, G., Smith, B. O., & Yarwood, S. J. (2009). EPAC proteins transduce diverse cellular actions of cAMP. In *British Journal of Pharmacology* (Vol. 158, Issue 1, pp. 70–86). John Wiley & Sons, Ltd. https://doi.org/10.1111/j.1476-5381.2008.00087.x

Bos, J. L. (2006). Epac proteins: multi-purpose cAMP targets. In *Trends in Biochemical Sciences* (Vol. 31, Issue 12, pp. 680–686). Elsevier Ltd. https://doi.org/10.1016/j.tibs.2006.10.002

Bos, J. L., De Bruyn, K., Enserink, J., Kuiperij, B., Rangarajan, S., Rehmann, H., Riedl, J., De Rooij, J., Van Mansfeld, F., & Zwartkruis, F. (2003). The role of Rap1 in integrin-mediated cell adhesion. *Biochemical Society Transactions*, *31*(1), 83–86. https://doi.org/10.1042/bst0310083

Branon, T. C., Bosch, J. A., Sanchez, A. D., Udeshi, N. D., Svinkina, T., Carr, S. A., Feldman, J. L., Perrimon, N., & Ting, A. Y. (2018). Efficient proximity labeling in living cells and organisms with TurboID. *Nature Biotechnology 2018 36:9*, *36*(9), 880–887. https://doi.org/10.1038/nbt.4201

Bucher, N. L. R., Robinson, G. S., & Farmer, S. R. (1990). Effects of extracellular matrix on hepatocyte growth and gene expression: implications for hepatic regeneration and the repair of liver injury. *Seminars in Liver Disease*, *10*(1), 11–19. https://doi.org/10.1055/S-2008-1040453

Cavalcanti-Adam, E. A., Volberg, T., Micoulet, A., Kessler, H., Geiger, B., & Spatz, J. P. (2007). Cell Spreading and Focal Adhesion Dynamics Are Regulated by Spacing of Integrin Ligands. *Biophysical Journal*, *92*(8), 2964. https://doi.org/10.1529/BIOPHYSJ.106.089730

Chang, N. C., Nguyen, M., & Shore, G. C. (2012). BCL2-CISD2: An ER complex at the nexus of autophagy and calcium homeostasis? *Autophagy*, *8*(5), 856–857. https://doi.org/10.4161/AUTO.20054

Cheng, X., Ji, Z., Tsalkova, T., & Mei, F. (2008). Epac and PKA: A tale of two intracellular cAMP receptors. In *Acta Biochimica et Biophysica Sinica* (Vol. 40, Issue 7, pp. 651–662). NIH Public Access. https://doi.org/10.1111/j.1745-7270.2008.00438.x

Cho, K. F., Branon, T. C., Udeshi, N. D., Myers, S. A., Carr, S. A., & Ting, A. Y. (2020). Proximity labeling in mammalian cells with TurboID and split-TurboID. *Nature Protocols 2020 15:12*, *15*(12), 3971–3999. https://doi.org/10.1038/s41596-020-0399-0

Choi, S. S., & Diehl, A. M. (2009). Epithelial-to-Mesenchymal Transitions in the Liver. *Hepatology (Baltimore, Md.)*, *50*(6), 2007. https://doi.org/10.1002/HEP.23196

De Vries, R. J., Banik, P. D., Nagpal, S., Weng, L., Ozer, S., Van Gulik, T. M., Toner, M., Tessier, S. N., & Uygun, K. (2018). Bulk Droplet Vitrification: An Approach to Improve Large-Scale Hepatocyte Cryopreservation Outcome. *Langmuir*, *35*(23), 7354–7363. https://doi.org/10.1021/ACS.LANGMUIR.8B02831

Du, Z., & Patel, T. B. (2003). Albumin: a Galpha(s)-specific guanine nucleotide dissociation inhibitor and GTPase activating protein. *Archives of Biochemistry and Biophysics*, *415*(2), 221–228. https://doi.org/10.1016/S0003-9861(03)00263-7

Enserink, J. M., Price, L. S., Methi, T., Mahic, M., Sonnenberg, A., Bos, J. L., & Taskén, K. (2004). The cAMP-Epac-Rap1 Pathway Regulates Cell Spreading and Cell Adhesion to Laminin-5 through the α3β1 Integrin but Not the α6β4 Integrin *. *Journal of Biological Chemistry*, *279*(43), 44889–44896. https://doi.org/10.1074/JBC.M404599200

Fleming, A., Bourdenx, M., Fujimaki, M., Karabiyik, C., Krause, G. J., Lopez, A., Martín-Segura, A., Puri, C., Scrivo, A., Skidmore, J., Son, S. M., Stamatakou, E., Wrobel, L., Zhu, Y., Cuervo, A. M., & Rubinsztein, D. C. (2022). The different autophagy

degradation pathways and neurodegeneration. In *Neuron* (Vol. 110, Issue 6). https://doi.org/10.1016/j.neuron.2022.01.017

Fonseca, S. G., Ishigaki, S., Oslowski, C. M., Lu, S., Lipson, K. L., Ghosh, R., Hayashi, E., Ishihara, H., Oka, Y., Permutt, M. A., & Urano, F. (2010). Wolfram syndrome 1 gene negatively regulates ER stress signaling in rodent and human cells. *The Journal of Clinical Investigation*, *120*(3), 744–755. https://doi.org/10.1172/JCI39678

Fredriksson, C., Khilman, S., Kasemo, B., & Steel, D. M. (1998). *In vitro real-time characterization of cell attachment and spreading*.

Friedman, S. L. (2005). Mac the knife? Macrophages - The double-edged sword of hepatic fibrosis. *Journal of Clinical Investigation*, *115*(1), 29–32. https://doi.org/10.1172/JCI200523928

Gallant, N. D., & García, A. J. (2007). Model of integrin-mediated cell adhesion strengthening. *Journal of Biomechanics*, *40*(6), 1301–1309. https://doi.org/10.1016/J.JBIOMECH.2006.05.018

Geerts, A. (2001). History, heterogeneity, developmental biology, and functions of quiescent hepatic stellate cells. *Seminars in Liver Disease*, *21*(3), 311–335. https://doi.org/10.1055/S-2001-17550

Gjessing, R., & Seglen, P. O. (1980a). Adsorption, simple binding and complex binding of rat hepatocytes to various in vitro substrata. *Experimental Cell Research*. https://doi.org/10.1016/0014-4827(80)90347-X

Gjessing, R., & Seglen, P. O. (1980b). Adsorption, simple binding and complex binding of rat hepatocytes to various in vitro substrata. *Experimental Cell Research*, *129*(1), 239–249. https://doi.org/10.1016/0014-4827(80)90347-X

Gkretsi, V., Apte, U., Mars, W. M., Bowen, W. C., Luo, J. H., Yang, Y., Yu, Y. P., Orr, A., St.-Arnaud, R., Dedhar, S., Kaestner, K. H., Wu, C., & Michalopoulos, G. K. (2008).

Liver-specific ablation of integrin-linked kinase in mice results in abnormal histology, enhanced cell proliferation, and hepatomegaly. *Hepatology*, *48*(6), 1932–1941. https://doi.org/10.1002/HEP.22537

Gkretsi, V., Bowen, W. C., Yang, Y., Wu, C., & Michalopoulos, G. K. (2007). Integrin-linked kinase is involved in matrix-induced hepatocyte differentiation. *Biochemical and Biophysical Research Communications*, *353*(3), 638–643. https://doi.org/10.1016/J.BBRC.2006.12.091

Gkretsi, V., Mars, W. M., Bowen, W. C., Barua, L., Yang, Y., Guo, L., St-Arnaud, R., Dedhar, S., Wu, C., & Michalopoulos, G. K. (2007). Loss of integrin linked kinase from mouse hepatocytes in vitro and in vivo results in apoptosis and hepatitis. *Hepatology (Baltimore, Md.)*, *45*(4), 1025–1034. https://doi.org/10.1002/HEP.21540

Gloerich, M., Ponsioen, B., Vliem, M. J., Zhang, Z., Zhao, J., Kooistra, M. R., Price, L. S., Ritsma, L., Zwartkruis, F. J., Rehmann, H., Jalink, K., & Bos, J. L. (2010). Spatial Regulation of Cyclic AMP-Epac1 Signaling in Cell Adhesion by ERM Proteins. *Molecular and Cellular Biology*, *30*(22), 5421–5431. https://doi.org/10.1128/mcb.00463-10

Godoy, P., Hewitt, N. J., Albrecht, U., Andersen, M. E., Ansari, N., Bhattacharya, S., Bode, J. G., Bolleyn, J., Borner, C., Böttger, J., Braeuning, A., Budinsky, R. A., Burkhardt, B., Cameron, N. R., Camussi, G., Cho, C. S., Choi, Y. J., Craig Rowlands, J., Dahmen, U., … Hengstler, J. G. (2013). Recent advances in 2D and 3D in vitro systems using primary hepatocytes, alternative hepatocyte sources and non-parenchymal liver cells and their use in investigating mechanisms of hepatotoxicity, cell signaling and ADME. In *Archives of Toxicology* (Vol. 87, Issue 8). https://doi.org/10.1007/s00204-013-1078-5

Graham, F. L., Smiley, J., Russell, W. C., & Nairn, R. (1977). Characteristics of a human cell line transformed by DNA from human adenovirus type 5. *Journal of General Virology*,

36(1). https://doi.org/10.1099/0022-1317-36-1-59

Green, C. J., Charlton, C. A., Wang, L. M., Silva, M., Morten, K. J., & Hodson, L. (2017). The isolation of primary hepatocytes from human tissue: optimising the use of small non-encapsulated liver resection surplus. *Cell and Tissue Banking*, *18*(4), 597–604. https://doi.org/10.1007/S10561-017-9641-6/FIGURES/2

Guo, X., Shen, S., Song, S., He, S., Cui, Y., Xing, G., Wang, J., Yin, Y., Fan, L., He, F., & Zhang, L. (2011). The E3 Ligase Smurf1 Regulates Wolfram Syndrome Protein Stability at the Endoplasmic Reticulum. *The Journal of Biological Chemistry*, *286*(20), 18037. https://doi.org/10.1074/JBC.M111.225615

Hacking, S. A., & Khademhosseini, A. (2013). Cells and Surfaces in vitro. *Biomaterials Science: An Introduction to Materials: Third Edition*, 408–427. https://doi.org/10.1016/B978-0-08-087780-8.00037-1

Han, M., Lim, S.-M., Kim, Y.-L., Kim, H.-L., Kim, K., Sacket, S. J., Jo, J.-Y., Bae, Y.-S., Okajima, F., & Im, D.-S. (2008). Albumin and Antioxidants Inhibit Serum-deprivation-induced Cell Adhesion in Hematopoietic Cells. *Biomolecules & Therapeutics*, *16*(4), 410–415. https://doi.org/10.4062/biomolther.2008.16.4.410

Hoefner, C., Bryde, T. H., Pihl, C., Tiedemann, S. N., Bresson, S. E., Hotiana, H. A., Khilji, M. S., Santos, T. Dos, Puglia, M., Pisano, P., Majewska, M., Durzynska, J., Klindt, K., Klusek, J., Perone, M. J., Bucki, R., Hägglund, P. M., Gourdon, P. E., Gotfryd, K., … Marzec, M. T. (2023). FK506-Binding Protein 2 Participates in Proinsulin Folding. *Biomolecules*, *13*(1). https://doi.org/10.3390/biom13010152

Hoivik, E. A., Witsoe, S. L., Bergheim, I. R., Xu, Y., Jakobsson, I., Tengholm, A., Doskeland, S. O., & Bakke, M. (2013). DNA Methylation of Alternative Promoters Directs Tissue Specific Expression of Epac2 Isoforms. *PLoS ONE*. https://doi.org/10.1371/journal.pone.0067925

Horner, R., Gassner, J. G. M. V., Kluge, M., Tang, P., Lippert, S., Hillebrandt, K. H., Moosburner, S., Reutzel-Selke, A., Pratschke, J., Sauer, I. M., & Raschzok, N. (2019). Impact of Percoll purification on isolation of primary human hepatocytes. *Scientific Reports*, *9*(1). https://doi.org/10.1038/S41598-019-43042-8

Howe, A. K. (2004). Regulation of actin-based cell migration by cAMP/PKA. In *Biochimica et Biophysica Acta - Molecular Cell Research* (Vol. 1692, Issues 2–3, pp. 159–174). https://doi.org/10.1016/j.bbamcr.2004.03.005

Huai, Q., Wang, H., Zhang, W., Colman, R. W., Robinson, H., & Ke, H. (2004). Crystal structure of phosphodiesterase 9 shows orientation variation of inhibitor 3-isobutyl-1-methylxanthine binding. *Proceedings of the National Academy of Sciences of the United States of America*, *101*(26), 9624–9629. https://doi.org/10.1073/pnas.0401120101

Hung, V., Udeshi, N. D., Lam, S. S., Loh, K. H., Cox, K. J., Pedram, K., Carr, S. A., & Ting, A. Y. (2016). Spatially resolved proteomic mapping in living cells with the engineered peroxidase APEX2. *Nature Protocols*, *11*(3). https://doi.org/10.1038/nprot.2016.018

Hurley, J. H. (1999). Structure, mechanism, and regulation of mammalian adenylyl cyclase. In *Journal of Biological Chemistry* (Vol. 274, Issue 12, pp. 7599–7602). https://doi.org/10.1074/jbc.274.12.7599

Hynes, R. O. (2002). Integrins: bidirectional, allosteric signaling machines. *Cell*, *110*(6), 673–687. https://doi.org/10.1016/S0092-8674(02)00971-6

Ishihara, H., Takeda, S., Tamura, A., Takahashi, R., Yamaguchi, S., Takei, D., Yamada, T., Inoue, H., Soga, H., Katagiri, H., Tanizawa, Y., & Oka, Y. (2004). Disruption of the WFS1 gene in mice causes progressive beta-cell loss and impaired stimulus-secretion coupling in insulin secretion. *Human Molecular Genetics*, *13*(11), 1159–1170. https://doi.org/10.1093/HMG/DDH125

Jones, T. R., Kang, I. H., Wheeler, D. B., Lindquist, R. A., Papallo, A., Sabatini, D. M.,

Golland, P., & Carpenter, A. E. (2008). CellProfiler Analyst: Data exploration and analysis software for complex image-based screens. *BMC Bioinformatics*, *9*. https://doi.org/10.1186/1471-2105-9-482

Jonsson-Schmunk, K., Wonganan, P., Choi, J. H., Callahan, S. M., & Croyle, M. A. (2016). Integrin receptors play a key role in the regulation of hepatic CYP3A. *Drug Metabolism and Disposition*, *44*(5), 758–770. https://doi.org/10.1124/dmd.115.068874

Junker, J. L., & Heine, U. I. (1987). Effect of Adhesion Factors Fibronectin, Laminin, and Type IV Collagen on Spreading and Growth of Transformed and Control Rat Liver Epithelial Cells. *Cancer Research*, *47*(14).

Kabeya, T., Qiu, S., Hibino, M., Nagasaki, M., Kodama, N., Iwao, T., & Matsunaga, T. (2018). Cyclic AMP signaling promotes the differentiation of human induced pluripotent stem cells into intestinal epithelial cells S. *Drug Metabolism and Disposition*, *46*(10), 1411–1419. https://doi.org/10.1124/DMD.118.082123/-/DC1

Kan, M., Minamoto, Y., Sunami, S., Yamane, I., & Umeda, M. (1982). *The Effects on Cell Adhesion of Fibronectin and Gelatin in a Serum-Free, Bovine Serum Albumin Medium*.

Kegel, V., Deharde, D., Pfeiffer, E., Zeilinger, K., Seehofer, D., & Damm, G. (2016). Protocol for Isolation of Primary Human Hepatocytes and Corresponding Major Populations of Non-parenchymal Liver Cells. *Journal of Visualized Experiments : JoVE*, *2016*(109), 53069. https://doi.org/10.3791/53069

Kido, K., Yamanaka, S., Nakano, S., Motani, K., Shinohara, S., Nozawa, A., Kosako, H., Ito, S., & Sawasaki, T. (2020). Airid, a novel proximity biotinylation enzyme, for analysis of protein–protein interactions. *ELife*, *9*. https://doi.org/10.7554/eLife.54983

Kikkawa, Y., Kataoka, A., Matsuda, Y., Takahashi, N., Miwa, T., Katagiri, F., Hozumi, K., & Nomizu, M. (2011). Maintenance of hepatic differentiation by hepatocyte attachment peptides derived from laminin chains. *Journal of Biomedical Materials Research Part A*,

99A(2), 203–210. https://doi.org/10.1002/JBM.A.33176

Kim, D. I., Jensen, S. C., Noble, K. A., Kc, B., Roux, K. H., Motamedchaboki, K., & Roux, K. J. (2016). An improved smaller biotin ligase for BioID proximity labeling. *Molecular Biology of the Cell*, *27*(8). https://doi.org/10.1091/mbc.E15-12-0844

Kim, T. H., Bowen, W. C., Stolz, D. B., Runge, D., Mars, W. M., & Michalopoulos, G. K. (1998). Differential expression and distribution of focal adhesion and cell adhesion molecules in rat hepatocyte differentiation. *Experimental Cell Research*, *244*(1), 93–104. https://doi.org/10.1006/excr.1998.4209

Kim, Y. L., Im, Y. J., Lee, Y. K., Ha, N. C., Bae, Y. S., Lim, S. M., Okajima, F., & Im, D. S. (2006). Albumin functions as an inhibitor of T cell adhesion in vitro. *Biochemical and Biophysical Research Communications*, *351*(4), 953–957. https://doi.org/10.1016/J.BBRC.2006.10.143

Kinbara, K., Goldfinger, L. E., Hansen, M., Chou, F. L., & Ginsberg, M. H. (2003). Ras GTPases: integrins' friends or foes? *Nature Reviews Molecular Cell Biology 2003 4:10*, *4*(10), 767–777. https://doi.org/10.1038/nrm1229

Klaas, M., Kangur, T., Viil, J., Mäemets-Allas, K., Minajeva, A., Vadi, K., Antsov, M., Lapidus, N., Järvekülg, M., & Jaks, V. (2016). The alterations in the extracellular matrix composition guide the repair of damaged liver tissue. *Scientific Reports 2016 6:1*, *6*(1), 1–12. https://doi.org/10.1038/srep27398

Lauschke, V. M., Shafagh, R. Z., Hendriks, D. F. G., & Ingelman-Sundberg, M. (2019). 3D Primary Hepatocyte Culture Systems for Analyses of Liver Diseases, Drug Metabolism, and Toxicity: Emerging Culture Paradigms and Applications. *Biotechnology Journal*, *14*(7), 1800347. https://doi.org/10.1002/BIOT.201800347

Lee, E. M., Verma, M., Palaniappan, N., Pope, E. M., Lee, S., Blacher, L., Neerumalla, P., An, W., Campbell, T., Brown, C., Hurst, S., Marshall, B., Hershey, T., Nunes, V., López

de Heredia, M., & Urano, F. (2023). Genotype and clinical characteristics of patients with Wolfram syndrome and WFS1-related disorders. *Frontiers in Genetics*, *14*. https://doi.org/10.3389/fgene.2023.1198171

Lee, S. M. L., Schelcher, C., Demmel, M., Hauner, M., & Thasler, W. E. (2013). Isolation of Human Hepatocytes by a Two-step Collagenase Perfusion Procedure. *Journal of Visualized Experiments : JoVE*, *79*, 50615. https://doi.org/10.3791/50615

Lezoualc'H, F., Fazal, L., Laudette, M., & Conte, C. (2016). Cyclic AMP Sensor EPAC Proteins and Their Role in Cardiovascular Function and Disease. *Circulation Research*, *118*(5), 881–897. https://doi.org/10.1161/CIRCRESAHA.115.306529

Lim, H. D., Lee, S. M., Yun, Y. J., Lee, D. H., Lee, J. H., Oh, S. H., & Lee, S. Y. (2023). WFS1 autosomal dominant variants linked with hearing loss: update on structural analysis and cochlear implant outcome. *BMC Medical Genomics*, *16*(1). https://doi.org/10.1186/s12920-023-01506-x

Lindblad, W. J., Schuetz, E. G., Redford, K. S., & Guzelian, P. S. (1991). Hepatocellular phenotype in Vitro is influenced by biophysical features of the collagenous substratum. *Hepatology*, *13*(2), 282–288. https://doi.org/10.1002/HEP.1840130213

Linxweiler, M., Schick, B., & Zimmermann, R. (2017). Let's talk about Secs: Sec61, Sec62 and Sec63 in signal transduction, oncology and personalized medicine. *Signal Transduction and Targeted Therapy 2017 2:1*, *2*(1), 1–10. https://doi.org/10.1038/sigtrans.2017.2

Lloyd, D. J., Wheeler, M. C., & Gekakis, N. (2009). A Point Mutation in Sec61α1 Leads to Diabetes and Hepatosteatosis in Mice. *Diabetes*, *59*(2), 460. https://doi.org/10.2337/DB08-1362

Lloyd, T. D. R., Orr, S., Berry, D. P., & Dennison, A. R. (2004). Development of a protocol for cryopreservation of hepatocytes for use in bioartificial liver systems. *Annals of*

Clinical and Laboratory Science, *34*(2), 165–174.

Loncke, J., Vervliet, T., Parys, J. B., Kaasik, A., & Bultynck, G. (2021). Uniting the divergent Wolfram syndrome–linked proteins WFS1 and CISD2 as modulators of Ca2+ signaling. In *Science Signaling* (Vol. 14, Issue 702). https://doi.org/10.1126/scisignal.abc6165

London, E., Bloyd, M., & Stratakis, C. A. (2020). PKA functions in metabolism and resistance to obesity: lessons from mouse and human studies. *Journal of Endocrinology*, *246*(3), R51–R64. https://doi.org/10.1530/JOE-20-0035

Longmuir, I. S., & Ap Rees, W. (1956). Preparation of Cell Suspensions from Rat Livers. *Nature 1956 177:4517*, *177*(4517), 997–997. https://doi.org/10.1038/177997a0

Loretz, L. J., Li, A. P., Flye, M. W., & Wilson, A. G. E. (1989). Optimization of cryopreservation procedures for rat and human hepatocytes. *Xenobiotica; the Fate of Foreign Compounds in Biological Systems*, *19*(5), 489–498. https://doi.org/10.3109/00498258909042288

Luchowska-Stańska, U., Morgan, D., Yarwood, S. J., & Barker, G. (2019). Selective small-molecule EPAC activators. *Biochemical Society Transactions*, *47*(5), 1415–1427. https://doi.org/10.1042/BST20190254

Machide, M., Hashigasako, A., Matsumoto, K., & Nakamura, T. (2006). Contact inhibition of hepatocyte growth regulated by functional association of the c-Met/hepatocyte growth factor receptor and LAR protein-tyrosine phosphatase. *Journal of Biological Chemistry*, *281*(13), 8765–8772. https://doi.org/10.1074/JBC.M512298200/ATTACHMENT/9F375979-E761-4FAA-A53F-526CC84EB893/MMC1.PDF

Matsunaga, K., Tanabe, K., Inoue, H., Okuya, S., Ohta, Y., Akiyama, M., Taguchi, A., Kora, Y., Okayama, N., Yamada, Y., Wada, Y., Amemiya, S., Sugihara, S., Nakao, Y., Oka,

Y., & Tanizawa, Y. (2014). Wolfram Syndrome in the Japanese Population; Molecular Analysis of WFS1 Gene and Characterization of Clinical Features. *PLOS ONE*, *9*(9), e106906. https://doi.org/10.1371/JOURNAL.PONE.0106906

Maurice, D. H., Palmer, D., Tilley, D. G., Dunkerley, H. A., Netherton, S. J., Raymond, D. R., Elbatarny, H. S., & Jimmo, S. L. (2003). Cyclic nucleotide phosphodiesterase activity, expression, and targeting in cells of the cardiovascular system. *Molecular Pharmacology*, *64*(3), 533–546. https://doi.org/10.1124/MOL.64.3.533

McBeath, R., Pirone, D. M., Nelson, C. M., Bhadriraju, K., & Chen, C. S. (1996). Cell shape, cytoskeletal tension, and RhoA regulate stem cell lineage commitment. *Developmental Cell*, *6*(4), 483–495. https://doi.org/10.1016/S1534-5807(04)00075-9/ATTACHMENT/9DA7BB14-1030-4B03-A548-AC2DFCFCF565/MMC1.JPG

McQuin, C., Goodman, A., Chernyshev, V., Kamentsky, L., Cimini, B. A., Karhohs, K. W., Doan, M., Ding, L., Rafelski, S. M., Thirstrup, D., Wiegraebe, W., Singh, S., Becker, T., Caicedo, J. C., & Carpenter, A. E. (2018). CellProfiler 3.0: Next-generation image processing for biology. *PLoS Biology*, *16*(7). https://doi.org/10.1371/journal.pbio.2005970

Menter, D. G., & Dubois, R. N. (2012). Prostaglandins in cancer cell adhesion, migration, and invasion. *International Journal of Cell Biology*, *2012*. https://doi.org/10.1155/2012/723419

Mesnil, M., Fraslin, J. M., Piccoli, C., Yamasaki, H., & Guguen-Guillouzo, C. (1987). Cell contact but not junctional communication (dye coupling) with biliary epithelial cells is required for hepatocytes to maintain differentiated functions. *Experimental Cell Research*, *173*(2), 524–533. https://doi.org/10.1016/0014-4827(87)90292-8

Miki, T., Awa, M., Nishikawa, Y., Kiyonaka, S., Wakabayashi, M., Ishihama, Y., & Hamachi, I. (2016). A conditional proteomics approach to identify proteins involved in

zinc homeostasis. *Nature Methods 2016 13:11*, *13*(11), 931–937. https://doi.org/10.1038/nmeth.3998

Miyazaki, J. I., Araki, K., Yamato, E., Ikegami, H., Asano, T., Shibasaki, Y., Oka, Y., & Yamamura, K. I. (1990). Establishment of a pancreatic β cell line that retains glucose-inducible insulin secretion: Special reference to expression of glucose transporter isoforms. *Endocrinology*, *127*(1). https://doi.org/10.1210/endo-127-1-126

Moeller, T. A., Shukla, S. J., & Xia, M. (2012). Assessment of compound hepatotoxicity using human plateable cryopreserved hepatocytes in a 1536-well-plate format. *Assay and Drug Development Technologies*, *10*(1), 78–87. https://doi.org/10.1089/adt.2010.0365

Mooney, D., Hansen, L., Vacanti, J., Langer, R., Farmer, S., & Ingber, D. (1992). Switching from differentiation to growth in hepatocytes: Control by extracellular matrix. *Journal of Cellular Physiology*, *151*(3), 497–505. https://doi.org/10.1002/jcp.1041510308

Niimura, M., Miki, T., Shibasaki, T., Fujimoto, W., Iwanaga, T., & Seino, S. (2009). Critical role of the N-terminal cyclic AMP-binding domain of Epac2 in its subcellular localization and function. *Journal of Cellular Physiology*, *219*(3), 652–658. https://doi.org/10.1002/JCP.21709

Ogura, N., Kawada, M., Chang, W. J., Zhang, Q., Lee, S. Y., Kondoh, T., & Abiko, Y. (2004). Differentiation of the human mesenchymal stem cells derived from bone marrow and enhancement of cell attachment by fibronectin. *Journal of Oral Science*, *46*(4), 207–213. https://doi.org/10.2334/JOSNUSD.46.207

Ojaniemi, M., & Vuori, K. (1997). Epidermal Growth Factor Modulates Tyrosine Phosphorylation of p130Cas: INVOLVEMENT OF PHOSPHATIDYLINOSITOL 3′-KINASE AND ACTIN CYTOSKELETON. *Journal of Biological Chemistry*, *272*(41), 25993–25998. https://doi.org/10.1074/JBC.272.41.25993

Ölander, M., Wiśniewski, J. R., Flörkemeier, I., Handin, N., Urdzik, J., & Artursson, P. (2019). A simple approach for restoration of differentiation and function in cryopreserved human hepatocytes. *Archives of Toxicology*, *93*(3), 819–829. https://doi.org/10.1007/s00204-018-2375-9

Pallotta, M. T., Tascini, G., Crispoldi, R., Orabona, C., Mondanelli, G., Grohmann, U., & Esposito, S. (2019). Wolfram syndrome, a rare neurodegenerative disease: From pathogenesis to future treatment perspectives. *Journal of Translational Medicine*, *17*(1), 1–12. https://doi.org/10.1186/S12967-019-1993-1/TABLES/2

Pinkse, G. G. M., Jiawan-Lalai, R., Bruijn, J. A., & Heer, E. De. (2005). RGD peptides confer survival to hepatocytes via the beta1-integrin-ILK-pAkt pathway. *Journal of Hepatology*, *42*(1), 87–93. https://doi.org/10.1016/J.JHEP.2004.09.010

Pinkse, G. G. M., Voorhoeve, M. P., Noteborn, M., Terpstra, O. T., Bruijn, J. A., & de Heer, E. (2004). Hepatocyte survival depends on β1-integrin-mediated attachment of hepatocytes to hepatic extracellular matrix. *Liver International*, *24*(3), 218–226. https://doi.org/10.1111/j.1478-3231.2004.0914.x

Qiao, J., Mei, F. C., Popov, V. L., Vergara, L. A., & Cheng, X. (2002). Cell Cycle-dependent Subcellular Localization of Exchange Factor Directly Activated by cAMP. *Journal of Biological Chemistry*, *277*(29), 26581–26586. https://doi.org/10.1074/JBC.M203571200

Qiao, L., & Farrell, G. C. (1999). The effects of cell density, attachment substratum and dexamethasone on spontaneous apoptosis of rat hepatocytes in primary culture. *In Vitro Cellular and Developmental Biology - Animal*, *35*(7), 417–424. https://doi.org/10.1007/s11626-999-0117-2

Rangarajan, S., Enserink, J. M., Kuiperij, H. B., De Rooij, J., Price, L. S., Schwede, F., & Bos, J. L. (2003). Cyclic AMP induces integrin-mediated cell adhesion through Epac and Rap1 upon stimulation of the β2-adrenergic receptor. *The Journal of Cell Biology*,

160(4), 487. https://doi.org/10.1083/JCB.200209105

Richter, J. R., de Guzman, R. C., & Van Dyke, M. E. (2011). Mechanisms of hepatocyte attachment to keratin biomaterials. *Biomaterials*, *32*(30), 7555–7561. https://doi.org/10.1016/J.BIOMATERIALS.2011.06.061

Rosanio, F. M., Di Candia, F., Occhiati, L., Fedi, L., Malvone, F. P., Foschini, D. F., Franzese, A., & Mozzillo, E. (2022). Wolfram Syndrome Type 2: A Systematic Review of a Not Easily Identifiable Clinical Spectrum. *International Journal of Environmental Research and Public Health*, *19*(2). https://doi.org/10.3390/IJERPH19020835

Roux, K. J., Kim, D. I., Raida, M., & Burke, B. (2012). A promiscuous biotin ligase fusion protein identifies proximal and interacting proteins in mammalian cells. *Journal of Cell Biology*, *196*(6). https://doi.org/10.1083/jcb.201112098

Rubin, K., Höök, M., öbrink, B., & Timpl, R. (1981). Substrate adhesion of rat hepatocytes: Mechanism of attachment to collagen substrates. *Cell*, *24*(2), 463–470. https://doi.org/10.1016/0092-8674(81)90337-8

Ruoslahti, E. (1996). RGD and other recognition sequences for integrins. *Annual Review of Cell and Developmental Biology*, *12*, 697–715. https://doi.org/10.1146/annurev.cellbio.12.1.697

Ruoslahti, E., & Reed, J. C. (1994). Anchorage dependence, integrins, and apoptosis. *Cell*, *77*(4), 477–478. https://doi.org/10.1016/0092-8674(94)90209-7

Saliem, M., Holm, F., Tengzelius, R. B., Jorns, C., Nilsson, L. M., Ericzon, B. G., Ellis, E., & Hovatta, O. (2012). Improved cryopreservation of human hepatocytes using a new xeno free cryoprotectant solution. *World Journal of Hepatology*, *4*(5), 176. https://doi.org/10.4254/WJH.V4.I5.176

Sassone-Corsi, P. (2012). The Cyclic AMP Pathway. *Cold Spring Harbor Perspectives in Biology*, *4*(12), a011148. https://doi.org/10.1101/CSHPERSPECT.A011148

Schuppan, D., Ruehl, M., Somasundaram, R., & Hahn, E. G. (2001). Matrix as a modulator of hepatic fibrogenesis. *Seminars in Liver Disease*, *21*(3), 351–372. https://doi.org/10.1055/S-2001-17556/ID/50

Seamon, K. B., Padgett, W., & Daly, J. W. (1981). Forskolin: Unique diterpene activator of adenylate cyclase in membranes and in intact cells. *Proceedings of the National Academy of Sciences of the United States of America*, *78*(6 I), 3363–3367. https://doi.org/10.1073/pnas.78.6.3363

Seglen, P. O. (1976). Preparation of isolated rat liver cells. *Methods in Cell Biology*, *13*(C), 29–83. https://doi.org/10.1016/S0091-679X(08)61797-5

Sharma, N. K., Das, S. K., Mondal, A. K., Hackney, O. G., Chu, W. S., Kern, P. A., Rasouli, N., Spencer, H. J., Yao-Borengasser, A., & Elbein, S. C. (2008). Endoplasmic Reticulum Stress Markers Are Associated with Obesity in Nondiabetic Subjects. *The Journal of Clinical Endocrinology and Metabolism*, *93*(11), 4532. https://doi.org/10.1210/JC.2008-1001

Shoemaker, J. T., Zhang, W., Atlas, S. I., Bryan, R. A., Inman, S. W., & Vukasinovic, J. (2020). A 3D Cell Culture Organ-on-a-Chip Platform With a Breathable Hemoglobin Analogue Augments and Extends Primary Human Hepatocyte Functions in vitro. *Frontiers in Molecular Biosciences*, *7*. https://doi.org/10.3389/FMOLB.2020.568777

Shrestha, N., Liu, T., Ji, Y., Reinert, R. B., Torres, M., Li, X., Zhang, M., Tang, C. H. A., Hu, C. C. A., Liu, C., Naji, A., Liu, M., Lin, J. D., Kersten, S., Arvan, P., & Qi, L. (2020). Sel1L-Hrd1 ER-associated degradation maintains β cell identity via TGF-β signaling. *The Journal of Clinical Investigation*, *130*(7), 3499–3510. https://doi.org/10.1172/JCI134874

Shrestha, N., Reinert, R. B., & Qi, L. (2020). Endoplasmic Reticulum Protein Quality Control in β Cells. *Seminars in Cell & Developmental Biology*, *103*, 59–67.

https://doi.org/10.1016/J.SEMCDB.2020.04.006

Smith, D. M., Kafri, G., Cheng, Y., Ng, D., Walz, T., & Goldberg, A. L. (2005). ATP binding to PAN or the 26S ATPases causes association with the 20S proteasome, gate opening, and translocation of unfolded proteins. *Molecular Cell*, *20*(5). https://doi.org/10.1016/j.molcel.2005.10.019

Sosef, M. N., Baust, J. M., Sugimachi, K., Fowler, A., Tompkins, R. G., & Toner, M. (2005). Cryopreservation of Isolated Primary Rat Hepatocytes: Enhanced Survival and Long-term Hepatospecific Function. *Annals of Surgery*, *241*(1), 125. https://doi.org/10.1097/01.SLA.0000149303.48692.0F

Stéphenne, X., Najimi, M., & Sokal, E. M. (2010). Hepatocyte cryopreservation: Is it time to change the strategy? *World Journal of Gastroenterology : WJG*, *16*(1), 1. https://doi.org/10.3748/WJG.V16.I1.1

Sugawara, K., Shibasaki, T., Takahashi, H., & Seino, S. (2016). Structure and functional roles of Epac2 (Rapgef4). In *Gene* (Vol. 575, Issue 2, pp. 577–583). https://doi.org/10.1016/j.gene.2015.09.029

Swift, B., & Brouwer, K. L. R. (2010). Influence of Seeding Density and Extracellular Matrix on Bile Acid Transport and Mrp4 Expression in Sandwich-Cultured Mouse Hepatocytes. *Molecular Pharmaceutics*, *7*(2), 491. https://doi.org/10.1021/MP900227A

Takato, M., Sakamoto, S., Nonaka, H., Valor, F. Y. T., Tomonori, T., & Hamachi, I. (2024). Photoproximity labeling of endogenous receptors in the live mouse brain in minutes. *Nature Chemical Biology*. https://doi.org/https://doi.org/10.1038/s41589-024-01692-4

Terry, C., Dhawan, A., Mitry, R. R., Lehec, S. C., & Hughes, R. D. (2010). Optimization of the cryopreservation and thawing protocol for human hepatocytes for use in cell transplantation. *Liver Transplantation : Official Publication of the American Association for the Study of Liver Diseases and the International Liver Transplantation Society*,

16(2), 229–237. https://doi.org/10.1002/LT.21983

Terry, C., Hughes, R. D., Mitry, R. R., Lehec, S. C., & Dhawan, A. (2007). Cryopreservation-induced nonattachment of human hepatocytes: Role of adhesion molecules. *Cell Transplantation*, *16*(6), 639–647. https://doi.org/10.3727/000000007783465000

Terry, C., Mitry, R. R., Lehec, S. C., Muiesan, P., Rela, M., Heaton, N. D., Hughes, R. D., & Dhawan, A. (2005). The effects of cryopreservation on human hepatocytes obtained from different sources of liver tissue. *Cell Transplantation*, *14*(8), 585–594. https://doi.org/10.3727/000000005783982765

Tokuma, H., Sakano, D., Tanabe, K., Tanizawa, Y., Shiraki, N., & Kume, S. (2023). Selective proteasome degradation of the C-terminal truncated human WFS1 mutants in the pancreatic beta-cells. *FEBS Open Bio*.

Ueda, K., Kawano, J., Takeda, K., Yujiri, T., Tanabe, K., Anno, T., Akiyama, M., Nozaki, J., Yoshinaga, T., Koizumi, A., Shinoda, K., Oka, Y., & Tanizawa, Y. (2005). Endoplasmic reticulum stress induces Wfs1 gene expression in pancreatic β-cells via transcriptional activation. *European Journal of Endocrinology*, *153*(1), 167–176. https://doi.org/10.1530/EJE.1.01945

Ueno, H., Shibasaki, T., Iwanaga, T., Takahashi, K., Yokoyama, Y., Liu, L. M., Yokoi, N., Ozaki, N., Matsukura, S., Yano, H., & Seino, S. (2001a). Characterization of the gene EPAC2: Structure, chromosomal localization, tissue expression, and identification of the liver-specific isoform. *Genomics*. https://doi.org/10.1006/geno.2001.6641

Ueno, H., Shibasaki, T., Iwanaga, T., Takahashi, K., Yokoyama, Y., Liu, L. M., Yokoi, N., Ozaki, N., Matsukura, S., Yano, H., & Seino, S. (2001b). Characterization of the gene EPAC2: structure, chromosomal localization, tissue expression, and identification of the liver-specific isoform. *Genomics*, *78*(1–2), 91–98.

https://doi.org/10.1006/GENO.2001.6641

Urano, F. (2016). Wolfram Syndrome: Diagnosis, Management, and Treatment. *Current Diabetes Reports*, *16*(1), 1–8. https://doi.org/10.1007/S11892-015-0702-6

Van Niel, G., D'Angelo, G., & Raposo, G. (2018). Shedding light on the cell biology of extracellular vesicles. In *Nature Reviews Molecular Cell Biology* (Vol. 19, Issue 4). https://doi.org/10.1038/nrm.2017.125

Vinken, M., & Hengstler, J. G. (2018). Characterization of hepatocyte-based in vitro systems for reliable toxicity testing. In *Archives of Toxicology*. https://doi.org/10.1007/s00204-018-2297-6

Wang, L., Liu, H., Zhang, X., Song, E., Wang, Y., Xu, T., & Li, Z. (2021). WFS1 functions in ER export of vesicular cargo proteins in pancreatic β-cells. *Nature Communications 2021 12:1*, *12*(1), 1–13. https://doi.org/10.1038/s41467-021-27344-y

Wang, Y., Kim, P. K. M., Peng, X., Loughran, P., Vodovotz, Y., Zhang, B., & Billiar, T. R. (2006). Cyclic AMP and cyclic GMP suppress TNFalpha-induced hepatocyte apoptosis by inhibiting FADD up-regulation via a protein kinase A-dependent pathway. *Apoptosis : An International Journal on Programmed Cell Death*, *11*(3), 441–451. https://doi.org/10.1007/S10495-005-4293-6

Whittard, J. D., & Akiyama, S. K. (2001). Positive regulation of cell-cell and cell-substrate adhesion by protein kinase A. *Journal of Cell Science*, *114*(18), 3265–3272. https://doi.org/10.1242/jcs.114.18.3265

Wu, H., & Hegde, R. S. (2023). Mechanism of signal-anchor triage during early steps of membrane protein insertion. *Molecular Cell*, *83*(6), 961-973.e7. https://doi.org/10.1016/j.molcel.2023.01.018

Yamamoto, H., & Matsui, T. (2024). Molecular Mechanisms of Macroautophagy, Microautophagy, and Chaperone-Mediated Autophagy. In *Journal of Nippon Medical*

School (Vol. 91, Issue 1). https://doi.org/10.1272/jnms.JNMS.2024_91-102

Yamasaki, C., Ishida, Y., Yanagi, A., Yoshizane, Y., Kojima, Y., Ogawa, Y., Kageyama, Y., Iwasaki, Y., Ishida, S., Chayama, K., & Tateno, C. (2020). Culture density contributes to hepatic functions of fresh human hepatocytes isolated from chimeric mice with humanized livers: Novel, long-term, functional two-dimensional in vitro tool for developing new drugs. *PLoS ONE*, *15*(9 September). https://doi.org/10.1371/journal.pone.0237809

Yan, K., Gao, L. N., Cui, Y. L., Zhang, Y., & Zhou, X. (2016). The cyclic AMP signaling pathway: Exploring targets for successful drug discovery (review). *Molecular Medicine Reports*, *13*(5), 3715–3723. https://doi.org/10.3892/MMR.2016.5005/HTML

Yeh, Y. C., Lin, H. H., & Tang, M. J. (2012). A tale of two collagen receptors, integrin β1 and discoidin domain receptor 1, in epithelial cell differentiation. In *American Journal of Physiology - Cell Physiology*. https://doi.org/10.1152/ajpcell.00253.2012

Yu, P., & Hua, Z. (2023). To Kill or to Be Killed: How Does the Battle between the UPS and Autophagy Maintain the Intracellular Homeostasis in Eukaryotes? In *International Journal of Molecular Sciences* (Vol. 24, Issue 3). https://doi.org/10.3390/ijms24032221

Zatyka, M., Rosenstock, T. R., Sun, C., Palhegyi, A. M., Hughes, G. W., Lara-Reyna, S., Astuti, D., di Maio, A., Sciauvaud, A., Korsgen, M. E., Stanulovic, V., Kocak, G., Rak, M., Pourtoy-Brasselet, S., Winter, K., Varga, T., Jarrige, M., Polvèche, H., Correia, J., … Sarkar, S. (2023). Depletion of WFS1 compromises mitochondrial function in hiPSC-derived neuronal models of Wolfram syndrome. *Stem Cell Reports*, *18*(5). https://doi.org/10.1016/j.stemcr.2023.04.002

Zhang, Y. L., Wang, R. C., Cheng, K., Ring, B. Z., & Su, L. (2017). Roles of Rap1 signaling in tumor cell migration and invasion. *Cancer Biology & Medicine*, *14*(1), 90–99. https://doi.org/10.20892/J.ISSN.2095-3941.2016.0086

Zhao, L., Zhao, J., Zhong, K., Tong, A., & Jia, D. (2022). Targeted protein degradation: mechanisms, strategies and application. In *Signal Transduction and Targeted Therapy* (Vol. 7, Issue 1). https://doi.org/10.1038/s41392-022-00966-4

Zhu, Y., Chen, H., Boulton, S., Mei, F., Ye, N., Melacini, G., Zhou, J., & Cheng, X. (2015). Biochemical and Pharmacological Characterizations of ESI-09 Based EPAC Inhibitors: Defining the ESI-09 "Therapeutic Window." *Scientific Reports 2015 5:1*, *5*(1), 1–8. https://doi.org/10.1038/srep09344

Academic Conference

The 44th Annual Meeting of the Molecular Biology Society of Japan

Authors : Grace Aprilia Helena, Teruhiko Watanabe, Nobuaki Shiraki, Shoen Kume

Title : Improvement of Primary Human Hepatocyte Attachment

Date : December 2, 2021

Venue : Pacifico Yokohama

The 47th Annual Meeting of the Molecular Biology Society of Japan

Authors : Grace A. Helena, Hiraku Tokuma, Airi Inoue, Tatsuya Niwa, Hideki Taguchi, Daisuke Sakano, Shoen Kume

Title : Unraveling WFS1 Selective Degradation through Proximity Labeling

Date : November 27, 2024

Venue : Marine Messe, Fukuoka

List of Publications

Helena G A, Watanabe T, Kato Y, Nobuaki S, Kume S. (2023) Activation of cAMP (EPAC2) signaling pathway promotes hepatocyte attachment. Sci Rep, 2023 Jul 31;13(1):12352. doi: 10.1038/s41598-023-39712-3.

Helena G A, Kume S. (2024) A sneak peek into chronic glucose exposure and insulin secretion impairment through translatome. J Diabetes Investig. 2024 Jul 1;15(9):1174–1176. doi: 10.1111/jdi.14258

eAprin Certification

Tokyo Tech Basic Course (RCR) Certificate number: AP0000469604.

Supplementary Data

Supplementary Table 1 *PHH qPCR Primer List*

Gene Id	Symbol	Name	Forward	Reverse
174	AFP	Homo sapiens alpha-fetoprotein (AFP), mRNA.	AGAAACCCACTGGAGATGAACAGTC	GGCTGCAGCAGTCTGAATGTC
213	ALB	Homo sapiens albumin (ALB), mRNA.	GCAGTGTCCATTTGAAGATCATGTA	TGCAACTGTGCATAATTTGTCTCC
1543	CYP1A1	Homo sapiens cytochrome P450, family 1, subfamily A, polypeptide 1	AAACAGGGCCACATAGATGC	AGGGTCCTGGTTTGGCTAGT
1576	CYP3A4	Homo sapiens cytochrome P450, family 3, subfamily A, polypeptide 4	GAAACACAGATCCCCCTGAA	CTGGTGTTCTCAGGCACAGA
1544	CYP1A2	Homo sapiens cytochrome P450, family 1, subfamily A, polypeptide 2	TGTTCAAGCACAGCAAGAAGG	TGCTCCAAAGATGTCATTGAC
1373	CPS1	Homo sapiens carbamoyl-phosphate synthase 1, mitochondrial (CPS1), nuclear gene encoding mitochondrial protein, transcript variant 1, mRNA.	AAGCCACATCAGACTGGCTCA	TCACTAGGTCAATGCTGCCATCTC
5243	ABCB1	Homo sapiens ATP binding cassette subfamily B member 1 (ABCB1), transcript variant 3, mRNA	GGAGCCTACTTGGTGGCACATAA	TGGCATAGTCAGGAGCAAATGAAC
9429	ABCG2	Homo sapiens ATP-binding cassette, sub-family G (WHITE), member 2 (ABCG2), transcript variant 1, mRNA.	GGAGGCCTTGGGATACTTTGA	TCTATGAGTGGCTTATCCTGCTTG
2168	FABP1	Homo sapiens fatty acid binding protein 1 (FABP1), mRNA	AGTACCAACTGCAGAGCCAGGAA	ACTTTGGACCCAGCGGTGA
5465	PPARA	Homo sapiens peroxisome proliferator-activated receptor alpha (PPARA), transcript variant 3, mRNA.	TCAGGCTATCATTACGGAGTCCAC	TTGAATGTCTTCAATGGGCTTCAC
8694	DGAT1	Homo sapiens diacylglycerol O-acyltransferase 1 (DGAT1), mRNA	AACACATGGAGGCCATAGCATAGAG	TCCTCGAAGATCACCTGCTTGTA
84649	DGAT2	Homo sapiens diacylglycerol O-acyltransferase 2 (DGAT2), transcript variant 2, mRNA	CCTGGCAAGAATGCAGTCAC	TTTGAAGACAACAAACGTGAACGAC
335	APOA1	Homo sapiens apolipoprotein A1 (APOA1), transcript variant 1, mRNA	ACTGTGTACGTGGATGTGCTCAAAG	CACGCTGTCCCAGTTGTCAAG
338	APOB	Homo sapiens apolipoprotein B (APOB), mRNA	CAGTGAGCCAGCCTTGCAGTAG	GCTTTGGTGCAGGTCCAGTTC
1581	CYP7A1	Homo sapiens cytochrome P450, family 7, subfamily A, polypeptide 1	GAGAAGGCAAACGGGTGAAC	GCACAACACCTTATGGTATGACA

Supplementary Table 2 Composition of M4 Medium

Component	Company, Catalog No	Concentration
William's E Medium	Kanto Chemical, 49432-15	
HEPES	Dojindo, GB10	
Penicillin-Streptomycin	Nacalai Tesque, 26252-94	P:100 μg/mL, S:100 μg/mL
Bovine Serum Albumin (BSA)	Proliant Biological, PRL68700	
Insulin Human Recombinant	Kanto Chemical, 49433-61	5 mg/L
Transferrin	Bioconcept	5 mg/L
Recombinant Human HGF	PeproTech, 100-39	10 ng/mL
Recombinant Human Oncostain M (OsM)	Peprotech, 300-10	10 ng/mL
6-Bromoindirubin-3'-oxime (BIO)	Peprotech, 6676296	1.5 μM
Dexamethasone (Dex)	PeproTech, 5000222	10 μM
Calcitriol	Wako, 3220632	1 μM
Forskolin (Frk)	Wako, 6652995	10 μM
3-Isobutyl-1-methylxanthine (IBMX)	Wako, 2885842	0.5 mM

Supplementary Table 3 cDNA Primer Sequences

Primer Name	Primer Sequence
HindIII_mSec61a1_ORF_F	TGACTGAAGCTTGCCGCCATGGCGATCAAATTTCTGG
mSec61a1_ORF_R_SacI	CAGTCAGAGCTCTCAGAAGAGAAGGGCTCCCATGCTGCCC
EcoRI_mFKBP2_ORF_F	CAGTCAGAATTCCATGAGGCTGAGCTGGATCCTGACAATACTGT
mFKBP2_ORF_R_SacI	GTCACAGAGCTCCTACAGTTCTGAGCGTCTCTCAATCTTGAGCAGCTC

Supplementary Table 4 First Antibody List

First Antibody Name	Company, Catalog No.	Dilution Factor
Goat anti Albumin	Bethyl Laboratories, A80-129A	1:100
Rabbit anti MRP2	Invitrogen, JA32-01	1:50
Rabbit anti Myc	GeneTex, GTX115046	1:1000
Mouse anti Flag	Sigma, F1804-200UG	1:1000
Goat anti Calnexin	Novus Biologicals, NBP1-37774	1:50

Supplementary Table 5 Secondary & Conjugated Antibody List

Secondary & Conjugated Antibody Name	Company, Catalog No.	Dilution Factor
DAPI	Roche Diagnostics, 10236276001	1:1000
Phalloidin-Alexa iFluor 488	Biotium, 20106	1:1000
Donkey Anti Goat CF 568	AAT Bioquest, 23155	1:1000
Donkey anti Goat IgG Alexa Fluor 647	Jackson Laboratories, 705-605-147	1:1000

Supplementary Table 6 Buffer Compositions

Buffer Name	Buffer Composition	Storage Condition
Phosphate Buffered Saline (PBS (-))	137.0 mM NaCl, 2.7 mM KCl, 8.1 mM Na2HPO4, 1.5 mM KH2PO4	Room temperature
PBS-T	137.0 mM NaCl, 2.7 mM KCl, 8.1 mM Na2HPO4, 1.5 mM KH2PO4, 0.1% Tween-20	Room temperature
4% PFA/PBS (-)	137.0 mM NaCl, 2.7 mM KCl, 8.1 mM Na2HPO4, 1.5 mM KH2PO4, 4% Paraformaldehyde	-20°C refrigerator
1% Triton/PBS (-)	137.0 mM NaCl, 2.7 mM KCl, 8.1 mM Na2HPO4, 1.5 mM KH2HPO4. 1% Tween	4°C refrigerator
×5 Blocking One/PBS-T	Blocking One (Nacalai Tesque, 03953-95) diluted with the ratio of 1/5 in PBS-T	4°C refrigerator
Tris-acetate EDTA Buffer (TAE)	40.0 mM Tris-acetate,1.0 mM EDTA	Room temperature

Supplementary Table 7 EB Medium Composition

EB Medium Composition	Concentration, Details
D-MEM (high glucose)	Glucose (4.6 g/L)
fetal bovine serum (FBS)	10%
Non-Essential Amino Acids (NEAA)	0.1 mM
L-glutamine	2 mM
Pennicilin-Streptomycin	1%
Beta-Mercaptoethanol in PBS (-)	0.037 mM

Supplementary Table 8 List of R Packages

Package Names
clusterProfiler
org.Mm.eg.db
AnnotationDbi
DOSE
ReactomePA
KEGGREST
pathview
dplyr
tidygraph
ggplot2
ggkegg
KEGGgraph
DESeq2